

การออกแบบแผ่นปะอย่างเหมาะสมที่สุดเพื่อซ่อมแซมแผ่นเหล็กที่มีรอยร้าวโดยใช้ขั้นตอนวิธีเชิง
พันธุกรรม



นายแบช คิม ดู

จุฬาลงกรณ์มหาวิทยาลัย

บทคัดย่อและแฟ้มข้อมูลฉบับเต็มของวิทยานิพนธ์ตั้งแต่ปีการศึกษา 2554 ที่ให้บริการในคลังปัญญาจุฬาฯ (CUIR)
เป็นแฟ้มข้อมูลของนิสิตเจ้าของวิทยานิพนธ์ ที่ส่งผ่านทางบัณฑิตวิทยาลัย

The abstract and full text of theses from the academic year 2011 in Chulalongkorn University Intellectual Repository (CUIR)
are the thesis authors' files submitted through the University Graduate School.

วิทยานิพนธ์นี้เป็นส่วนหนึ่งของการศึกษาตามหลักสูตรปริญญาวิศวกรรมศาสตรมหาบัณฑิต

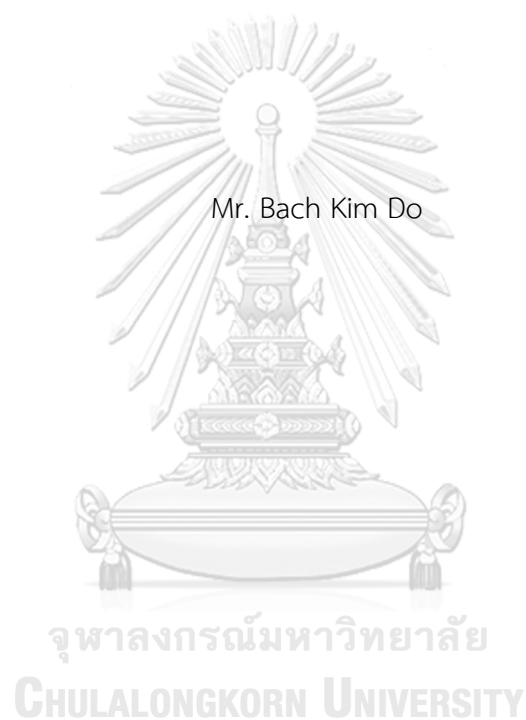
สาขาวิชาวิศวกรรมโยธา ภาควิชาวิศวกรรมโยธา

คณะวิศวกรรมศาสตร์ จุฬาลงกรณ์มหาวิทยาลัย

ปีการศึกษา 2560

ลิขสิทธิ์ของจุฬาลงกรณ์มหาวิทยาลัย

OPTIMUM PATCH DESIGN FOR REPAIRING CRACKED STEEL PLATES USING
GENETIC ALGORITHM



A Thesis Submitted in Partial Fulfillment of the Requirements
for the Degree of Master of Engineering Program in Civil Engineering

Department of Civil Engineering

Faculty of Engineering

Chulalongkorn University

Academic Year 2017

Copyright of Chulalongkorn University

Thesis Title OPTIMUM PATCH DESIGN FOR REPAIRING
 CRACKED STEEL PLATES USING GENETIC
 ALGORITHM
By Mr. Bach Kim Do
Field of Study Civil Engineering
Thesis Advisor Associate Professor Akhrawat Lenwari, Ph.D.

Accepted by the Faculty of Engineering, Chulalongkorn University in Partial
Fulfillment of the Requirements for the Master's Degree

.....Dean of the Faculty of Engineering
(Associate Professor Supot Teachavorasinskun, D.Eng.)

THESIS COMMITTEE

.....Chairman
(Professor Teerapong Senjuntichai, Ph.D.)

.....Thesis Advisor
(Associate Professor Akhrawat Lenwari, Ph.D.)

.....Examiner
(Sawekchai Tangaramvong, Ph.D.)

.....External Examiner
(Professor Thaksin Thepchatri, Ph.D.)

แบช คิม ดู : การออกแบบแผ่นปะอย่างเหมาะสมที่สุดเพื่อซ่อมแซมแผ่นเหล็กที่มีรอยร้าว โดยใช้ขั้นตอนวิธีเชิงพันธุกรรม (OPTIMUM PATCH DESIGN FOR REPAIRING CRACKED STEEL PLATES USING GENETIC ALGORITHM) อ.ที่ปรึกษาวิทยานิพนธ์หลัก: อัครวัชร เล่นวารี, 119 หน้า.

งานวิจัยนี้นำเสนอการออกแบบแผ่นปะอย่างเหมาะสมที่สุดเพื่อซ่อมแซมแผ่นเหล็กที่มีรอยร้าวโดยใช้ขั้นตอนวิธีเชิงพันธุกรรม ในขั้นตอนการออกแบบได้ใช้วิธีไฟไนต์เอลิเมนต์ (FE) การโปรแกรมเชิงพันธุกรรม (GP) ขั้นตอนวิธีทางพันธุกรรม (GA) และการโปรแกรมไม่เชิงเส้น เพื่อหาปริมาณที่น้อยที่สุดของแผ่นปะที่ทำให้ช่วงของตัวประกอบความเข้มของความเค้น (SIF) ที่ปลายรอยร้าวภายหลังการซ่อมแซมมีค่าต่ำกว่าขีดจำกัดความล้าของเหล็กภายใต้แรงกระทำเป็นรอบ ในงานวิจัยได้สร้างแบบจำลองไฟไนต์เอลิเมนต์สามมิติจำนวน 864 แบบเพื่อสร้างฐานข้อมูลของ SIF โดยพิจารณาค่าตัวแปรออกแบบต่างๆ ในกรณีการใช้แผ่นปะสองด้านที่สมมาตรกันซ่อมแซมรอยร้าวที่กึ่งกลางในแผ่นเหล็กภายใต้แรงดึงกระทำเป็นรอบ จากนั้นทำการวิเคราะห์การถดถอยโดย GP เพื่อพัฒนาผลเฉลยรูปแบบปิดของ SIF จากฐานข้อมูลของ SIF ที่ได้สร้างขึ้น และทำการวิเคราะห์เพื่อหาปริมาณที่น้อยที่สุดของแผ่นปะโดยขั้นตอนวิธีทางพันธุกรรม (GA) และการโปรแกรมไม่เชิงเส้น ซึ่งผลการออกแบบที่ได้คือ ความยาว ความกว้าง และความหนาแผ่นปะที่เหมาะสมที่สุด ในขั้นตอนสุดท้ายทำการตรวจสอบผลการออกแบบที่ได้ว่าไม่นำไปสู่การวิบัติในรูปแบบการขาดของแผ่นปะและการหลุดล่อนโดยพิจารณาเกณฑ์ที่เกี่ยวข้อง ในงานวิจัยนี้ได้แสดงตัวอย่างเพื่ออธิบายขั้นตอนการออกแบบที่เหมาะสมที่สุดในกรณีแผ่นปะสองด้านที่สมมาตรกันเพื่อซ่อมแซมแผ่นเหล็กที่มีรอยร้าวที่กึ่งกลางภายใต้แรงดึงกระทำเป็นรอบ โดยจากตัวอย่างพบว่า มอดุลัสของแผ่นปะมีอิทธิพลต่อผลการออกแบบที่ได้ และเมื่อพิจารณาเกณฑ์การวิบัติรูปแบบการหลุดล่อนพบว่า หน่วยแรงที่ผิวสัมผัสและวัสดุประสานมีค่าสูงขึ้นเมื่อเพิ่มค่ามอดุลัสของวัสดุประสาน จึงมีข้อเสนอแนะว่าควรใช้แผ่นปะที่มีค่ามอดุลัสสูงร่วมกับวัสดุประสานที่มีค่ามอดุลัสต่ำในการซ่อมแซมรอยร้าว และการเพิ่มความหนาและมอดุลัสของแผ่นปะจะมีประสิทธิภาพที่สุดสำหรับรอยร้าวขนาดใหญ่

ภาควิชา วิศวกรรมโยธา

ลายมือชื่อนิสิต

สาขาวิชา วิศวกรรมโยธา

ลายมือชื่อ อ.ที่ปรึกษาหลัก

ปีการศึกษา 2560

5970367021 : MAJOR CIVIL ENGINEERING

KEYWORDS: CRACK PATCHING / STRESS INTENSITY FACTOR SOLUTION / FATIGUE CRACK / CENTER-CRACKED PLATES / DESIGN OPTIMIZATION / GENETIC ALGORITHM

BACH KIM DO: OPTIMUM PATCH DESIGN FOR REPAIRING CRACKED STEEL PLATES USING GENETIC ALGORITHM. ADVISOR: ASSOC. PROF. AKHRAWAT LENWARI, Ph.D., 119 pp.

This research presents a design optimization process that combines the finite element (FE) method, genetic programming (GP), and optimization solvers, i.e., genetic algorithm (GA) and nonlinear programming, for double-sided fiber-reinforced polymer (FRP) patches used to repair center-cracked steel plates under tension fatigue. An optimization statement is to minimize the patch volume and reduce the stress intensity factor (SIF) range at crack tips below the fatigue threshold range. A detailed three-dimensional (3D) FE model of patch-repaired cracked plates is developed to compute SIF. A total of 864 FE models of patch-repaired cracked plates with different combinations of design parameters are then analyzed to obtain a SIF database. Based on the database, a symbolic regression via GP analysis is implemented to develop a closed-form SIF solution that helps visualize the effects of design parameters on SIF, facilitates the repair design, and is used as an inequality constraint in the optimization. Finally, optimization solvers are employed to find an optimum solution (patch length, width, and thickness) that is then checked for patch rupture and debonding failure based on some failure criteria. An example is given to illustrate the design process. The example results reveal that the optimum patch design is significantly influenced by patch modulus, meanwhile, the effect of adhesive modulus is not pronounced. Furthermore, in view of debonding failure, the maximum Tresca and interfacial stresses significantly increase when adhesive modulus increases. As both stresses are relatively insensitive to patch modulus, the use of high modulus patch and low modulus adhesive is recommended for fatigue crack repairs. For large cracks, using a thick and high elastic modulus patch is the most effective.

Department: Civil Engineering Student's Signature

Field of Study: Civil Engineering Advisor's Signature

Academic Year: 2017

ACKNOWLEDGEMENTS

First, and above all, I would like to express my sincerest gratitude to my academic supervisor Assoc. Prof. Akhrawat Lenwari. Thank you, Ajarn, not only for your outstanding technical guidance but also for your trust, your comments, your counsel, and for your time you put into discussing and revising my thesis work and my very first publications.

I would also like to thank the examiners of this thesis, Prof. Teerapong Senjuntichai, Prof. Thaksin Thepchatri, and Dr. Sawekchai Tangaramvong for their time, their interest in reading and discussing this thesis work.

The work presented in this thesis has been funded by the ASEAN University Network/Southeast Asia Engineering Education Development Network (AUN/SEED-Net) and Chulalongkorn University. Their support is gratefully acknowledged.

Last but not least, I dedicate this thesis to my parents, my younger brothers, my lover, Tran Tuyet, and my friends, Linh, Duy, Binh, Thu, Tek, Chanachai who always support and keep me going through difficult times during the implementation of this thesis.

จุฬาลงกรณ์มหาวิทยาลัย
CHULALONGKORN UNIVERSITY

CONTENTS

	Page
THAI ABSTRACT	iv
ENGLISH ABSTRACT	v
ACKNOWLEDGEMENTS	vi
CONTENTS	vii
LIST OF TABLES	x
LIST OF FIGURES	xi
NOTATION	xiv
CHAPTER 1 INTRODUCTION	1
1.1. Problem statement.....	1
1.2. Research objectives	3
1.3. Scope	4
1.4. Thesis outline.....	4
CHAPTER 2 LITERATURE REVIEW.....	6
2.1. Structural advantages of bonding composite patches.....	6
2.2. Determination of SIF of patch-repaired structures.....	7
2.3. Design criteria for crack patching	9
2.4. Optimization patch design for repairing cracked structures.....	10
CHAPTER 3 THEORETICAL BACKGROUND.....	12
3.1. Linear elastic fracture mechanics	12
3.1.1. Energy approach	12
3.1.2. Stress intensity factor approach	14
3.2. Computation of SIF with the interaction integral method	15

	Page
3.3. Genetic algorithm methodology	17
3.4. Genetic programming methodology	20
3.5. Symbolic regression via GP with HeuristicLab	22
3.6. MATLAB global optimization toolbox	22
3.7. Optimization with inequality constraints	23
CHAPTER 4 THREE-DIMENSIONAL FINITE ELEMENT MODEL	26
4.1. Element types and mesh density	26
4.2. Materials, geometries, and constraints	28
4.3. Validation of FE models	31
CHAPTER 5 STRESS INTENSITY FACTOR SOLUTIONS FOR PATCH-REPAIRED CENTER- CRACKED PLATES	36
5.1. Stress intensity factor solutions	36
5.2. Symbolic regression via genetic programming in HeuristicLab	37
5.3. Correction factor F_2 function	40
5.4. Verification of proposed SIF solution	42
CHAPTER 6 PATCH VOLUME OPTIMIZATION	48
6.1. Optimization problem statement	48
6.2. MATLAB optimization solver input and default values	49
6.3. A comparison of an optimum patch design with a previous work solution	51
CHAPTER 7 DESIGN EXAMPLE	53
7.1. Problem definition	53
7.2. Design optimization results	54
7.3. Assessment of composite patch and adhesive layer failures	65

	Page
CHAPTER 8 CONCLUSIONS	73
8.1. Conclusions	73
8.2. Recommendations for future works.....	74
REFERENCES	75
APPENDIX A THREE-DIMENSIONAL FINITE ELEMENT MODELING	84
APPENDIX B COMPARISON OF FINITE ELEMENT WITH PREVIOUS FE STUDY RESULTS	106
APPENDIX C VERIFICATION OF CLOSED-FORM SIF SOLUTION.....	108
APPENDIX D SYMBOLIC REGRESSION VIA GENETIC PROGRAMMING IN HEURISTICLAB.	111
APPENDIX E OPTIMIZATION SOLVERS IN MATLAB	116
E.1. Genetic algorithm.....	116
E.2. Nonlinear programming.....	117
E.3. A comparison between GA and nonlinear programming solutions.....	118
VITA.....	119

LIST OF TABLES

Table 4.1 Material and geometrical properties of steel plates, FRP patches, and adhesive layers.....	29
Table 5.1 Groups and subgroups used for GP analyses.....	38
Table 5.2 Control parameters used for GP analyses (HeuristicLab).....	38
Table 5.3 Person's R^2 values at several generations from GP analyses.....	39
Table 5.4 Constant coefficients of F_2 function.....	41
Table 5.5 Application range of closed-form SIF solution.....	42
Table 5.6 Cases for verification of SIF solution.....	43
Table 5.7 Fatigue crack growth calculation.....	45
Table 7.1 Optimum FRP patch for different material combinations, $2a = 0.2W_s$	61
Table 7.2 Optimum FRP patch for different material combinations, $2a = 0.3W_s$	63
Table 7.3 Failure indexes for optimum patch design solutions.....	68
Table B.1 Comparison of SIF from FE and handbook solutions [12] (unrepaired). ...	106
Table B.2 Comparison of SIF from FE and solutions [13] (one-sided patch).	107
Table B.3 Comparison of SIF from FE results and solutions [11] (two-sided patch). 107	
Table C.1 Comparison of the proposed F_2 solution and ABAQUS for case 1.....	108
Table C.2 Comparison of the proposed F_2 solution and ABAQUS for case 2.....	109
Table C.3 Comparison of the proposed F_2 solution and ABAQUS for case 3.....	109
Table C.4 Comparison of the proposed F_2 solution and ABAQUS for case 4.....	110

LIST OF FIGURES

Fig. 1.1. A crack was detected in a steel girder using red dye penetrant [5].	2
Fig. 1.2. A fracture occurred on a truss member of Turnpike Toll Bridge [6].	2
Fig. 3.1. Three basic modes of fracture mechanics [12].	14
Fig. 3.2. Example of GA candidate solutions.	18
Fig. 3.3. Example of GA operators.	18
Fig. 3.4. Example of a GP individual.	20
Fig. 3.5. Example of GP operators [75].	21
Fig. 4.1. Three element types used [9].	27
Fig. 4.2. FE meshes near the crack front.	28
Fig. 4.3. Sensitive analysis results.	28
Fig. 4.4. A-quarter finite element model in ABAQUS.	31
Fig. 4.5. Tie constraint regions in the finite element model.	31
Fig. 4.6. Comparison of FE results with referenced solutions [12] (unrepaired).	33
Fig. 4.7. Comparison of FE results with published solutions [13] (single-sided patch).	33
Fig. 4.8. Comparison of FE results with previously published results [11] (double-sided patch).	35
Fig. 5.1. Pearson's R^2 versus generation for four GP analyses.	39
Fig. 5.2. Scatter plot of F_2 at 2000 th generation with $R^2 = 0.906$ (Group 4).	40
Fig. 5.3. GP tree structure from the GP analysis for Group 4.	40
Fig. 5.4. Comparison of F_2 results from proposed solution and ABAQUS.	44

Fig. 5.5. Geometry and configuration of repaired specimen [34].....	45
Fig. 5.6. Crack propagation curves of the specimen.....	47
Fig. 6.1. Visualization of the inequality constraint.....	50
Fig. 6.2. Evolution of patch volume in GA analysis.....	52
Fig. 7.1. Cracked steel plate in the design example (dimension in mm).....	53
Fig. 7.2. Evolution of patch volume in GA analyses for $2a = 0.2W_s$, $E_p = 460$ MPa, and $E_a = 2944$ MPa.....	55
Fig. 7.3. Evolution of patch volume in fmincon analysis for $2a = 0.2W_s$, $E_p = 460$ MPa, and $E_a = 2944$ MPa.....	56
Fig. 7.4. Evolution of patch volume in GA analyses for $2a = 0.3W_s$, $E_p = 460$ MPa, and $E_a = 2944$ MPa.....	58
Fig. 7.5. Evolution of patch volume in fmincon analysis for $2a = 0.3W_s$, $E_p = 460$ MPa, and $E_a = 2944$ MPa.....	59
Fig. 7.6. Optimum patch volumes for different material combinations.....	60
Fig. 7.7. Distribution of Tresca along adhesive thickness ($2a = 0.2W_s$, $E_a = 2944$ MPa).....	66
Fig. 7.8. Effect of patch modulus on longitudinal stress in FRP patch ($2a = 0.2W_s$, $E_a = 2944$ MPa).....	69
Fig. 7.9. Effect of patch modulus on Tresca in adhesive layer ($2a = 0.2W_s$, $E_a = 2944$ MPa).....	70
Fig. 7.10. Effect of adhesive modulus on Tresca and interfacial stresses in adhesive layer ($2a = 0.2W_s$, $E_p = 460$ GPa).....	71
Fig. 7.11. Effect of adhesive modulus on Tresca and interfacial stresses in adhesive layer ($2a = 0.3W_s$, $E_p = 460$ GPa).....	72
Fig. A.1. Creating parts for FE model.....	86
Fig. A.2. Assemblage of five parts of FE model.....	87

Fig. A.3. Creating steel and adhesive sections.....	89
Fig. A.4. Creating composite layup for FRP patch.....	92
Fig. A.5. Meshing FE model.....	95
Fig. A.6. Defining surfaces for tie constraints.....	96
Fig. A.7. Creating four tie constraints.....	98
Fig. A.8. Material properties.....	100
Fig. A.9. Assigning boundary conditions.....	101
Fig. A.10. Creating tension load.....	102
Fig. A.11. Creating a crack and SIF output.....	105
Fig. D.1. Database for GP analyses.....	111
Fig. D.2. Starting HeuristicLab.....	112
Fig. D.3. Import the database and define the target variable in HeuristicLab.....	112
Fig. D.4. Define the maximum numbers of tree depth and tree length.....	113
Fig. D.5. Define function and terminal sets for GP.....	114
Fig. D.6. Define some control parameters for GP algorithm.....	115

NOTATION

a	one-half of crack length
A	crack area
\mathbf{B}	pre-logarithmic energy factor matrix
$c_0 - c_9$	constant coefficients
D	surface energy
E_{2p}	transverse in-plane modulus of FRP patch
E_a	elastic modulus of adhesive
E_p	longitudinal modulus of FRP patch
E_s	elastic modulus of steel
f	objective function
F	function set in genetic programming
F_1	finite-width correction factor
F_2	correction factor for patching effect
F_3	correction factor for debonding effect
g	inequality constraint
G	energy release rate
G_c	critical value of energy release rate
h	equality constraint
H	particular schema in a GA generation
k_I, k_{II}, k_{III}	SIF values for an auxiliary pure mode <i>I</i> , <i>II</i> , and <i>III</i>
$K, K_I, K_{II}, K_{III}, K_{IC}$	SIF, SIF mode <i>I</i> , mode <i>II</i> , mode <i>III</i> , fracture toughness
K_{FE}	stress intensity factor from finite element

K_{Ref}	stress intensity factor from handbook
L_e	crack front element length
L_p	length of patch
n	number of contours
n	number of design parameters of a general optimization problem
N	number data points
m	number of inequality constraints of a general optimization problem
p_{ap}	peeling strength of adhesive-patch interface
p_{as}	peeling strength of steel-adhesive interface
p_{ay}	shear strength of adhesive material
R_e	radius of the semi-cylinder
S	nonnegative slack variable vector
S_{11}	ultimate longitudinal stress in patch
S_{12}	ultimate shear stress in patch
S_{22}	ultimate transverse stress in patch
t	time
T	terminal set in genetic programming
T_s	Tsai-Hill failure index
t_a	thickness of adhesive layer
T_{ay}, T_{as}, T_{ap}	adhesive failure indexes
t_p	thickness of patch
t_s	thickness of steel plate

V_p	patch volume
W_{ext}	work done by external loads
W_{int}	the internal energy
W_p	width of patch
W_s	width of steel plate
\mathbf{X}	design parameter vector
$x_1 - x_4$	independent variables of F_2 function
$X_1 - X_3$	design parameters
X_i	i^{th} prediction of F_2 value
\mathbf{X}_L	lower bound of \mathbf{X}
X_i	mean of all F_2 predictions
\mathbf{X}_U	upper bound of \mathbf{X}
Y_i	F_2 value of i^{th} FE analysis
Y_m	mean of all F_2 values
ΔK_{th}	fatigue threshold SIF
δ	schema defining length
\mathcal{L}	Lagrange function
$\lambda = [\lambda_1, \lambda_2, \dots, \lambda_m]^T$	multiplier vector
γ	material constant related to surface energy D
ν	Poisson's ratio
o	schema order
σ	remote tensile stress
σ_1	maximum principal stress
σ_3	minimum principal stress

σ_{11}	longitudinal stress in patch
σ_{12}	shear stress in patch
σ_{22}	transverse stress in patch
σ_{33}	normal stress
σ_{\max}	maximum fatigue stress
σ_{\min}	minimum fatigue stress
μ	shear modulus



CHAPTER 1

INTRODUCTION

1.1. Problem statement

The need of finding an effective technique for strengthening and repairing old metallic bridges to ensure that the structures are still in good condition before new constructions is perceived. According to a report of United States Department of Transportation in 2016 [1] and a survey by Bien, *et al.* [2], almost half of 614,387 bridges in the US and about 70% of metallic bridges in Europe are 50 years or older.

Fatigue cracks appearing at high-stress zones in old-metallic structural members subjected to cyclic loadings are natural phenomena. In a report, Kuehn, *et al.* [3] revealed that fatigue is one of the leading causes of old bridge collapses among the other ones, such as the decreased static strength, instability, elastic deformation, and environmental conditions (seawater or industrial environment). In a survey, Fisher and Yuceoglu [4] indicated twenty-eight types of metallic bridge details experienced cracks, e.g. web gap, cope, eyebar, pin plate, cover plate, etc. These cracks can seriously damage the integrity of the structures if they are not detected and repaired in time. Fig. 1.1 shows a crack developed from a web gap of a steel girder detected by the red dye penetrant inspection [5]. Fig. 1.2 presents a crack initiated at a steel truss member of Turnpike Toll Bridge, in the US, that was closed for two months for the repair [6].

Owing to many good mechanical properties, adhesive-bonded fiber-reinforced polymer (FRP) patches have become a suitable choice for strengthening and repairing cracked and defective structures. Particularly for cracked structures, by sharing stresses in the main structures, FRP patches reduce stress intensity factor (SIF) that characterizes the stress and strain fields near the crack tip. As SIF reduces, the service life of repaired-cracked structures is extended. Therefore, the quantification of SIF values after the crack repairs is significant to predict the increased lifetime of repaired structures. Particularly for steel plates, however, a closed-form solution for SIF of repaired cracks does not exist. This drives a search for finding a correction factor for SIF in this study

to take into account the positive effects of FRP patches on SIF reduction. Center-cracked steel plates under tension fatigue loadings repaired with double-sided FRP patches are studied in this research.

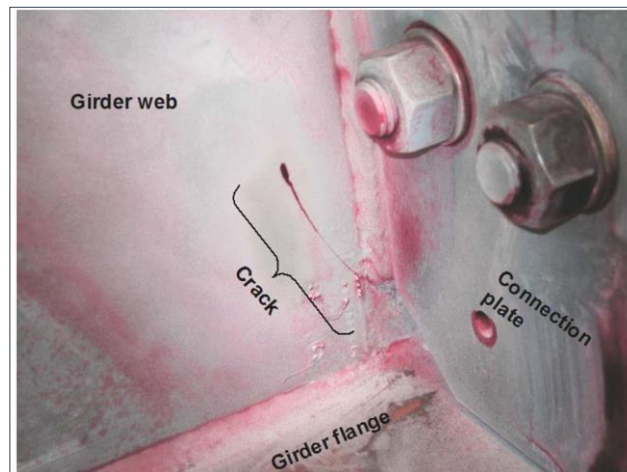


Fig. 1.1. A crack was detected in a steel girder using red dye penetrant [5].



Fig. 1.2. A fracture occurred on a truss member of Turnpike Toll Bridge [6].

This research also addresses the optimum FRP patch design for repairing foregoing cracked steel plates. Thereby, an optimum patch design is defined as a combination of design parameters that simultaneously minimizes the patch volume and limits SIF range below the fatigue threshold range. Additionally, the optimum design must satisfy the failure criteria, described in [7, 8], for the patch and adhesive layer.

In the study, a general finite element (FE) program ABAQUS/CAE [9], genetic programming (GP) in HeuristicLab [10], which is an important application of genetic algorithm (GA), and two optimization solvers in MATLAB are executed sequentially in a numerical process as follows. First, a detailed FE model of FRP-patched cracked plates built with ABAQUS is validated with previously published results [11-13]. Secondly, a total of 864 FE models are employed to create a SIF database for FRP-patched cracked plates. Thirdly, based on SIF database, the HeuristicLab is used to perform a symbolic regression via GP analyses to develop an empirical SIF solution to be used as an inequality constraint in a minimization problem for patch volume. Fourthly, an optimum solution (length, width, and thickness of patch) is obtained using GA and nonlinear programming in MATLAB. Finally, the optimum patch design is analyzed with ABAQUS to assess the FRP patch rupture and debonding phenomenon.

1.2. Research objectives

Following are four major objectives of this study:

1. To compute SIF of FRP-patched cracked steel plates under tension using FE analyses in which the layer-wise theory [14] is applied for modeling FRP patches.
2. To study the effects of geometrical and material properties of FRP patch and adhesive layer on SIF of FRP-patched cracked steel plates.
3. To develop closed-form empirical SIF solutions for cracked steel plates repaired with adhesive-bonded double-sided FRP patches under tension for ready use of practicing engineers.
4. To determine the optimum combination of width, length, and thickness of FRP patches for repairing center-cracked steel plates under tension fatigue loadings when FRP and adhesive material properties are specific.

1.3. Scope

The following statements limit the scope of this study:

1. Material models of steel and adhesive are linear elastic isotropic, while FRP is analyzed as a linear elastic orthotropic material.
2. Debonding phenomenon that may occur in the adhesive layer, at the steel-adhesive, or adhesive-patch interface [15] is not included in FE analyses. However, the possibility of appearing in this phenomenon is analyzed when the optimum patch design has already been accomplished.
3. Symbolic regression via GP and two optimization solvers are limited in the algorithms of HeuristicLab and MATLAB optimization toolbox, respectively.

1.4. Thesis outline

The thesis contents are organized as follows:

Chapter 2 provides a summary of previously published studies on structural advantages of bonding composite patches, methods used for determining SIF of FRP-patched cracked structures, some design criteria for crack patching, and different statements of optimization patch design for repairing cracked structures.

Chapter 3 focuses on the theoretical background used for this research. Two novel approaches to deal with crack problems in linear elastic fracture mechanics, the method of interaction energy release rate for the computation of SIF, a brief introduction to GA and GP methodologies, and the method of Lagrange multipliers for solving inequality constrained optimization problems are presented.

Chapter 4 describes in detail a three-dimensional (3D) FE model built with ABAQUS/CAE to compute SIF of center-cracked steel plates repaired with double-sided FRP patches under tension. A validation scheme for FE models is then presented at the end of the chapter.

Chapter 5 provides a closed-form SIF solution for FRP-patches cracked plates under tension. The solution is a result obtained from a symbolic regression via a GP

analysis in HeuristicLab. An independent verification of SIF solution for different combinations of design parameters is also introduced.

Chapter 6 formulates the optimization statement in this study. Two optimization solvers in MATLAB are presented briefly. A comparison of an optimum patch design with a previous work result is also introduced.

Chapter 7 presents a design example to illustrate the optimization process. The optimum combination of the width, length, and thickness of FRP patches repairing a center-cracked steel plate under tension fatigue loadings for predefined FRP and adhesive material properties is solved.

Chapter 8 gives main conclusions of this thesis work, including recommendations and perceptions for future works.



CHAPTER 2

LITERATURE REVIEW

This chapter summarizes previous studies focusing on four aspects of using composite patches for cracked structure repairs related to the present study. First, major structural advantages of bonding composite patches observed in the literature are listed. Secondly, previous works concentrating on characterizing SIF reduction of cracked structures due to the presence of composite patches are summarized. Thirdly, some design criteria for crack patching used in some aerospace engineering applications are provided. Finally, published studies on optimizing composite patch design are summarized.

2.1. Structural advantages of bonding composite patches

Due to their excellent mechanical properties, i.e., high modulus and strength of composite materials, good resistance to damage by fatigue, high formability, easy installation [16], adhesive-bonded fiber-reinforced polymer (FRP) patches have been considered as a suitable choice for repairing cracked and defective structural members, among other techniques, such as hole drilling, welding repair, adding doubler or splice plates, and post-tensioning [5]. Their applications have expanded in diverse fields, ranging from repairing cracks in aircraft structures to reinforcing old metallic bridges in civil engineering and applying to some structural problems in offshore and marine infrastructure engineering [17]. In practical application, FRP composite patches are usually used to strengthen old and corroded structures of infrastructure systems, such as old cast iron bridges, old steel bridges, and onshore and offshore pipelines [18]. In academia, many published studies verify that the adhesive-bonded composite patches beneficially influence the flexural strength [15, 19-24], lateral-torsional buckling capacity [25-28], and fatigue behavior [29-32] of steel structures; successfully oppose local buckling in hollow sections [15]; enhance the shear strength of reinforced concrete structures [33]; and enhance the strength and ductility of concrete-filled steel tubes [24].

It is the fact that bonding composite patches into the tension flange of metallic girders can significantly increase the flexural capacity and stiffness of these girders. In the study by Miller, *et al.* [19], four 7m-S24x80 steel girders strengthened by adhesive-bonded 12GPa-carbon fiber reinforced polymer (CFRP) plates increased the stiffness from 10% to 37% and ultimate strength from 17% to 25%. Schnerch and Rizkalla [23] found that the stiffness and ultimate strength of steel-concrete composite beams strengthened by high modulus CFRP strips also increased from 10% to 34% and up to 46%, respectively.

The applications of using the adhesive-bonded FRP patches to extend the fatigue life of cracked structures subjected to cyclic loadings have been reported for both steel plates [29-31, 34, 35] and beams [32, 36-39]. Colombi, *et al.* [29] concluded that fatigue life of a cracked steel plate repaired with different types of CFRP material increased by three times when using 174GPa-CFRP and up to 16 times when 216GPa-CFRP with a pre-stress level of 632 MPa was applied. Liu, *et al.* [30] conducted a series of experiments on cracked steel plates and revealed that elastic modulus of patch material and the number of patch layers play an important role in the fatigue life of repaired cracked plates. Täljsten *et al.* [31] performed an experimental program for old steel plates with a center notch strengthened by using prestressed and non-prestressed CFRP laminates and found that using non-prestressed CFRP increased fatigue life almost four times while using pre-stressing CFRP completely stopped the crack propagation. Jiao, *et al.* [32] showed that the fatigue life of 1.2m-steel beams repaired by using 210GPa-CFRP plates increased about seven times as compared with those repaired by welding method only. Colombi, *et al.* [37-39] demonstrated that bonding CFRP strips into the tension flange of cracked steel beams can significantly reduce the fatigue crack growth of the structures.

2.2. Determination of SIF of patch-repaired structures

A significant SIF reduction of cracked structures after bonding composite patches has attracted the attention of many researchers. The literature includes analytical, numerical, and experimental studies to characterize this phenomenon. The following is a brief summary of these studies.

In analytical works by Erdogan and Arin [40] and Ratwani [41], the solutions of stresses in the composite patch, SIF, and adhesive shear stresses for patched plates were provided using a two-step analysis with treating adhesive layer as two-dimensional shear springs. In the first step, stress distributions in an uncracked plate with the presence of composite patch were computed. The second step then introduced a crack into the patched plate to determine SIF values using the computed normal stress in the uncracked plate from the first step and two components of shearing spring stress that was the solution of a system of two integral equations. Rose [42-44] applied the two-step analysis for an infinite orthotropic plate containing a center-crack repaired with a bonded elliptical orthotropic patch and an adhesive layer considered as a shearing spring in the load direction to determine the solutions of tensile stress in the composite patch, the upper bond of SIF, and maximum shear stress in the adhesive layer. The aforementioned analytical works, however, are based on certain assumptions that may not be suitable for complex problems.

On the other hand, as a capacity for analyzing complex structures with different geometrical and material models and without any assumptions, the FE analysis has been popularly used to compute SIF of patch repaired cracks. Sun, *et al.* [45] presented a simple analysis method using Mindlin plate elements for a cracked plate and composite patch and three springs for adhesive layer. Naboulsi and Mall [46] proposed the three-layer technique in which two-dimensional Mindlin plate elements with the transverse shear deformation capability were used for all three parts: cracked plate, composite patch, and adhesive layer. Ayatollahi and Hashemi [13] computed SIF values for composite patched cracks in pure mode *I* and mixed mode *I/II* by using 3D brick elements for the three parts and the quarter point crack tip singular elements for crack tip region. Lam, *et al.* [47] proposed the modified three-layer technique using 3D brick elements for a cracked plate and conventional shell elements for both a composite patch and an adhesive layer. Gu, *et al.* [48] used 3D hex-dominated quadratic elements for all the three parts with collapsed 20 node brick elements for crack tip region. Wang, *et al.* [49] employed 8-node 3D solid elements for both a

cracked structure and a composite patch and 3D spring-damper elements for an adhesive layer.

Meanwhile, experimental works on SIF of the repaired structures have been very limited in the literature. Using the experimental methods, SIF can be interpreted from the X-ray back reflection [50], caustics method [51, 52], photoelasticity technique [53, 54], thermoelasticity technique [55], and piezoelectric sensor measurement [56].

2.3. Design criteria for crack patching

The effectiveness of a crack repair with FRP patches is assessed based on some design criteria for the three parts of the repair, i.e. the repaired structure, adhesive layer, and FRP patch in terms of design ultimate (DUL) and design fatigue (DFL) loads.

According to Marioli-Riga, *et al.* [57], a crack patching is successful if the following criteria are satisfied.

For repaired structure:

$$\Delta K_{\text{repaired}} < \left(\frac{1}{\delta}\right)^{\frac{1}{m}} \Delta K_{\text{unrepaired}} \quad (2.1)$$

where $\Delta K = K_{\text{max}} - K_{\text{min}}$ for cyclic loading; δ = the ration of life increase; m = Paris' law exponent.

and

$$\sigma_{V_s}^{\text{repaired}} < 0.7 \sigma_{V_s}^{\text{unrepaired}} \quad (2.2)$$

$$\sigma_{Ed}^{\text{repaired}} < \sigma_y \quad (2.3)$$

where $\sigma_{V_s}^{\text{repaired}}$ = von Mises stress at points in the structure underneath the patch; $\sigma_{Ed}^{\text{repaired}}$ = stresses in the structure at the edges of the patch; σ_y = yield stress of the structure material.

For the adhesive layer, shear strain is less than the allowable.

$$\gamma_a < \gamma_{al} \quad (2.4)$$

For the composite patch, Two criteria are required: stress in the load direction, σ_{yy} , is less than the allowable, σ_{al} , and some interactive criteria for composite materials are satisfied (e.g., Tsai–Hill).

$$\sigma_{yy} < \sigma_{al} \quad (2.5)$$

In a book on the theory of composite repair, Duong and Wang [58] provided design criteria for a crack patching applied in aerospace engineering whereby the repaired structure, adhesive layer, and composite patch must have sufficient static strength and fatigue resistance after the crack repair. For the repaired structure, the following three design criteria are required: 1) stress concentration factor in the repaired structure at patch's edge due to DUL is below 1.3, 2) SIF must be less than 80% of fracture toughness of the repaired structure at DUL, and 3) the difference in SIF at DFL must be less than the fatigue threshold range. For the composite patch, the maximum stress in the patch at DUL is less than 83% of the tensile ultimate strength of patch material and the maximum stress in the patch at DFL is less than 40% of the strength allowable of patch material. For adhesive layer, the maximum shear strain at DUL is below 80% of the maximum allowable strain and the maximum shear strain at DFL is less than twice the elastic shear strain limit.

2.4. Optimization patch design for repairing cracked structures

Research on composite patch design optimization for repairing cracked structures can be classified as two types of the problem formulation: 1) minimizing a structural cost function under constraints on mechanical properties and 2) maximizing a mechanical property under a constraint on the structural cost. Volume or area of the patch is usually used for representing the structural cost while SIF or the fatigue life of repaired structures is considered as the mechanical property. However, published studies in this field have been very limited.

Kumar and Hakeem [11] conducted a series of parameter finite element studies on different patch configurations to determine a patch shape that has the most effect

on SIF reduction. Brighenti [59] developed a tool in which GA was embedded within a finite element code to provide a patch topology that minimizes SIF or maximizes fatigue life of cracked steel plates. Although his work provided the best geometry of the patch by determining its topology, the optimization procedure presented was very complicated and almost cannot be applied by practicing engineers who just have a scant background of the finite element code, as well as GA. Yala and Megueni [60] used the design of experiments method to find an optimum combination of the patch and adhesive thicknesses and shear modulus of adhesive to minimize SIF of a rectangular center-cracked aluminum plate. Ramji, *et al.* [61] conducted 3D finite element analyses to find an optimum composite patch shape (circular, rectangle, square, elliptical, or octagonal) that provides the highest SIF reduction for an inclined center crack panel containing a crack inclination angle of 45° . Errouane, *et al.* [62] presented a combination of the ANSYS software and first-order optimization method to the volume optimization of a composite patch bonded on a cracked aluminum sheet to reduce SIF and restrict interfacial shear stress in adhesive layer by some constraints. Recently, Rasane, *et al.* [63] provided optimum patch designs for repairing a center-cracked aluminum sheet by using response surface methodology for an optimization problem with patch area was considered as an objective function and failure stress at aluminum-patch interface was as a constraint.

CHAPTER 3

THEORETICAL BACKGROUND

In this chapter, two approaches to deal with crack problems in linear elastic fracture mechanics, followed by the interaction integral method that is applied to compute SIF in ABAQUS/CAE are briefly presented. Basic backgrounds of GA and GP methodologies are then introduced. This chapter ends with the method of Lagrange multipliers that is used to find the optimum solution of inequality constrained optimization problem in the present study.

3.1. Linear elastic fracture mechanics

The basic of linear fracture mechanics theory (LEFM) includes energy balance and stress intensity factor (SIF) approaches to handle crack problems in structures. In the energy approach proposed by Griffith [64], the condition for an unstable crack extension in a brittle material is when a critical value of an energy release rate per unit crack growth exceeds an increasing rate of surface energy. Meanwhile, Irwin [65] proposed using a new quantity called stress intensity factor (SIF) to characterize the near crack-tip stress and strain fields. According to Irwin, a fracture occurs if SIF reaches a critical value that is related to the critical energy release rate proposed by Griffith [64].

3.1.1. Energy approach

Considering a static problem with a deformable body containing a crack in an adiabatically closed system, applying the first law of thermodynamics to the body, a change in energy per time is represented as

$$\dot{W}_{ext} = \dot{W}_{int} + \dot{D} \quad (3.1)$$

where the left-hand side of Eq. (3.1) = energy goes into the body per time in terms of the work done by external loads (body forces and boundary tractions); right-hand side of Eq. (3.1) = energy absorbed by the body per time = the internal energy per time,

\dot{W}_{int} , adds (+) the dissipative energy (surface energy) per time, \dot{D} , consumed during the creation of two new surfaces of the crack.

The surface energy, needed to create two new crack surfaces, is proportional to the crack area, A , with a material constant, γ , as follow

$$D = 2\gamma A \quad (3.2)$$

Now, considering two moments of time of a crack extension t_i and t_{i+1} where at t_i , $A_i = A$ and at t_{i+1} , $A_{i+1} = A_i + \Delta A = A + \Delta A$.

Substituting D from Eq. (3.2) into Eq. (3.1) and applying the propagation of the crack corresponding to the above two moments of time, Eq. (3.1) becomes

$$\frac{W_{ext,i+1} - W_{ext,i}}{t_{i+1} - t_i} = \frac{W_{int,i+1} - W_{int,i}}{t_{i+1} - t_i} + 2\gamma \frac{A_{i+1} - A_i}{t_{i+1} - t_i} \quad (3.3)$$

Eq. (3.3) can be rewritten as

$$\Delta W_{ext} = \Delta W_{int} + 2\gamma \Delta A \quad (3.4)$$

Based on Eq. (3.4), Griffith [64] provided the energetic fracture criterion, as follow

$$G = \frac{\Delta W_{ext} - \Delta W_{int}}{\Delta A} \geq 2\gamma \quad (3.5)$$

In Eq. (3.5), G is the energy release rate defined for finite or infinitesimal crack extension. Based on this concept, a fracture criterion regarding the energy dissipated during the crack extension is produced, whereby a crack propagates if the following condition is satisfied

$$G = \frac{\Delta W_{ext} - \Delta W_{int}}{\Delta A} \geq G_c = 2\gamma \quad (3.6)$$

where G_c represents the critical material parameter.

3.1.2. Stress intensity factor approach

Fig. 3.1 shows three basic modes of crack extensions in which mode *I* is dominant in the real world. Each mode is characterized by the displacement of the crack surface with respect to the plane of the crack. A polar coordinate system (r, θ) is defined with the crack tip is referred as the reference point of the system, illustrated in Fig. 3.1. The stress field in the vicinity of the crack tip corresponding to three crack extension modes are characterized by three stress intensity factor values K_I , K_{II} , and K_{III} , detailed in Eqs. (3.7) – (3.9).

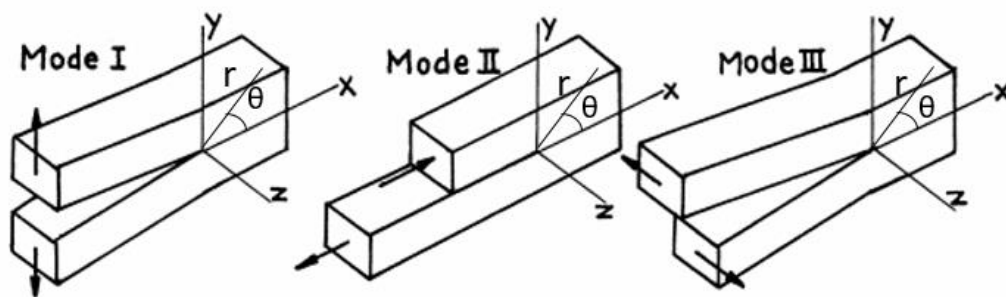


Fig. 3.1. Three basic modes of fracture mechanics [12].

Mode *I*, for a plane stress condition

$$\begin{bmatrix} \sigma_{xx} \\ \sigma_{yy} \\ \sigma_{xy} \end{bmatrix} = \frac{K_I}{\sqrt{2\pi r}} \cos \frac{\theta}{2} \begin{bmatrix} 1 - \sin \frac{\theta}{2} \sin \frac{3\theta}{2} \\ 1 + \sin \frac{\theta}{2} \sin \frac{3\theta}{2} \\ \sin \frac{\theta}{2} \cos \frac{3\theta}{2} \end{bmatrix} + \text{terms containing } r^0, r^{1/2}, r^1, r^{3/2} \dots \quad (3.7)$$

Mode *II*, for a plane stress condition

$$\begin{bmatrix} \sigma_{xx} \\ \sigma_{yy} \\ \sigma_{xy} \end{bmatrix} = \frac{K_{II}}{\sqrt{2\pi r}} \begin{bmatrix} -2 \sin \frac{\theta}{2} - \sin \frac{\theta}{2} \cos \frac{\theta}{2} \cos \frac{3\theta}{2} \\ \sin \frac{\theta}{2} \cos \frac{\theta}{2} \cos \frac{3\theta}{2} \\ \cos \frac{\theta}{2} - \cos \frac{\theta}{2} \sin \frac{\theta}{2} \sin \frac{3\theta}{2} \end{bmatrix} + \text{terms containing } r^0, r^{1/2}, r^1, r^{3/2} \dots \quad (3.8)$$

Mode *III*

$$\begin{bmatrix} \sigma_{xz} \\ \sigma_{yz} \end{bmatrix} = \frac{K_{III}}{\sqrt{2\pi r}} \begin{bmatrix} -\sin \frac{\theta}{2} \\ \cos \frac{\theta}{2} \end{bmatrix} + \text{terms containing } r^0, r^{1/2}, r^1, r^{3/2} \dots \quad (3.9)$$

It is seen that the singular stress field described by the three SIF values is dominated in a finite region around the crack tip only where r approaches to 0. If r is beyond that region, the higher terms get their influences.

Based on the concept of SIF, Irwin [65] provided a fracture criterion for a crack problem, whereby the crack propagates if the following condition is satisfied (for the case of mode *I*)

$$K_I > K_{IC} \quad (3.10)$$

where K_{IC} = the critical value of mode *I* SIF, namely fracture toughness, representing the material resistance against crack initiation under monotonic loadings.

The relationship between $\mathbf{K} = [K_I \ K_{II} \ K_{III}]^T$ and G is expressed by

$$G = \begin{cases} \frac{K_I^2 + K_{II}^2}{E_s} + \frac{K_{III}^2}{2\mu} & \text{plane stress} \\ \frac{K_I^2 + K_{II}^2}{E_s} (1 - \nu^2) + \frac{K_{III}^2}{2\mu} & \text{plane strain} \end{cases} \quad (3.11)$$

where E_s = elastic modulus; ν = Poison's ratio; μ = shear modulus.

3.2. Computation of SIF with the interaction integral method

SIF values are extracted in ABAQUS/CAE from the interaction integral method [66]. In this method, an auxiliary pure mode *I* crack-tip field [Eq. (3.13)] is assumed to superimpose onto the mixed-mode actual field [Eq. (3.12)]. An interaction energy release rate [Eq. (3.15)] is computed by subtracting the energy release rate of the auxiliary and actual fields from the energy release rate of the superimposed field [Eq. (3.14)]. SIF values are directly computed from the computed interaction energy release rate [66]. Following is a brief summary of the interaction integral method.

The energy release rate for the actually mixed-mode crack field is

$$G = \frac{1}{8\pi} [K_I B_{11}^{-1} K_I + 2K_I B_{12}^{-1} K_{II} + 2K_I B_{13}^{-1} K_{III}] \quad (3.12)$$

+ (terms not involving K_I)

where \mathbf{B} = pre-logarithmic energy factor matrix [66, 67].

The energy release rate for the auxiliary pure mode I is given by

$$G_{aux}^I = \frac{1}{8\pi} k_I B_{11}^{-1} k_I \quad (3.13)$$

The energy release rate of the superimposed field is

$$G_{tot}^I = \frac{1}{8\pi} [(K_I + k_I) B_{11}^{-1} (K_I) + 2(K_I + k_I) B_{12}^{-1} (K_{II}) + 2(K_I + k_I) B_{13}^{-1} K_{III}] \quad (3.14)$$

+ (terms not involving K_I or k_I)

Subtracting the actual and auxiliary energy release rates in Eqs. (3.12) and (3.13) from the superimposed energy release rate in Eq. (3.14), the interaction energy release rate is given

$$G_{int}^I = G_{tot}^I - G - G_{aux}^I = \frac{k_I}{4\pi} [B_{11}^{-1} K_I + B_{12}^{-1} K_{II} + B_{13}^{-1} K_{III}] \quad (3.15)$$

If the foregoing steps are also repeated for mode II and mode III , a linear system of equations results

$$\begin{cases} G_{int}^I = \frac{k_I}{4\pi} [B_{11}^{-1} K_I + B_{12}^{-1} K_{II} + B_{13}^{-1} K_{III}] \\ G_{int}^{II} = \frac{k_{II}}{4\pi} [B_{21}^{-1} K_I + B_{22}^{-1} K_{II} + B_{23}^{-1} K_{III}] \\ G_{int}^{III} = \frac{k_{III}}{4\pi} [B_{31}^{-1} K_I + B_{32}^{-1} K_{II} + B_{33}^{-1} K_{III}] \end{cases} \quad (3.16)$$

If $k_I = k_{II} = k_{III} = 1$, a solution of system (3.16) provides SIF values as

$$\mathbf{K} = 4\pi \mathbf{B} \mathbf{G}_{int} \quad (3.17)$$

where $\mathbf{G}_{int} = [G_{int}^I \ G_{int}^{II} \ G_{int}^{III}]^T$

In ABAQUS, the energy release rate is determined using the method of virtual crack extensions. For more detail, see section 2.16.1 of ABAQUS theory manual [68].

3.3. Genetic algorithm methodology

Genetic algorithms (GAs) are iterative numerical solvers for optimization problems inspired by natural selection and natural genetics [69-71]. Each GA operates on a population of candidate solutions of binary strings in a computer program.

To start a GA, randomly numeric values of independent variables in a solution space are encoded to binary strings in a computer program with respect to the 1-to-1 mapping property in which each binary string in the computer program space represents exactly one point in the solution space, and vice versa. For example, Fig. 3.2 shows four numeric numbers in a solution space that are encoded to become corresponding four binary strings of length 10 in a computer program. The opposite process of encode is decode that turns binary strings into numeric numbers for the assessment and visualization of the algorithm results.

Immediately after the encode process, the GA determines the fitness of each string in the current generation (iteration). The string fitness is the value of a given objective function, namely fitness function, at a particular point that corresponds to the binary string being considered. The algorithm then arranges all strings in descending order of their fitness values. Based on this arrangement, the algorithm performs orderly the following three genetic operators: elite transfer [Fig. 3.3(a)], crossover [Fig. 3.3(b)], and mutation [Fig. 3.3(c)] to produce a new population of binary strings for the next generation.

Numeric values	GA process	Binary strings									
-30	encode →	1	1	1	1	1	0	0	0	1	0
-10		1	1	1	1	1	1	0	1	1	0
10	← decode	0	0	0	0	0	0	1	0	0	0
30		0	0	0	0	0	1	1	1	1	0

Fig. 3.2. Example of GA candidate solutions.

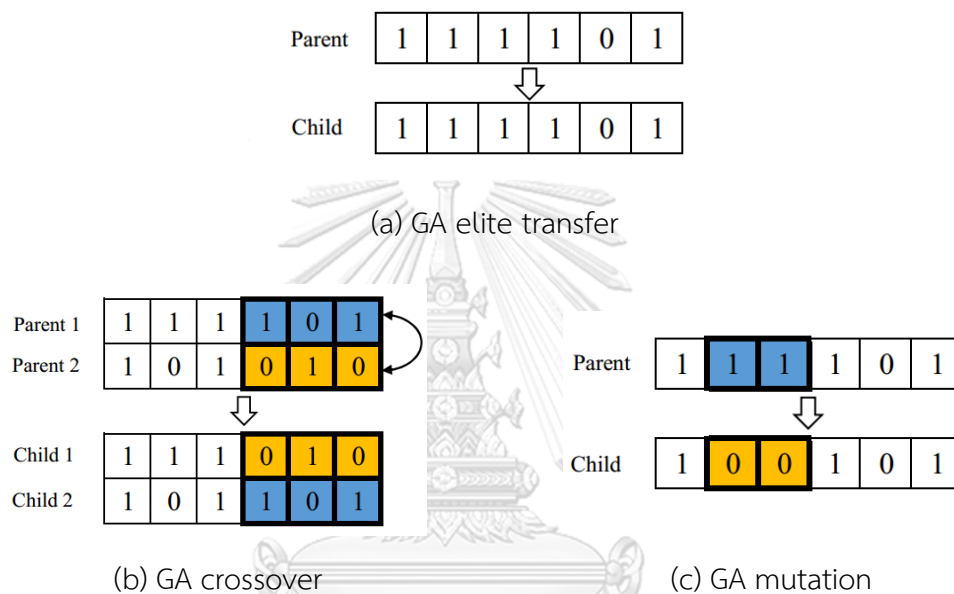


Fig. 3.3. Example of GA operators.

In GA elite transfer scheme [Fig. 3.3(a)], strings that have the best fitness values in the current generation are automatically survived to the next generation. Two strings will be the elites in this study. Meanwhile, most of the strings in the population are to be experienced through the crossover operator [Fig. 3.3(b)]. To implement the crossover, each pair of strings is selected randomly; a crossover point is determined at a random location of these strings. By exchanging all binary bits coming after the crossover point of the two strings, two new crossover offspring are created for the next generation. Finally, a small proportion of the population containing strings with the worst fitness values can be through the mutation operator [Fig. 3.3(c)] in which a binary bit of the mutation string is randomly selected and changed its value from 0 to 1, or vice versa.

As an iterative algorithm, the GA repeats the aforementioned operators for the next generation until reaching a stopping criterion that usually is a specific number of generations of the algorithm. In MATLAB, some stopping criteria are also applied such as the run-time complexity limit, the function and constraint tolerances, etc. The designation of the GA solution is determined as the best-so-far binary string that has the greatest fitness value stored in the computer cache as soon as the algorithm satisfies at least one stopping criterion.

Focusing on the foundation of GAs, Holland [69] first proposed the schema theory that attempted to explain how a GA process directly guided the search for improving the fitness of the current GA population. This theory can be able to predict the development in the number of a particular schema, namely \mathbf{H} , contained within a population at a certain time to be increased or decreased after each generation.

As defined by Holland [69], followed by Goldberg [70], a schema \mathbf{H} is a subset of strings that have the same values at certain loci. Let all strings in a population are constructed from three alphabets $(0\ 1\ *)$ in which the star $*$ can be either a 1 or a 0 at a certain locus. For example, $\mathbf{H}=11*1*101$, a schema of length 8, describes a subset including the following four strings: **11010101**, **11111101**, **11110101**, and **11011101**.

Each schema has two properties: schema defining length, $\delta(\mathbf{H})$ and schema order, $o(\mathbf{H})$. The schema defining length is defined as the distance between the first and the last locus of given bits of the schema being considered. For example, a schema $11*1*101$ with the first given bit is 1 at locus 1 and the last one is 1 at locus 8 has $\delta(\mathbf{H}) = 8-1 = 7$. The schema order is the numbers of given bits of the schema. For example, the schema $11*1*101$ with 6 given bits at loci 1, 2, 4, 6, 7, 8 has $o(\mathbf{H}) = 6$.

According to the schema theory, schemas with above-average fitness, short length, and lower order can have more chance to increase their number in future generations.

3.4. Genetic programming methodology

Genetic programming (GP) [72, 73] is one important application of GA for regression analysis. The major difference between GP and GA is the representation of candidate solutions that are binary strings in GA [Fig. 3.2] and are tree structures in GP [Fig. 3.4].

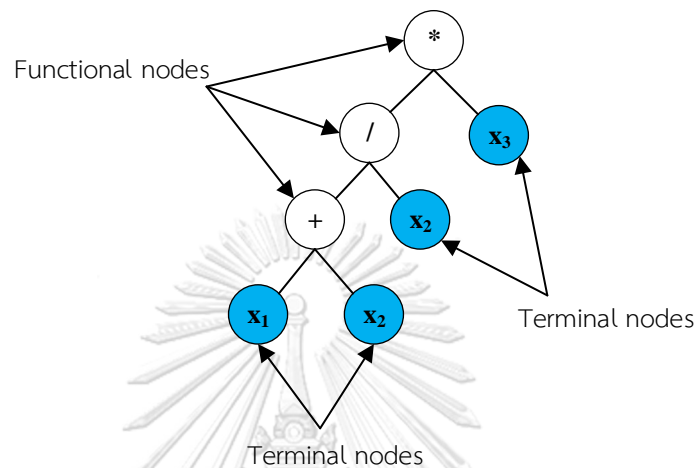


Fig. 3.4. Example of a GP individual.

In this research, GP provides the best fit solution for a new correction factor F_2 (see section 5.1) by maximizing the squared Pearson correlation coefficient R^2 (Pearson's R^2) [74], as given in Eq. (3.18). The R^2 is widely used to reveal the linear correlation between two quantitative parameters. Here, the two quantitative parameters are the validated FE results of the correction factor F_2 and corresponding predictions from a GP analysis. The larger the R^2 is, the better the GP result is

$$R^2 = \left[\sum_{i=1}^N (X_i - X_m)(Y_i - Y_m) \right]^2 / \sum_{i=1}^N (X_i - X_m)^2 \sum_{i=1}^N (Y_i - Y_m)^2 \quad (3.18)$$

where N = the number of observations of F_2 database from FE analyses; $Y_i = F_2$ value of the i^{th} FE analysis; Y_m = the mean of all Y_i values; X_i = the prediction value of Y_i ; X_m = the mean of all X_i values.

SIF of the repaired plates is sensitive to the variation of design parameters. Thus, traditional regression techniques, namely numeric regression, may not work well since it is difficult to predict a regression mathematical model at first with unknown coefficients before applying regression theory to determine these coefficients. In this

case, simultaneously finding the regression mathematical model and unknown coefficients, namely symbolic regression, is a reasonable requirement. The GP allows performing the symbolic regression.

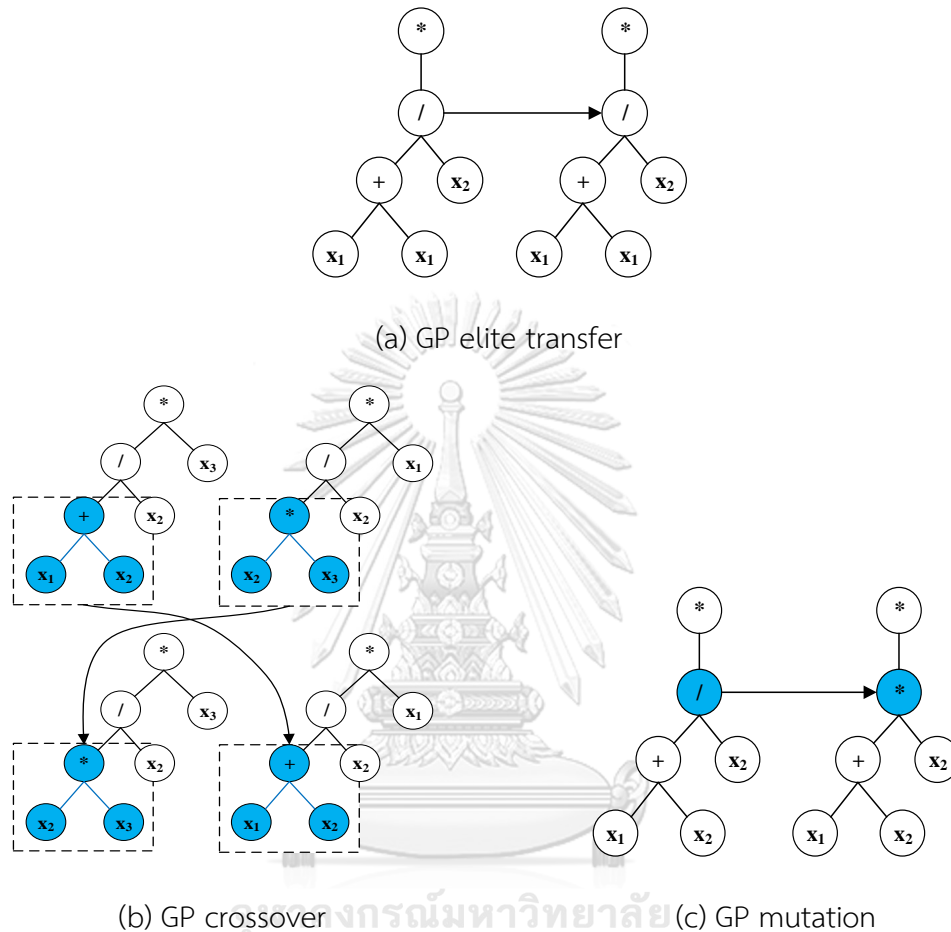


Fig. 3.5. Example of GP operators [75].

A GP analysis consists of the following three steps. First, an initial population of a given number of tree structures is randomly created by using atoms from the following two given sets: function (**F**) and terminal (**T**). Atoms of the **F** set can be arithmetic operations, mathematical functions, Boolean operations, conditional operators, or any user-defined functions [72]. Within a tree structure, **F**'s atoms occupy functional nodes that have two arguments, presented Fig. 3.4. Meanwhile, **T**'s atoms are independent variables and constants [72]. These atoms are to be located at terminal nodes of the GP tree structure that have no argument, illustrated in Fig. 3.4. Secondly, the GP computes R^2 values for all tree structures existing in the current

generation. Based on these R^2 values, the algorithm stores all tree structures in a column vector and arranges them in a descending order of R^2 values. After the arrangement, the GP performs the following three genetic operators in a sequence: elite transfer [Fig. 3.5(a)], crossover [Fig. 3.5(b)], and mutation [Fig. 3.5(c)] to produce a new population of tree structures for the next generation. Finally, similarly to GA solution definition, the solution of the GP analysis is determined as the best-so-far tree structure stored in the cache of the computer program.

3.5. Symbolic regression via GP with HeuristicLab

This research uses HeuristicLab for GP analyses [10]. It is an open source software for heuristic and evolutionary algorithms developed on C# programming language by members of the Heuristic and Evolutionary Algorithms Laboratory in Austria since 2002.

Symbolic regression in HeuristicLab is a database modeling technique that works on a set of examples, namely training set, with identified properties. On the basis of the training set, the algorithm works with solution candidates that are tree structure representations of symbolic expressions, as presented in section 3.5, and produces a formula that maps a vector of object features into one of the given classes. A procedure for performing a symbolic regression via GP in HeuristicLab environment is introduced in **APPENDIX D**.

3.6. MATLAB global optimization toolbox

Global optimization toolbox [76] provides MATLAB functions that search for global solutions to optimization problems. The toolbox includes global search, nonlinear programming, genetic algorithm, multi-objective genetic algorithm, pattern search, quadratic programming, and simulated annealing solvers. These solvers can be used to solve optimization problems where the objective or constraint function is continuous, discontinuous, does not have derivatives, or includes simulations [76].

For comparison purpose, this study uses two solvers: genetic programming (command `ga`) and nonlinear programming, (command `fmincon`). Both solvers are completely different in the way of searching the optimum solution. While the GA only looks at the objective function values at every point in the solution space during the

searching process, the fmincon is based on calculating the gradient of the objective function.

Considering the following optimization problem: Min $f(\mathbf{X})$ such that

$$\begin{cases} c(\mathbf{X}) \leq 0 \\ c_{eq}(\mathbf{X}) = 0 \\ \mathbf{A}\mathbf{X} = \mathbf{b} \\ \mathbf{A}_{eq}\mathbf{X} = \mathbf{b}_{eq} \\ \mathbf{X}_L \leq \mathbf{X} \leq \mathbf{X}_U \end{cases} \quad (3.19)$$

where \mathbf{b} and \mathbf{b}_{eq} = vectors; \mathbf{A} and \mathbf{A}_{eq} = matrices; $c(\mathbf{X})$ and $c_{eq}(\mathbf{X})$ = functions that return vectors; $f(\mathbf{X})$ = a function that returns a scalar; and \mathbf{X}_L and \mathbf{X}_U = lower and upper bound vectors, respectively.

In MATLAB, the genetic algorithm and nonlinear programming commands for the optimization are as follows

$$\mathbf{X} = \text{ga}(f(\mathbf{X}), \text{size}(\mathbf{X}), \mathbf{A}, \mathbf{b}, \mathbf{A}_{eq}, \mathbf{b}_{eq}, \mathbf{X}_L, \mathbf{X}_U, [c(\mathbf{X}), c_{eq}(\mathbf{X})], \text{options}) \quad (3.20)$$

$$\mathbf{X} = \text{fmincon}(f(\mathbf{X}), \mathbf{X}_0, \mathbf{A}, \mathbf{b}, \mathbf{A}_{eq}, \mathbf{b}_{eq}, \mathbf{X}_L, \mathbf{X}_U, [c(\mathbf{X}), c_{eq}(\mathbf{X})], \text{options}) \quad (3.21)$$

The “options” for each solver is clearly described in [76] and in **APPENDIX E**.

3.7. Optimization with inequality constraints

The method of Lagrange multipliers [77] is applied to deal with the inequality-constrained optimization problem in the present study. The background of this method is presented as follows.

An optimization problem is given as

$$\text{Min } f(\mathbf{X})$$

subject to

$$g_j(\mathbf{X}) \leq 0, j = 1, 2, \dots, m \quad (3.22)$$

where $\mathbf{X} = [x_1, x_2, \dots, x_n]^T$ = design parameter vector; n = the number of design parameters; and m = the total number of constraints, including explicit lower and upper bounds on the design parameters.

The constraints in Eq. (3.19) is to be transformed to equality constraints by adding nonnegative slack variables, S_j , as

$$g_j(\mathbf{X}) + S_j = 0, j = 1, 2, \dots, m \quad (3.23)$$

Then, the optimization problem becomes

Min $f(\mathbf{X})$

subject to

$$h_j(\mathbf{X}, \mathbf{S}) = g_j(\mathbf{X}) + S_j = 0, j = 1, 2, \dots, m \quad (3.24)$$

where $\mathbf{S} = [S_1, S_2, \dots, S_m]^T$

The new problem can be solved conveniently by the method of Lagrange multipliers with the Lagrange function, \mathcal{L} , is as

$$\mathcal{L}(\mathbf{X}, \mathbf{S}, \boldsymbol{\lambda}) = f(\mathbf{X}) + \sum_{j=1}^m \lambda_j h_j(\mathbf{X}, \mathbf{S}) \quad (3.25)$$

where $\boldsymbol{\lambda} = [\lambda_1, \lambda_2, \dots, \lambda_m]^T$ = multiplier vector.

The Karush-Kuhn-Tucker (KKT) conditions that are necessary conditions for a global minimum of the above problem are as follows

$$\frac{\partial \mathcal{L}}{\partial x_i} = \frac{\partial f}{\partial x_i} + \sum_{j=1}^m \lambda_j \frac{\partial g_j}{\partial x_i} = 0, \quad i = 1, 2, \dots, n \quad (3.26)$$

$$\lambda_j g_j = 0, \quad j = 1, 2, \dots, m \quad (3.27)$$

$$g_j \leq 0, \quad j = 1, 2, \dots, m \quad (3.28)$$

$$\lambda_j \geq 0, \quad j = 1, 2, \dots, m \quad (3.29)$$

If the optimization problem is convex, the KKT conditions are necessary as well as sufficient conditions and any local minimum becomes a global minimum. The above optimization problem is convex if $f(\mathbf{X})$ and $g_j(\mathbf{X})$ are convex functions [77].



CHAPTER 4

THREE-DIMENSIONAL FINITE ELEMENT MODEL

In this chapter, a detailed FE model of FRP-patched plates built with ABAQUS/CAE is provided. The FE models are then validated with previous studies in the literature for two cases of unrepaired and repaired (with single-sided and double-sided patches) plates.

4.1. Element types and mesh density

A total of 864 three-dimensional (3D) FE models are analyzed with ABAQUS/CAE [9] to compute SIF values of FRP-patched plates under tension for different combinations of steel plate configuration, crack length, and geometrical and material properties of the patch and adhesive layer. Fig. 4.1 shows three element types used in all FE models. A 20-node quadratic solid element, C3D20, is assigned to the cracked plate and adhesive layer elements while an 8-node continuum shell element with reduced integration, SC8R, is used for FRP patch. The SC8R element is designed to resemble 8-node solid element but has only three displacement degrees of freedom at each node. Kinematic assumptions and constitutive relations for the element are similar to the 3D conventional shell element given at a reference surface [78]. A layer-wise theory of Reddy [14] is applied for modeling FRP patch by stacking SC8R elements through the patch thickness with the command `*SHELL SECTION, STACK DIRECTION = 3`, which means the stacking direction and patch thickness are identical. Additionally, to capture the square root singularity of stress and strain fields in the vicinity of the crack front, a collapsed 3D element, collapsed C3D20, is appointed to a small region around the crack front in the steel plate.

In Fig. 4.2, surrounding the crack front are strips of wedge-shaped elements that fill a semi-cylinder with the center at the crack front and the radius, R_e , is equal to $a/12 - a/5$. The amount of these strips spanning the radial length of the semi-cylinder depends on the crack front element size, L_e . To determine an appropriate L_e value, a sensitivity analysis [79] is implemented on the 6×90×1300 mm center-cracked steel

plate. SIF values in the variation of a/L_e ratio ranging from 20 to 100 for two normalized crack lengths, i.e. $2a/W_s = 0.1$ and 0.9 are computed using ABAQUS, K_{FE} . These computed results are then compared with referenced handbook solutions [12], K_{Ref} . The sensitivity analysis results show that the ratio of K_{FE}/K_{Ref} for two crack length levels approached unity as a/L_e approached 100, as detailed in Fig. 4.3. Therefore, $a/L_e = 100$ is chosen for this study. The number of the wedge-shaped strips is computed with $R_e = a/10$ and $a/L_e = 100$ would be equal to 10. Each strip is divided into 48 equally sized elements spanning the angular distance from 0 to π . The global size of the steel plate, patch, and adhesive elements are 1.5, 1, and 1 mm, respectively.

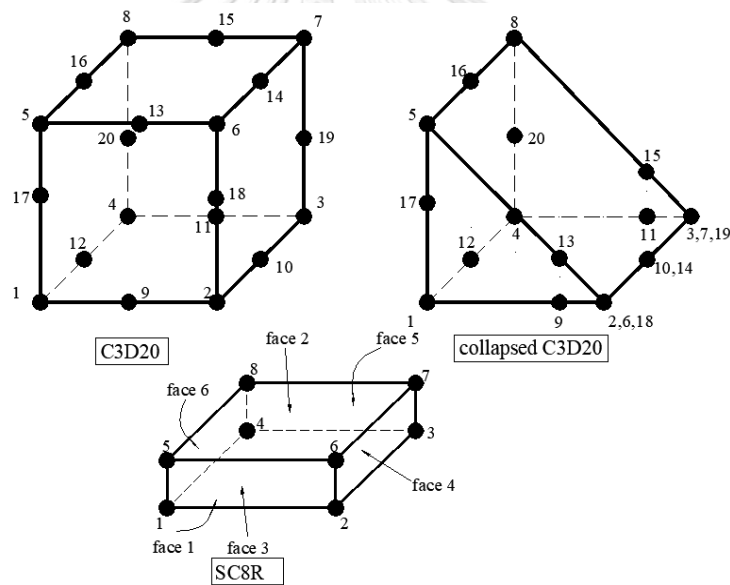


Fig. 4.1. Three element types used [9].

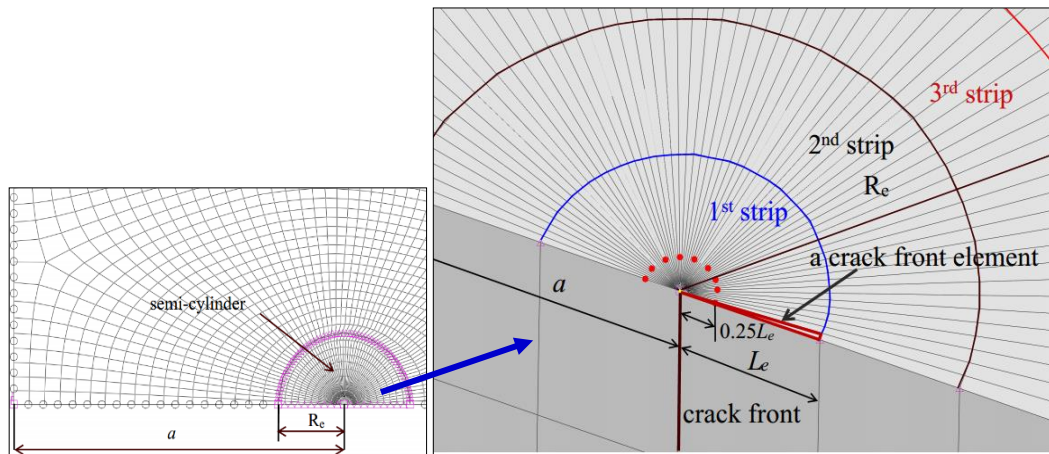


Fig. 4.2. FE meshes near the crack front.

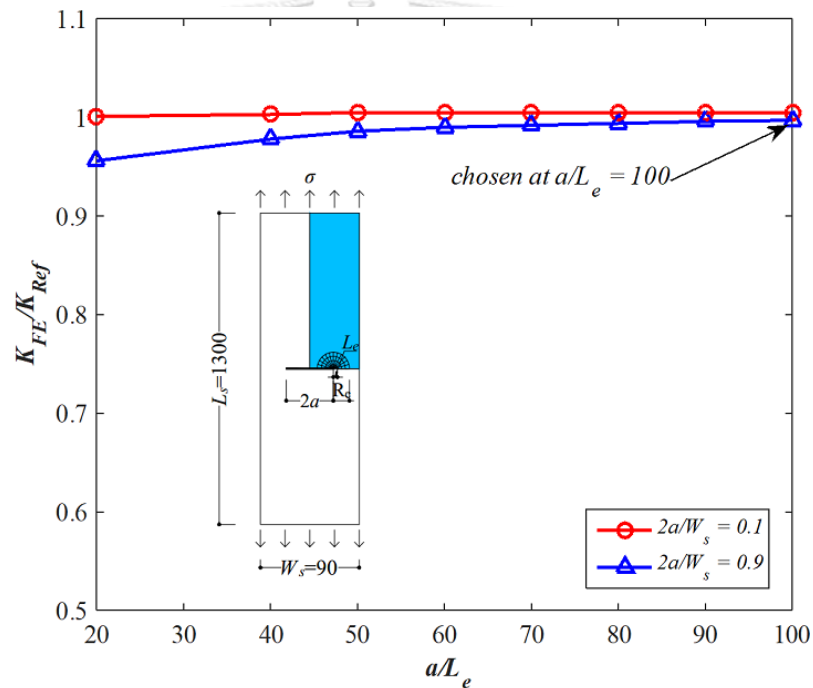


Fig. 4.3. Sensitive analysis results.

4.2. Materials, geometries, and constraints

Table 4.1 shows material and geometrical properties of steel plates, FRP patches, and adhesive layers used in all ABAQUS models. Four different steel plates are used for two different purposes. Plate 1=6×90×1300 mm and Plate 2=16×180×2600 mm are employed to create a so-called F_2 database to be used to obtain the closed-form SIF solution by symbolic regression via GP analyses, see section 5.1. Meanwhile, Plate

3=10×100×1500 mm and Plate 4=12×150×2200 mm are used to obtain independent results for verification of the developed SIF solutions. The modulus of elasticity, Poisson's ratio, and fatigue threshold SIF range for steel material are 200 GPa, 0.3, and 6.6 MPa.m^{1/2} (taken at stress ratio = 0.13) [80], respectively. Three types of unidirectional FRP and adhesive materials are chosen from the literature [30, 58, 81, 82]. The mechanical behavior of steel and adhesive materials is isotropic and linearly elastic. FRP material is assumed to be linear orthotropic under plane stress condition.

Table 4.1 Material and geometrical properties of steel plates, FRP patches, and adhesive layers.

Material	Material		Geometry			
	E_s, E_p , or E_a (MPa)	E_{2p} (MPa)	ν	t_s, t_p , or t_a (mm)	W_s or W_p (mm)	L_s or L_p (mm)
Steel [30]						
Plate 1	200×10 ³		0.30	6	90	1300
Plate 2	200×10 ³		0.30	16	180	2600
Plate 3	200×10 ³		0.30	10	100	1500
Plate 4	200×10 ³		0.30	12	150	2200
Patch [81, 82]						
Type 1	210×10 ³	8×10 ³	0.30	1.2	varied	varied
Type 2	300×10 ³	12×10 ³	0.30	1.4	varied	varied
Type 3	460×10 ³	12×10 ³	0.36	2.0	varied	varied
Adhesive						
[58]						
FM-73	959		0.35	1.0	varied	varied
FM36	1815		0.35	1.0	varied	varied
FM400	2944		0.36	1.0	varied	varied

here E_s = elastic modulus of steel; E_p = longitudinal modulus of the patch; E_{2p} = transverse in-plane modulus of the patch; E_a = elastic modulus of adhesive;

W_p and L_p = width and length of the patch, respectively; t_s , t_p , and t_a = thickness of the steel plate, patch, and adhesive layer, respectively; ν = Poisson's ratio.

Debonding phenomenon that may occur in the adhesive layer, at the steel-adhesive interface, or adhesive-patch interface [15] will be assessed after the optimum patch design has been accomplished (see section 7.3).

Fig. 4.4 shows a quarter section of the model of a center-cracked steel plate repaired with adhesive-bonded double-sided FRP patches. Displacement symmetric constraints, i.e., Xsym and Ysym are applied on corresponding symmetric planes. To enforce the geometric compatibility conditions along steel-adhesive and adhesive-patch interfaces, tie constraints, with a command *TIE, NAME = CONSTRAINT NAME "Enter key" SLAVE SURFACE NAME, MASTER SURFACE NAME, are used. A master surface and a slave surface must be designated for the definition of each tie constraint, as shown in Fig. 4.5.

Finally, SIF values at crack tips of FRP-patched cracked plates are computed in ABAQUS/CAE based on the methodology of the interaction integral method [66], detailed in section 3.2. A command used in ABAQUS for computing SIF is *CONTOUR INTEGRAL, CONTOURS = n, TYPE = K FACTORS, where n = number of contours.

A matrix of 864 rows for all FE models is constructed for two steel plate configurations, three levels of crack length, three patch types, four levels of patch width, four levels of patch length, and three levels of the adhesive modulus. Material and geometrical properties for each FE model are taken from each row of this matrix. Once the SIF database has been created, the so-called correction factor F_2 can be obtained by normalizing SIF values with applied tensile stress, crack length, and the finite-width correction factor.

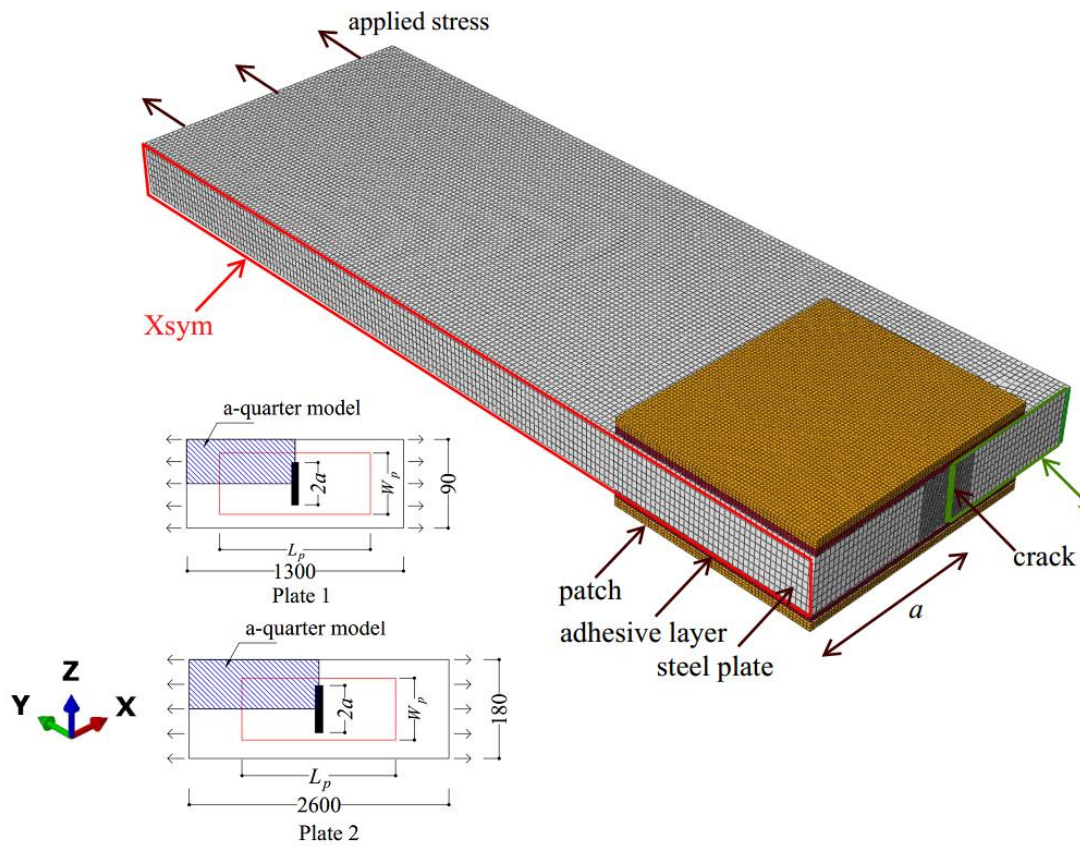


Fig. 4.4. A-quarter finite element model in ABAQUS.

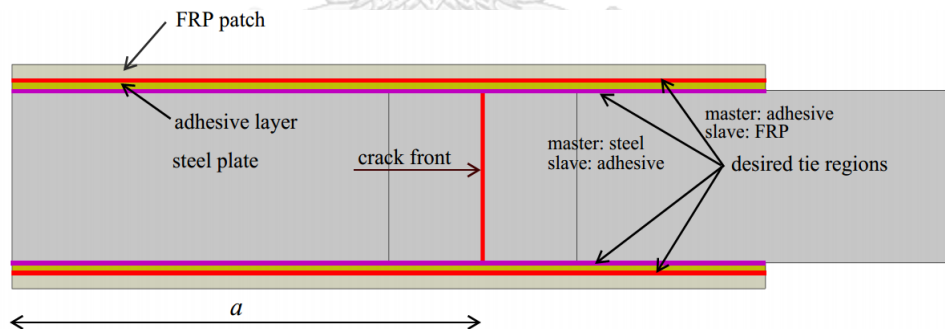


Fig. 4.5. Tie constraint regions in the finite element model.

4.3. Validation of FE models

An accuracy of FE models to represent both unrepaired and repaired plates is validated against published results from Tada *et al.* [12] (unrepaired), Ayatollahi and Hashemi [13] (single-sided patch), and Kumar and Hakeem [11] (double-sided patch). The validation consists of two steps. First, the calculated SIF for two cracked steel plates (Plates 1 and 2) without bonded FRP patches are compared with the handbook

solutions [12]. Secondly, the validation is then performed on cracked aluminum plates repaired with different configurations of single-sided composite patches, in Ayatollahi and Hashemi [13] and double-sided composite patches, in Kumar and Hakeem [11]. In a comparison, the materials, geometries, and loadings used in FE models are the same as those described in the related original studies [11, 13].

Figs. 4.6, 4.7, and 4.8 show that SIF values obtained from ABAQUS for both unrepaired and patch-repaired cases are in very good agreement with published results. In Fig. 4.6, the average difference between the FE results and the handbook solutions [12] with for unrepaired plates is 0.3%, demonstrating a suitability of element sizes used for the steel plate, especially near the crack front region. Fig. 4.7 shows that the numerical models also can accurately capture the singular stress field in the vicinity of the crack front for cracked aluminum plates with single-sided patches. The average difference between the FE results and Ayatollahi and Hashemi solutions [13] is 1.64%. For cracked aluminum plates with double-side patches as in Kumar and Hakeem [11], the mean difference is 1.9%, as illustrated in Figs. 4.8(a)-(c). Obviously, the FE models predict the effects of patch material [Fig. 4.7] and patch geometry [Figs. 4.8(a)-(c)] on the fluctuation of SIF values which are identical to ones observed in the original papers [11, 13]. Databases represented by Figs. 4.6-4.8 are given in **APPENDIX B**.

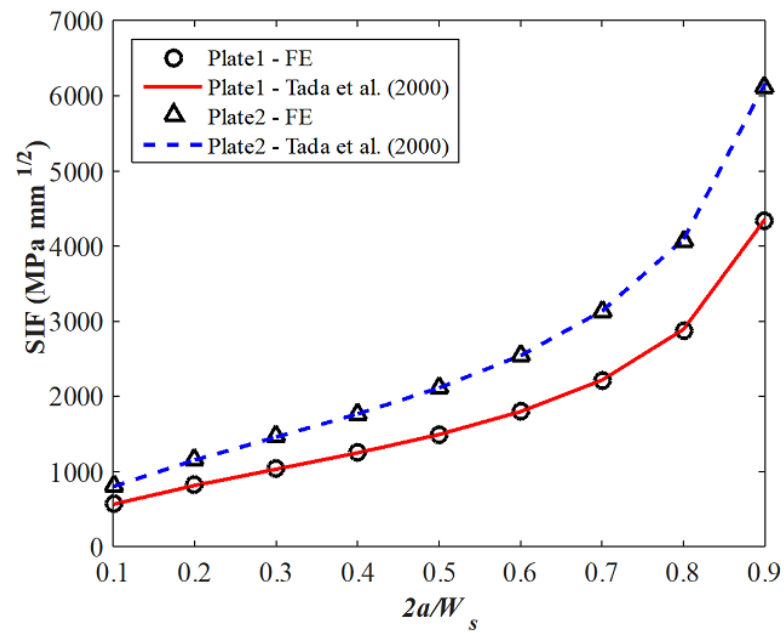


Fig. 4.6. Comparison of FE results with referenced solutions [12] (unrepaired).

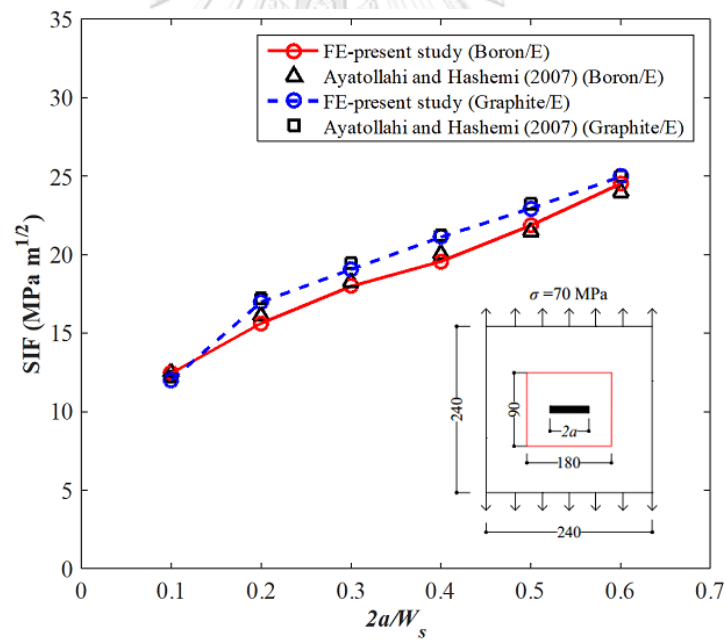
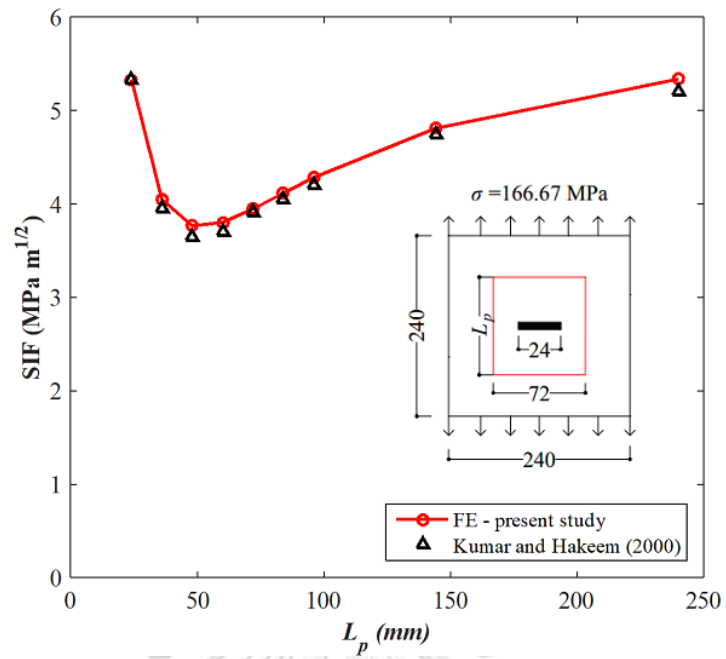
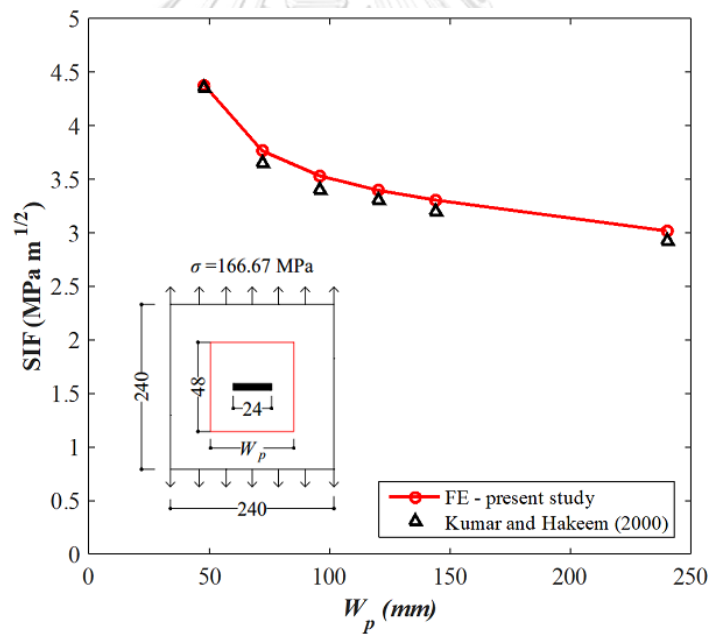


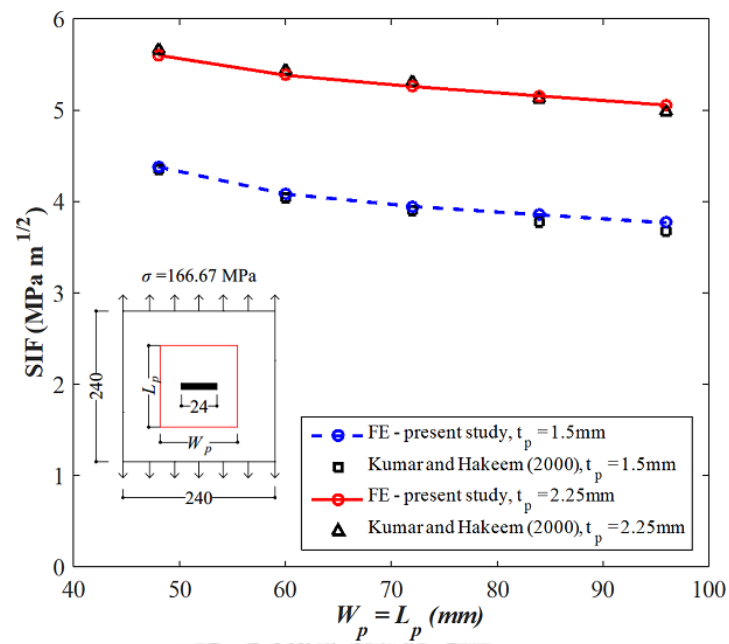
Fig. 4.7. Comparison of FE results with published solutions [13] (single-sided patch).



(a) rectangular patch with variation in patch length



(b) rectangular patch with variation in patch width



(c) square patch with variations in patch length and patch thickness

Fig. 4.8. Comparison of FE results with previously published results [11] (double-sided patch).

CHAPTER 5

STRESS INTENSITY FACTOR SOLUTIONS FOR PATCH-REPAIRED CENTER-CRACKED PLATES

This chapter introduces a new correction factor to SIF solution for FRP-patched cracked plates to take into account the positive effect of FRP patch on the SIF reduction. The solution is then tested for its capability to predict SIF of FRP-patched cracked steel plates under tension.

5.1. Stress intensity factor solutions

SIF solutions for finite-width center-cracked plates subjected to a remote tensile stress can be found in Tada *et al.* [12]. The solutions are expressed as

$$K = F_1 \sigma (\pi a)^{1/2} \quad (5.1)$$

where

$$F_1 = \left[1 - 0.025(2a/W_s)^2 + 0.06(2a/W_s)^4 \right] \sqrt{\sec(\pi a/W_s)} \quad (5.2)$$

and K = stress intensity factor; F_1 = correction factor for finite-width of steel plates given in Eq. (5.2); a = one-half of the crack length; W_s = width of steel plates; and σ = remote tensile stress.

In the case of FRP-patched cracked plates, a new correction factor F_2 , namely patching correction factor that takes into account the positive effects of material and geometrical properties of the patch and adhesive layer on SIF reduction is proposed. Therefore, Eq. (5.1) becomes

$$K = F_1(x_1) F_2(x_1, x_2, x_3, x_4) \sigma (\pi a)^{1/2} \quad (5.3)$$

where

$$x_1 = \frac{2a}{W_s}; \quad x_2 = \frac{W_p}{W_s}; \quad x_3 = \frac{L_p}{2a}; \quad x_4 = \frac{2(E_p t_p + E_a t_a)}{E_s t_s} \quad (5.4)$$

A process for determining F_2 function expressed will be described in the subsequent sections of this chapter.

5.2. Symbolic regression via genetic programming in HeuristicLab

In HeuristicLab [10], the F_2 database is randomly shuffled into four groups for GP analyses, i.e. 1, 2, 3, and 4 to avoid the bias of GP performance on a certain group. Each group has four subgroups, i.e. A, B, C, D and each subgroup contains 216 data points (25% database). In Table 5.1, each subgroup is sequentially used as a test set (25% database) and the remaining three groups are training set (75% database). This is consistent with the principle of separating a database in the data mining where most of the database will be assigned as the training set and a smaller portion of the database will be the test set. The training set creates an approximate model while the test set measures the generalization ability of that model [83]. In this research, four different functions of F_2 corresponding to the four groups are achieved and the best one with the largest R^2 value is selected.

The function and terminal sets for the GP analyses in this research are $F = \{+, -, *, \text{exponential, square, power}\}$ and $T = \{x_1, x_2, x_3, x_4, [-10,10]\}$. Here, the independent variable atoms are x_1, x_2, x_3 , and x_4 given in Eq. (5.4) while the constant atoms are initially generated in the interval $[-10,10]$. Additional control parameters defined at the beginning of each GP analysis are given in Table 5.2. The termination for all GP analyses is at 2000 generations of the algorithm. All GP analyses are performed on Intel ® Core™ i7-7700HQ CPU @ 2.80-2.81Ghz.

Fig. 5.1 shows the variation of Pearson's R^2 during four GP analyses. Table 5.3 provides the training R^2 values at several generations of these GP analyses. It is seen that Pearson's R^2 is improved or remained constant after each GP generation. After 2000 generations, the training R^2 values corresponding to the four groups are 0.902, 0.901, 0.899, and 0.906, respectively. Fig. 5.2 shows the scatter diagram of F_2 at the

2000th generation in the case of $R^2 = 0.906$ (Group 4) is plotted that demonstrates a high correlation between ABAQUS and GP results.

Table 5.1 Groups and subgroups used for GP analyses.

GP group	analysis	Training set		Testing set	
		Subgroup	Number of data points	Subgroup	Number of data points
1		A, B, C	648	D	216
2		A, B, D	648	C	216
3		A, C, D	648	B	216
4		B, C, D	648	A	216

Table 5.2 Control parameters used for GP analyses (HeuristicLab).

Parameter	Value
Number of tree structures	10 000
Probability of mutation	25%
Elite count (reproduction option)	2
Maximum number of tree depth	10
Maximum number of tree length	30

Table 5.3 Person's R^2 values at several generations from GP analyses.

Generation	Group 1	Group 2	Group 3	Group 4
	Training R^2	Training R^2	Training R^2	Training R^2
0	0.769	0.757	0.789	0.766
250	0.902	0.888	0.897	0.899
500	0.902	0.893	0.898	0.903
750	0.902	0.898	0.898	0.905
1000	0.902	0.900	0.898	0.905
1250	0.902	0.901	0.898	0.905
1500	0.902	0.901	0.898	0.905
1750	0.902	0.901	0.898	0.906
2000	0.902	0.901	0.899	0.906

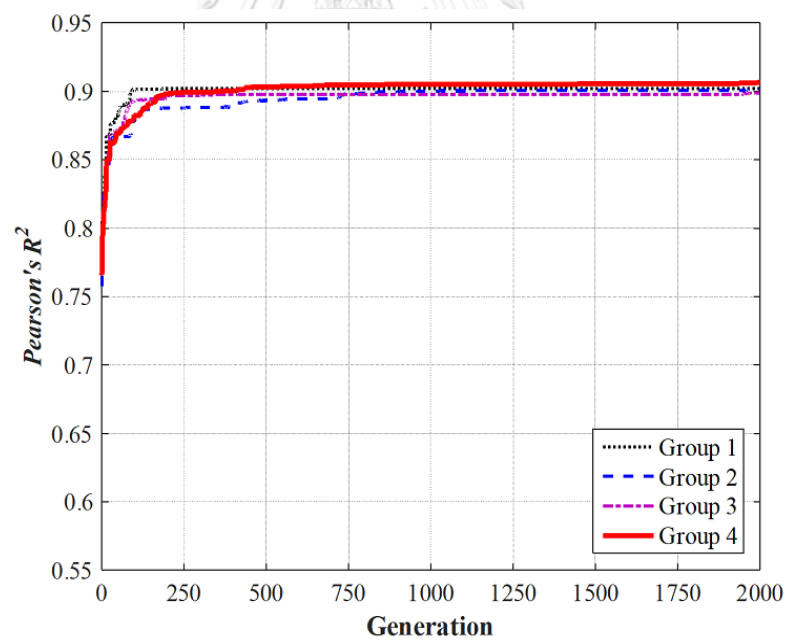


Fig. 5.1. Pearson's R^2 versus generation for four GP analyses.

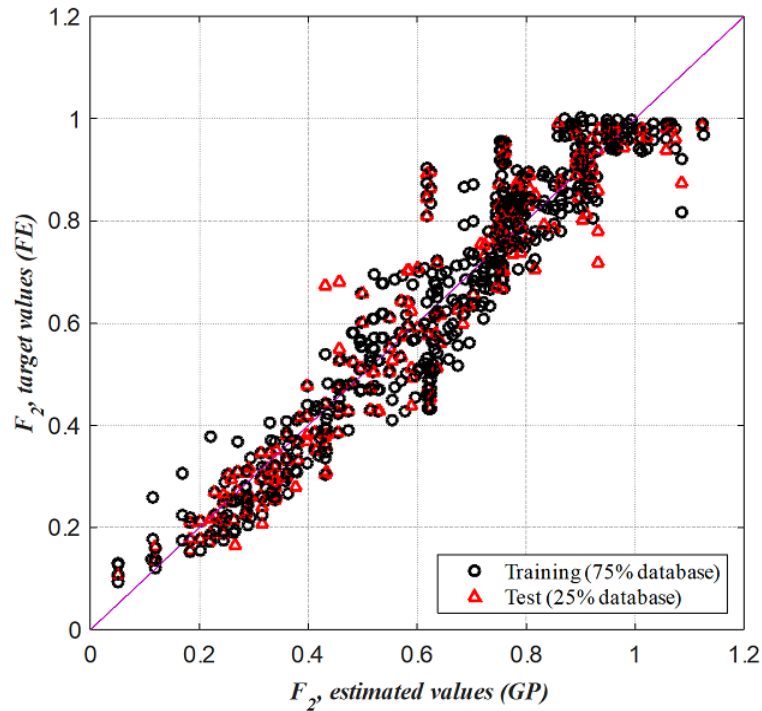


Fig. 5.2. Scatter plot of F_2 at 2000th generation with $R^2 = 0.906$ (Group 4).

5.3. Correction factor F_2 function

Fig. 5.3 shows the GP tree structure corresponding to $R^2 = 0.906$ selected to represent the correction factor F_2 in Eq. (5.3).

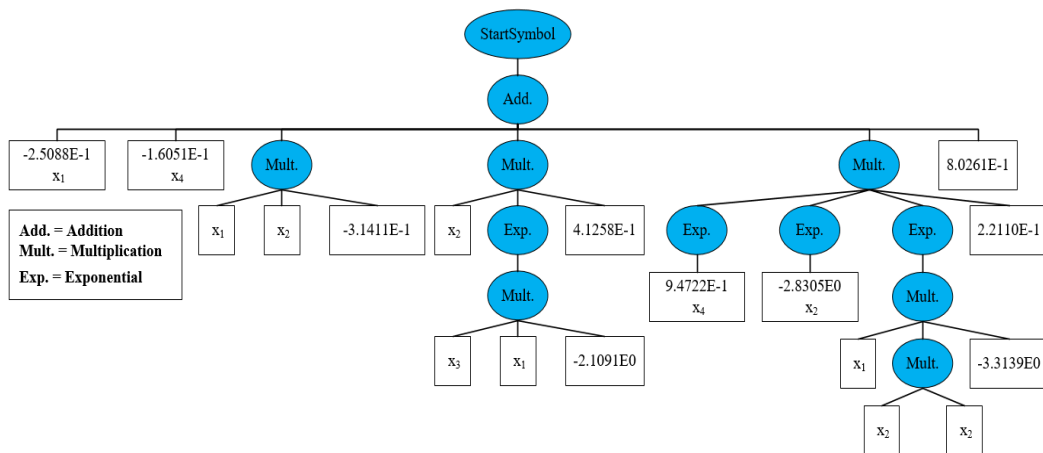


Fig. 5.3. GP tree structure from the GP analysis for Group 4.

The mathematical function corresponding to the above GP tree structure is written as

$$F_2 = c_0x_1 + c_1x_4 + c_2x_1x_2 + c_3x_2e^{c_4x_1x_3} + c_5e^{c_6x_2}e^{c_7x_4}e^{c_8x_1x_2^2} + c_9 \quad (5.5)$$

where

c_0, c_1, \dots, c_9 = constant coefficients given in Table 5.4.

Table 5.4 Constant coefficients of F_2 function.

c_0	c_1	c_2	c_3	c_4
-0.25088	-0.16051	-0.31411	0.42158	-2.10910
c_5	c_6	c_7	c_8	c_9
0.22110	-2.83052	0.94722	-3.31392	0.80261

Substituting F_2 in Eq. (5.5) into Eq. (5.3), a closed-form empirical SIF solution is obtained. The application range of Eq. (5.5) is shown in Table 5.5.

Table 5.5 Application range of closed-form SIF solution.

	Unit	Min	Max
Steel plate			
E_s	GPa	200	200
W_s	mm	90	180
t_s	mm	6	16
$2a / W_s$		0.1	0.9
FRP patch			
E_p	GPa	210	460
W_p / W_s		0.2	1.0
$L_p / 2a$		1	16
t_p	mm	1.2	2.0
Adhesive layer			
E_a	MPa	959	2944
t_a	mm	1	1

5.4. Verification of proposed SIF solution

First, the accuracy of proposed SIF solution is compared with the one from FE analysis. In Table 5.6, Plate 3 (10×100×1500 mm) and Plate 4 (12×150×2200 mm) with four combinations of crack length and material and geometrical properties of FRP patch and adhesive layer are used to verify the proposed F_2 solution given in Eq. (5.5) for FRP-patched cracked plates. The correction factor F_2 values are computed using Eq. (5.5) and ABAQUS. Figs. 5.4(a)-(d) show that the correction factor F_2 values from Eq. (5.5) and ABAQUS are in a good agreement. For Plate 3, the average differences between both methods for case 1, case 2, case 3, and case 4 respectively are 3%, 5%, 3%, and 5%, while they are 2%, 4%, 2%, 7% for Plate 4. As shown in Fig. 5.4(d), the difference became bigger when the patch width does not cover the crack entirely. Effects of design parameters on the fluctuation of SIF from both methods are identical. Databases represented by Figs. 5.4(a)-(d) are given in four tables in **APPENDIX C**.

Table 5.6 Cases for verification of SIF solution.

Verification cases	Plate 3	Plate 4
Case 1	$2a = 0.1W_s - 0.9W_s$	$2a = 0.1W_s - 0.9W_s$
Effect of a	$[W_p L_p t_p t_a] = [100 \ 400 \ 1.2 \ 1] \text{ (mm)}$ $[E_p E_a] = [210 \times 10^3 \ 959] \text{ (MPa)}$	$[W_p L_p t_p t_a] = [150 \ 250 \ 1.4 \ 1] \text{ (mm)}$ $[E_p E_a] = [300 \times 10^3 \ 1815] \text{ (MPa)}$
Case 2	$2a = 0.5W_s$	$2a = 0.5W_s$
Effect of L_p	$L_p = 2a - 16 \times 2a$ $[W_p t_p t_a] = [100 \ 1.2 \ 1] \text{ (mm)}$ $[E_p E_a] = [210 \times 10^3 \ 959] \text{ (MPa)}$	$L_p = 2a - 16 \times 2a$ $[W_p t_p t_a] = [150 \ 1.4 \ 1] \text{ (mm)}$ $[E_p E_a] = [300 \times 10^3 \ 1815] \text{ (MPa)}$
Case 3	$2a = 0.5W_s$	$2a = 0.5W_s$
Effect of W_p	$W_p = 0.2W_s - W_s$ $[L_p t_p t_a] = [400 \ 1.2 \ 1] \text{ (mm)}$ $[E_p E_a] = [210 \times 10^3 \ 959] \text{ (MPa)}$	$W_p = 0.2W_s - W_s$ $[L_p t_p t_a] = [250 \ 1.4 \ 1] \text{ (mm)}$ $[E_p E_a] = [300 \times 10^3 \ 1815] \text{ (MPa)}$
Case 4	$2a = 0.9W_s$	$2a = 0.9W_s$
Effect of W_p	$W_p = 0.2W_s - W_s$ $[L_p t_p t_a] = [400 \ 1.2 \ 1] \text{ (mm)}$ $[E_p E_a] = [210 \times 10^3 \ 959] \text{ (MPa)}$	$W_p = 0.2W_s - W_s$ $[L_p t_p t_a] = [250 \ 1.4 \ 1] \text{ (mm)}$ $[E_p E_a] = [300 \times 10^3 \ 1815] \text{ (MPa)}$

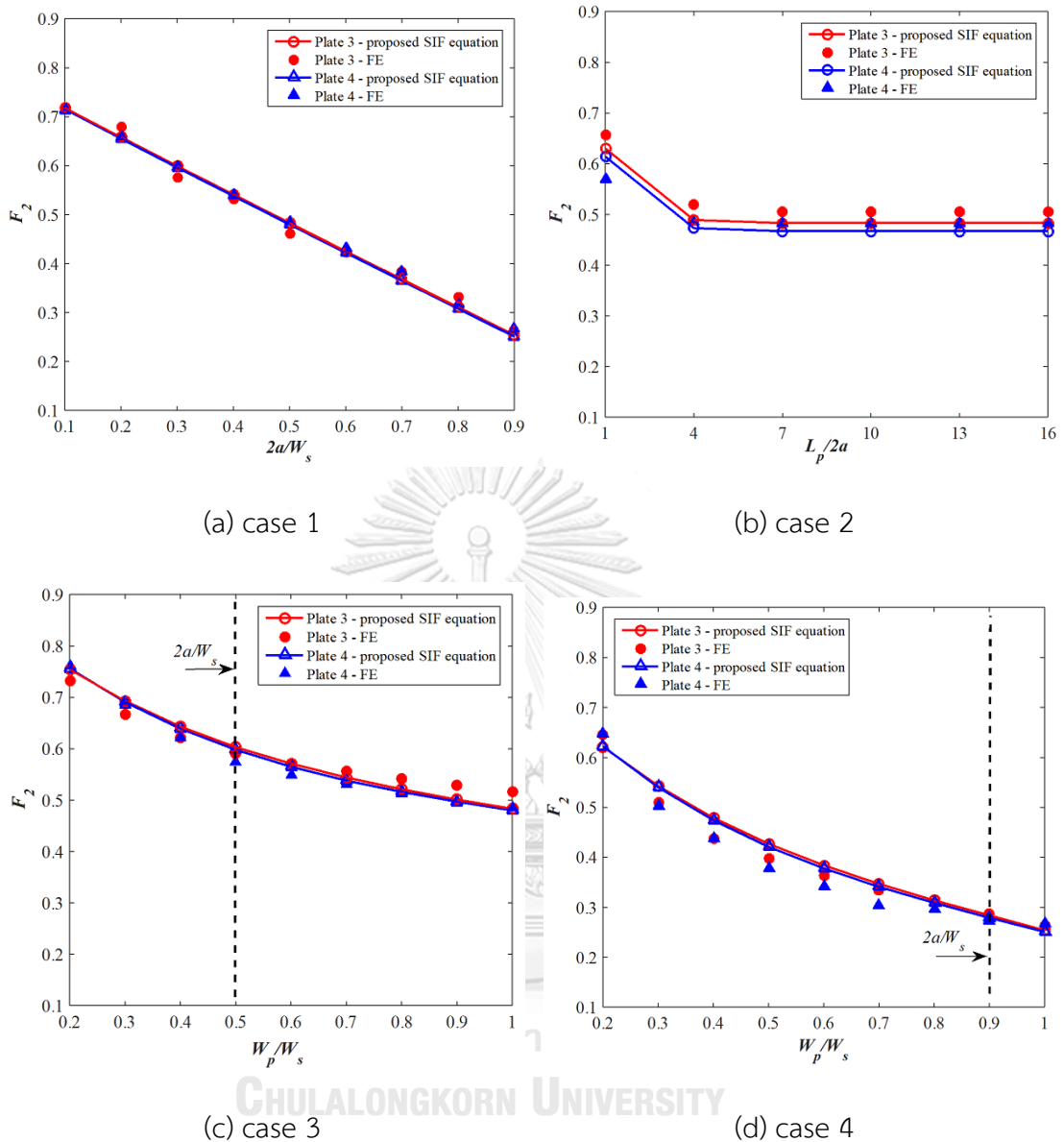


Fig. 5.4. Comparison of F_2 results from proposed solution and ABAQUS.

Second, the accuracy of the proposed SIF solution is compared with a result of a fatigue test in Wang *et al.* [34]. The configuration of a repaired specimen with a central crack is shown in Fig. 5.2. The specimen having $E_s = 200$ GPa is subjected to a constant amplitude loading with $\sigma_{\min} = 30$ MPa and $\sigma_{\max} = 150$ MPa and repaired with a double-sided FRP patch having $E_p = 165$ GPa, $W_p = 100$ mm, $L_p = 500$ mm, and $t_p = 1.4$ mm. The crack grows from its initial length, $2a_0 = 19$ mm, to a critical one, $2a_c = 108.6$ mm [34]. Fatigue life of the repaired specimen is calculated using the proposed SIF solution in Eq. (5.3) and compared with the fatigue test result. To

calculate the fatigue life of the repaired specimen, Paris' law in Eq. (5.6) [84] is employed. Fatigue life of the specimen is predicted by the integration given in Eq. (5.7).

$$da / dN = C (\Delta K)^m \quad (5.6)$$

$$N = \frac{1}{C} \int_{a_0}^{a_c} \frac{da}{(\Delta K)^m} \quad (5.7)$$

where Paris law constants are $C = 2.427 \times 10^{-12}$ (MPa, m units) and $m = 3.3$ [85].

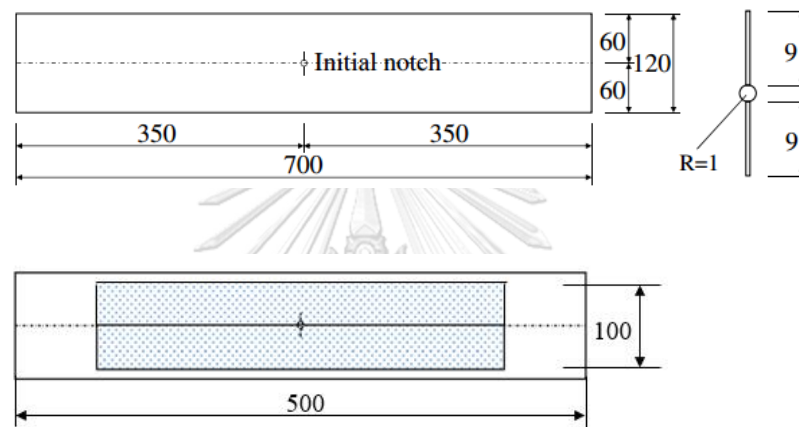


Fig. 5.5. Geometry and configuration of repaired specimen [34].

Table 5.7 shows the calculation of the fatigue crack life of the repaired specimen. In Fig. 5.6, the total number of cycles required to propagate the crack from 19 mm to 108.6 mm is 735,412, 9% larger than the experimental test result with 672,200 cycles. The fatigue life prediction becomes less accurate as the crack length is larger.

Table 5.7 Fatigue crack growth calculation.

a_0 mm	a_c mm	ΔK MPa m ^{1/2}	ΔN cycles	N cycles
9.5	11.0	14.78	77,391.8	77,391.8
11.0	12.5	15.67	64,745.1	142,136.9
12.5	14.0	16.47	55,571.6	197,708.5
14.0	15.5	17.19	48,646.7	246,355.2
15.5	17.0	17.85	43,248.8	289,604.0

a_0 mm	a_c mm	ΔK MPa m ^{1/2}	ΔN cycles	N cycles
17.0	18.5	18.46	38,927.9	328,531.9
18.5	20.0	19.03	35,389.8	363,921.7
20.0	21.5	19.56	32,434.7	396,356.4
21.5	23.0	20.07	29,922.3	426,278.7
23.0	24.5	20.54	27,751.5	454,030.2
24.5	26.0	21.00	25,847.4	479,877.6
26.0	27.5	21.45	24,153.2	504,030.7
27.5	29.0	21.88	22,625.1	526,655.8
29.0	30.5	22.31	21,228.7	547,884.6
30.5	32.0	22.75	19,936.3	567,820.9
32.0	33.5	23.18	18,725.4	586,546.3
33.5	35.0	23.63	17,577.2	604,123.5
35.0	36.5	24.09	16,476.0	620,599.5
36.5	38.0	24.57	15,408.5	636,008.0
38.0	39.5	25.08	14,362.9	650,370.9
39.5	41.0	25.64	13,329.3	663,700.2
41.0	42.5	26.25	12,298.9	675,999.1
42.5	44.0	26.92	11,264.0	687,263.1
44.0	45.5	27.68	10,218.1	697,481.2
45.5	47.0	28.56	9,156.1	706,637.4
47.0	48.5	29.58	8,074.3	714,711.7
48.5	50.0	30.81	6,971.2	721,682.9
50.0	51.5	32.33	5,847.9	727,530.8
51.5	53.0	34.27	4,710.0	732,240.8
53.0	54.3	36.84	3,170.9	735,411.6

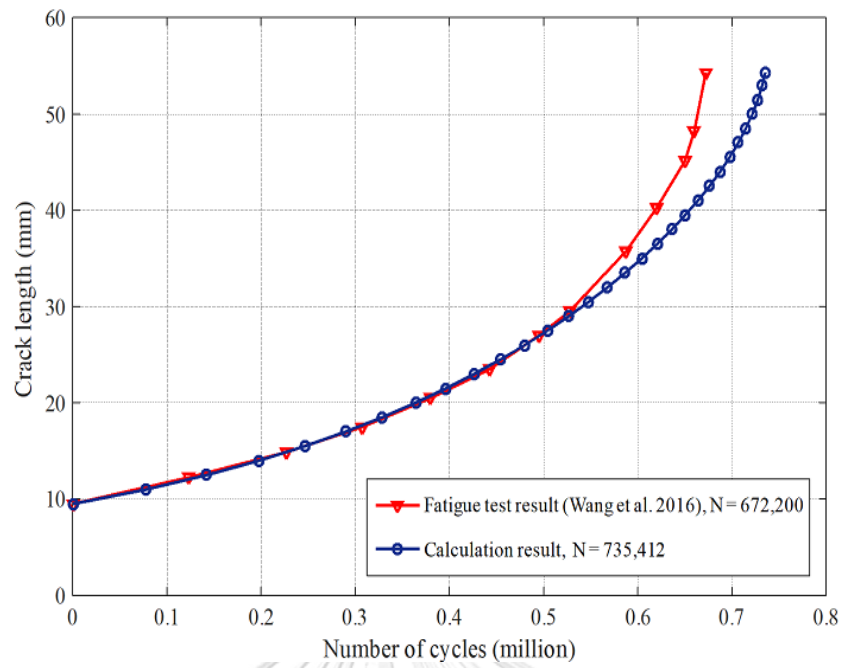


Fig. 5.6. Crack propagation curves of the specimen.

CHAPTER 6

PATCH VOLUME OPTIMIZATION

This chapter formulates the optimization statement. Two optimization solvers in MATLAB are presented. A comparison of an optimum patch design with a previous work result is also introduced.

6.1. Optimization problem statement

When the crack length, FRP and adhesive material properties, and the adhesive thickness are specific, the correction factor F_2 in Eq. (5.5) and SIF formulation in Eq. (5.3) become functions of FRP patch geometries. The SIF solution in Eq. (5.3) can be rewritten as

$$K(\mathbf{X}) = F_1 \left(\frac{a}{W_s} \right) F_2 \left(\frac{a}{W_s}, X_1, X_2, X_3 \right) \sigma(\pi a)^{1/2} \quad (6.1)$$

where

$$X_1 = W_s x_2 = W_p; \quad X_2 = 2ax_3 = L_p; \quad X_3 = (E_s t_s x_4 - 2E_a t_a) / (2E_p) = t_p \quad (6.2)$$

and x_2, x_3, x_4 = given in Eq. (5.4); F_1 = given in Eq. (5.2); F_2 = given in Eq. (5.5).

The optimization statement is developed and analyzed in the context of patch volume optimization as follows

Minimize $V_p(\mathbf{X})$, subject to

$$\mathbf{X}_L \leq \mathbf{X} \leq \mathbf{X}_U \quad (6.3)$$

$$\Delta K(\mathbf{X}) \leq \Delta K_{th} \quad (6.4)$$

where

$$\mathbf{X} = [X_1 \ X_2 \ X_3]^T = [W_p \ L_p \ t_p]^T \quad (6.5)$$

$$V_p(\mathbf{X}) = X_1 X_2 X_3 \quad (6.6)$$

and $\mathbf{K}(\mathbf{X}) =$ given in Eq. (6.1); \mathbf{X}_L and $\mathbf{X}_U =$ lower and upper bound of design parameters, respectively.

$$\mathbf{X}_L (mm) = [0.2W_s \ 2a \ 1.2]^T \quad (6.7)$$

$$\mathbf{X}_U (mm) = [W_s \ 16 \times 2a \ 2]^T \quad (6.8)$$

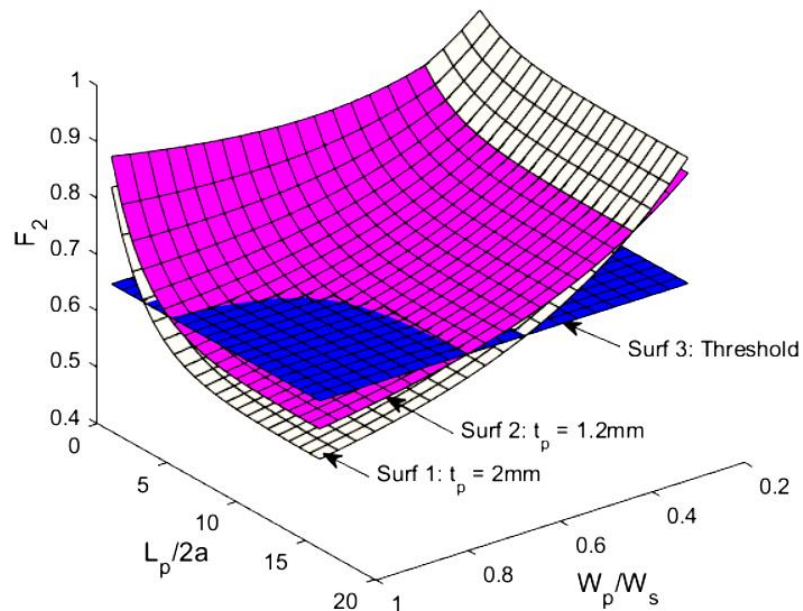
$\Delta K_{th} = 6.6 \text{ MPa.m}^{1/2} =$ threshold SIF range of the steel material (ASTM A572 - Grade 60) [80].

Fig. 6.1(a) shows three surfaces of F_2 values corresponding to $t_p = 2$ mm, Surf 1, $t_p = 1.2$ mm, Surf 2, and SIF = threshold, Surf 3, for the visualization of the inequality constraint given in Eq. (6.4). As shown in Figs. 6.1(b) and (c), the under-threshold area (blued area) of Surf 1 is larger than the one of Surf 2 as the SIF reduction is greater if the thicker FRP patch is used. The thicker the FRP patch layer is, the larger the solution space is. When the FRP patch thickness increases from 1.2 mm to 2 mm, the solution space expands from the smallest value [Fig. 6.1(b)] to the largest one [Fig. 6.1(c)]. When the crack length is too long or the remote tensile stress is too large, Surf 3 may lie completely under Surf 1 and Surf 2 and no feasible solution can be found. Changing material properties, increasing the number of FRP patch layers, reducing the thickness of the adhesive layer, or loosening the constraint in Eq. (6.4) can be selected.

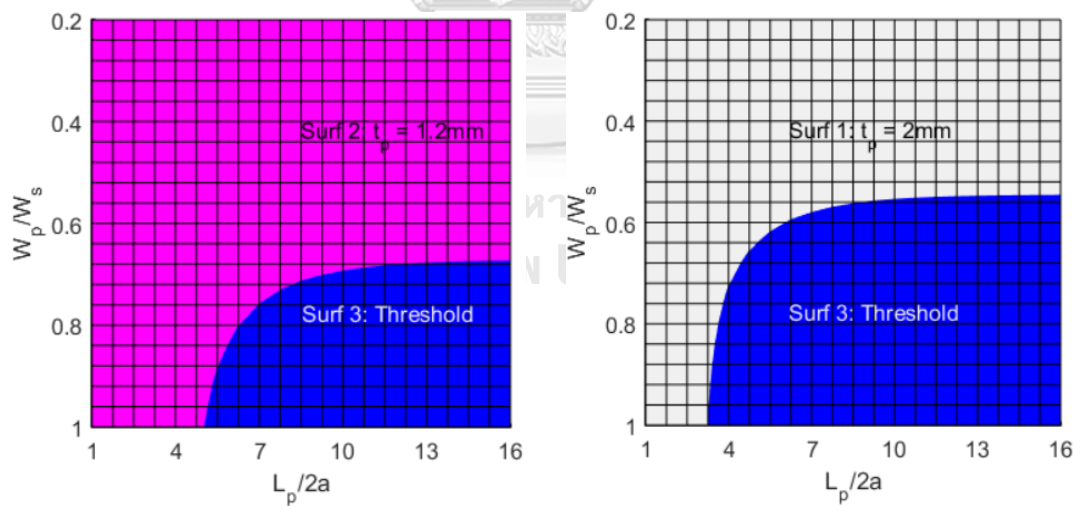
6.2. MATLAB optimization solver input and default values

Using MATLAB r2018a [76], the GA (command `ga`) and nonlinear programming, (command `fmincon`) are employed to solve the minimization of FRP patch volume. For a comparison, the input is identical for both solvers as follows: initial point = upper bound, function tolerance = 10^{-20} , constraint tolerance = 10^{-15} , and maximum number of generations (iterations) = 100. Both solvers used the method of Lagrange multipliers, presented in section 3.5, to deal with the inequality-constrained

optimization problem in this study. Two MATLAB functions of both solvers are given in APPENDIX E.



(a) F_2 surfaces in the cases of $t_p = 1.2$ mm, $t_p = 2$ mm, and SIF = threshold



(b) top view, $t_p = 1.2$ mm

(c) top view, $t_p = 2$ mm

Fig. 6.1. Visualization of the inequality constraint.

6.3. A comparison of an optimum patch design with a previous work solution

A comparison between an optimum patch design for a cracked steel plate and the one from a fatigue test [86, 87] is performed. The optimum patch volume is then compared with the patch volume used in the test. The width, length, and thickness of the cracked plate are $W_s = 100$ mm, $L_s = 700$ mm, and $t_s = 10$ mm. In the fatigue test, the plate having $E_s = 210$ GPa is repaired with a double-sided FRP patch with $E_p = 320$ GPa, $W_p = 100$ mm, $L_p = 300$ mm, $t_p = 1.4$ mm, and $V_p = 42,000$ mm³ and tested under a constant amplitude loading with $\sigma_{\min} = 60$ MPa and $\sigma_{\max} = 150$ MPa. The adhesive used is Araldite 2015 with $E_p = 2430$ MPa and $t_p = 1$ mm.

In the fatigue test, a crack needs over three million load cycles to grow from an initial value, $2a_0 = 6$ mm, to a critical value. Thus, a runout can be assumed to occur. The optimum patch design is determined by solving the optimization problem in section 6.1 for the FRP-patched cracked steel plate in the fatigue test. The fatigue threshold SIF range is assumed to equal to 6.1 MPa.m^{1/2} (lower bound) [88] in the case of $\sigma_{\min} / \sigma_{\max} = 0.4$.

Fig. 6.2 shows the convergence history of a GA analysis for the optimum patch design. The calculated optimum patch volume is $V_p = 38,200$ mm³ ($W_p = 100$ mm, $L_p = 191$ mm, and $t_p = 2$ mm) that is 10% smaller than the one in the test, $42,000$ mm³. Furthermore, using closed-form SIF solution in Eq. (5.3), SIF ranges in the cases of using the patch geometries in the fatigue test and the optimum one are calculated. Consequently, $\Delta K = 6.28$ MPa.m^{1/2}, larger than ΔK_{th} , for the test and $\Delta K = 6.1$ MPa.m^{1/2}, equal to ΔK_{th} , for the optimum solution. The result indicates the developed optimization process is capable of providing an optimum patch design that can stop the crack propagation and is better than another one used in a fatigue test in terms of patch volume minimization.

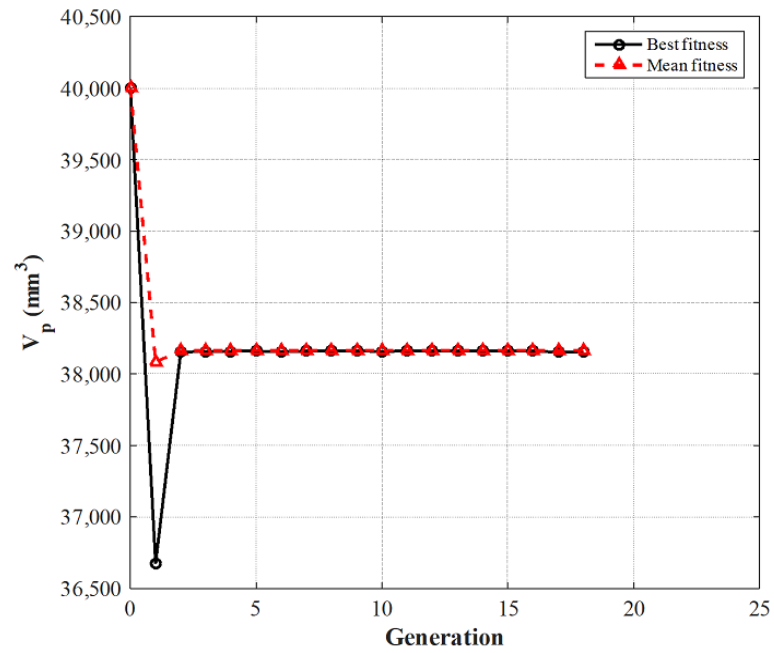


Fig. 6.2. Evolution of patch volume in GA analysis.



CHAPTER 7

DESIGN EXAMPLE

In this chapter, a design example of an FRP-patched cracked steel plate is presented to illustrate the optimization process. Basic criteria for composite patch rupture and debonding phenomenon when using the optimum patch design for the crack repair are also checked.

7.1. Problem definition

Fig. 7.1 shows the center-cracked steel plate in the example. The plate thickness is $t_s = 10$ mm. Properties of steel material are the modulus of elasticity, $E_s = 200$ GPa, Poisson's ratio, $\nu = 0.3$, and fatigue threshold SIF range, $\Delta K_{th} = 6.6 \text{ MPa}\cdot\text{m}^{1/2} = 209 \text{ MPa}\cdot\text{mm}^{1/2}$ [80]. The plate is subjected to a constant amplitude fatigue loading with $\sigma_{\max} = 55$ MPa and $\sigma_{\min} = 0$ MPa. Two crack length levels are considered, i.e. $2a = 0.2W_s$ and $0.3W_s$. For each crack length level, FRP patch and adhesive materials are specific. The adhesive layer thickness, t_a , is 1 mm.

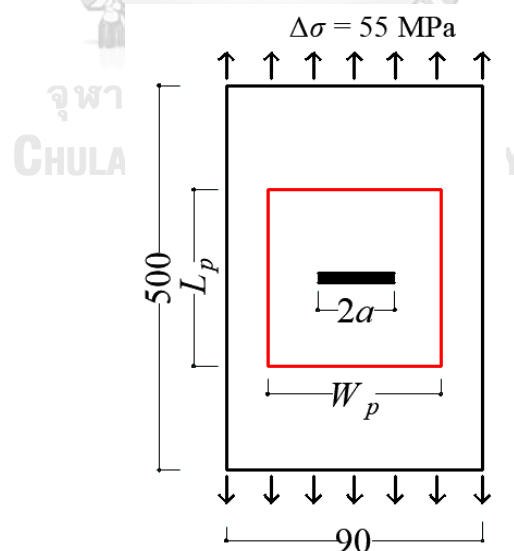


Fig. 7.1. Cracked steel plate in the design example (dimension in mm).

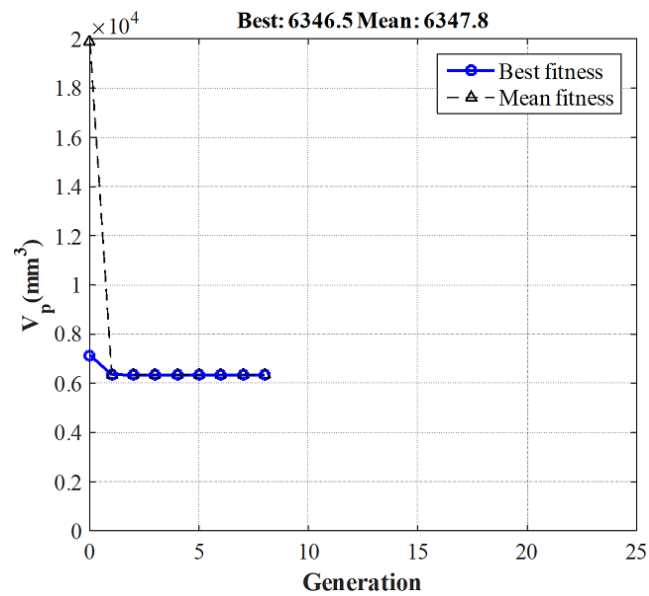
7.2. Design optimization results

A total of nine combinations of FRP patch and adhesive layer materials are investigated to consider the effects of material properties on optimum patch geometry at the specific crack length. For each combination, GA is performed twice to examine its stochastic property. Then, these GA's solutions are compared with the fmincon solution.

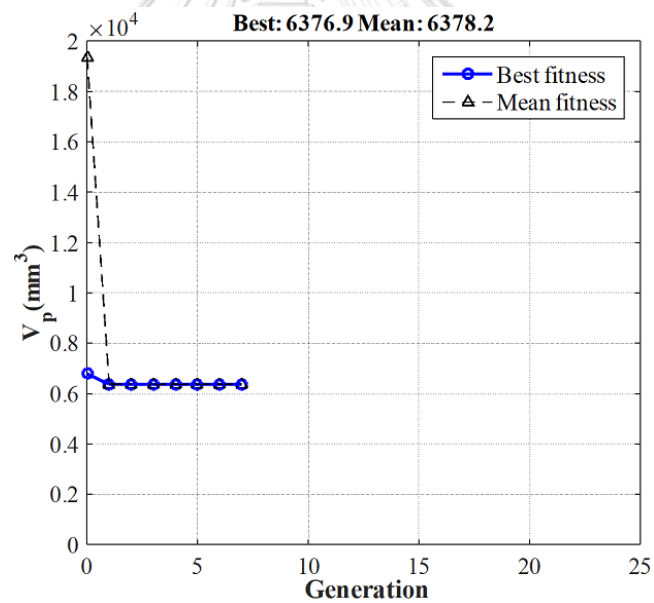
For GA solver, the fitness function is the patch volume function in Eq. (6.6). Based on lower and upper bounds of design parameters, given in Eqs. (6.7) and (6.8), a total of 500 binary strings are randomly initiated. A string represented a point in the solution space and had a particular fitness value. Therefore, there are 500 different fitness values in each GA generation. The lowest and mean values refer to the best fitness and mean fitness. For the patch volume minimization, the mean fitness is always larger than or equal to the best fitness.

Figs. 7.2(a) and (b) show the convergence histories of the 1st and 2nd GA analyses in the case of a small crack ($2a = 0.2W_s$, $E_p = 460$ MPa, and $E_a = 2944$ MPa). The best and mean fitness (patch volume) values are plotted versus GA's generation. Although the mean fitness values at the beginning of both analyses are much larger than the optimum ones, GA is possible to quickly achieve the solutions, i.e., at the 8th and 7th generation for the 1st and 2nd GA analyses, respectively. A signal to recognize GA solutions is when the best fitness started to coincide with the mean one as, at that time, the cache of a computer program has been occupied by identical binary strings. Furthermore, the difference in solutions between two GA analyses is about 0.5% due to the stochastic property of GA. GA solutions in Figs. 7.2(a) and (b) are all near-optimal solutions.

In Figs. 7.3(a) and (b), the fmincon needs 23 iterations to achieve the optimum solution as well as zero value of the first-order optimality that is the first condition in Eq. (3.23) of KKT conditions (see section 3.7). The obtained patch volume is less than GA solutions in Figs. 7.2(a) and (b) by 0.6%.

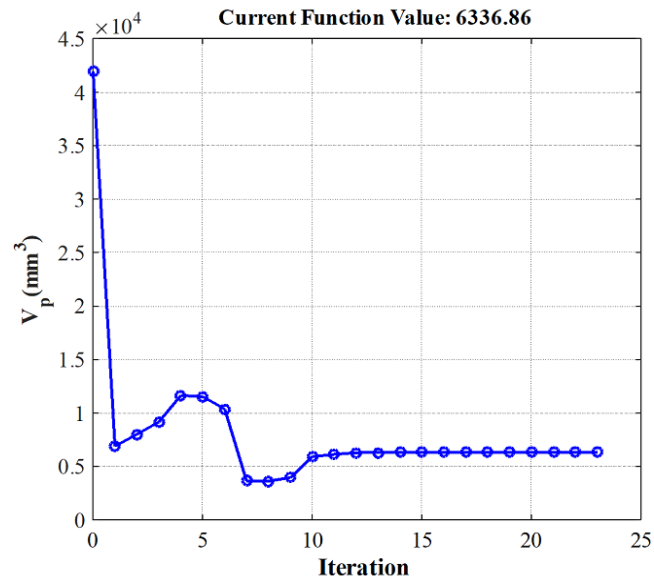
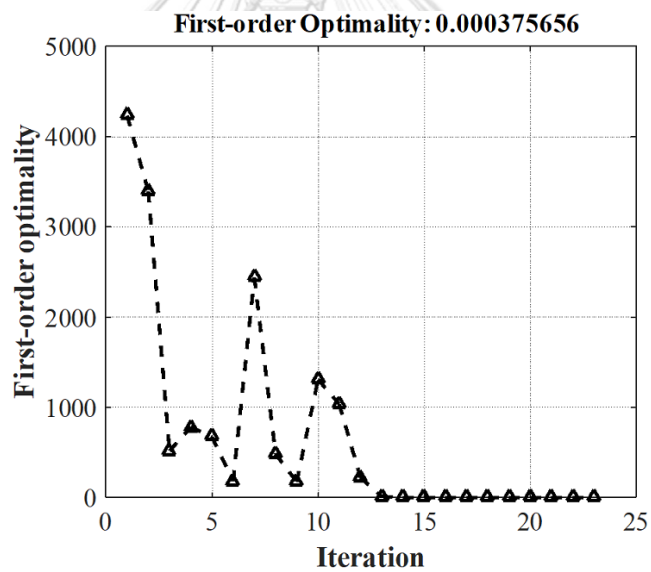


(a) V_p versus GA generation, 1st GA analysis



(b) V_p versus GA generation, 2nd GA analysis

Fig. 7.2. Evolution of patch volume in GA analyses for $2a = 0.2W_s$, $E_p = 460 \text{ MPa}$, and $E_a = 2944 \text{ MPa}$.

(a) V_p versus fmincon iteration

(b) First-order optimality evaluation

Fig. 7.3. Evolution of patch volume in fmincon analysis for $2a = 0.2W_s$,
 $E_p = 460$ MPa, and $E_a = 2944$ MPa.

For a larger crack ($2a = 0.3W_s$), the same conclusions can be drawn. Figs. 7.4 and 7.5 show that the way GA searching for optimum solutions is smoother than fmincon. The fmincon in Fig. 7.5, again, needs more time to come up with the optimum

solution as compared with GAs in Figs. 7.4(a) and (b). The fmincon solution is lower than GA solution by 2.2%.

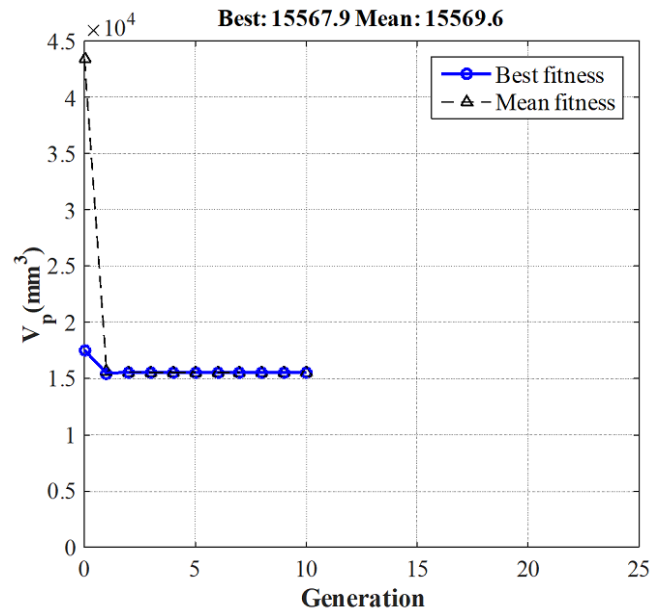
In Figs. 7.3 (a), 7.4(b), and 7.5(a), the patch volume values at the 7th, 1st, and 2nd iterations are less than the optimum ones but not the optimum solutions because at least one of KKT conditions is violated. For example, at the 7th iteration in Fig. 7.3 and the 2nd iteration in Fig. 7.5, the first-order optimality values are not equal to zero, as detailed in Figs. 7.3(b) and 7.5(b).

Tables 7.1 and 7.2 show the optimum patch solutions for the different patch and adhesive materials at two crack length levels. Typically, GA provides solutions having volumes equal to or slightly higher than fmincon solutions. The maximum difference between two solvers is 0.6% for $2a = 0.2W_s$ and 2.2% for $2a = 0.3W_s$. The stochastic property of GA is not pronounced as the difference between two GA solutions for the same combination is trivial.

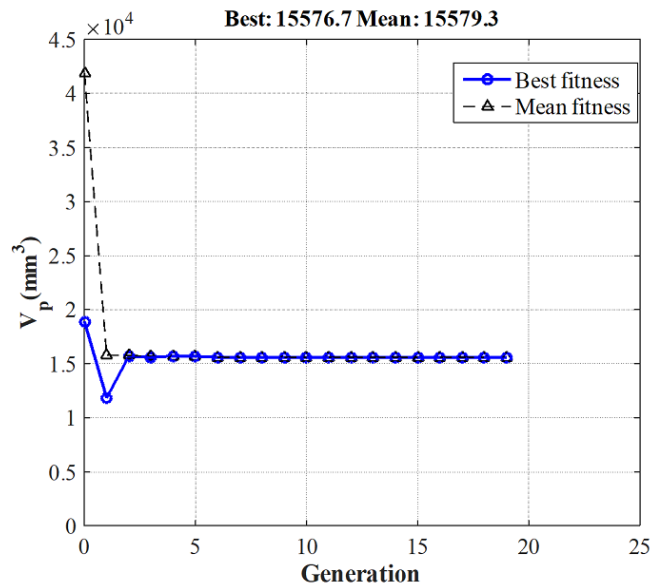
In the case of $2a = 0.2W_s$, the optimum patch width increases from 0.75 to 0.9 times the steel plate width, while optimum patch length varies from 4.4 to 6.1 times the crack length. The optimum patch thickness equals to 1.2 mm. The optimum patch volume is 10565 mm³ in the case of $E_p = 210$ GPa. It decreases by 18.4% and 40.1% when $E_p = 300$ GPa and $E_p = 460$ GPa, respectively. The patch volume takes the smallest value of 6337 mm³, roughly 1.4% of steel plate volume, when $E_p = 460$ GPa and $E_a = 2944$ MPa. Conversely, the optimum patch volume is almost unchanged with the modulus of adhesive material, as shown in Fig. 7.6(a). Although E_a increases significantly from 89% (from 959 to 1815 MPa) to 207% (from 959 to 2944 MPa), optimum patch volume slightly decreases from 0.1% to 0.2%.

In the case of $2a = 0.3W_s$ and $E_p = 210$ GPa, no feasible patch volume exists because the threshold surface (Surf 3) is completely under Surf 1 and Surf 2, as shown in Fig. 6.1(a). The optimum patch, however, can be achieved when elastic modulus of patch material increases from $E_p = 210$ to 300 and 460 GPa. The patch volume decreases roughly two times from 31616 mm³ to 15568 mm³ when E_p increases from 300 GPa to 460 GPa. Again, as shown in Fig. 7.6(b), the impact of adhesive modulus on

optimum patch volume is negligible. In summary, the optimum FRP patch for $2a = 0.3W_s$ has the geometry as patch width = 0.96 to 1 times the steel plate width, patch length = 3.3 to 6.6 times the crack length, and patch thickness = 2 mm.

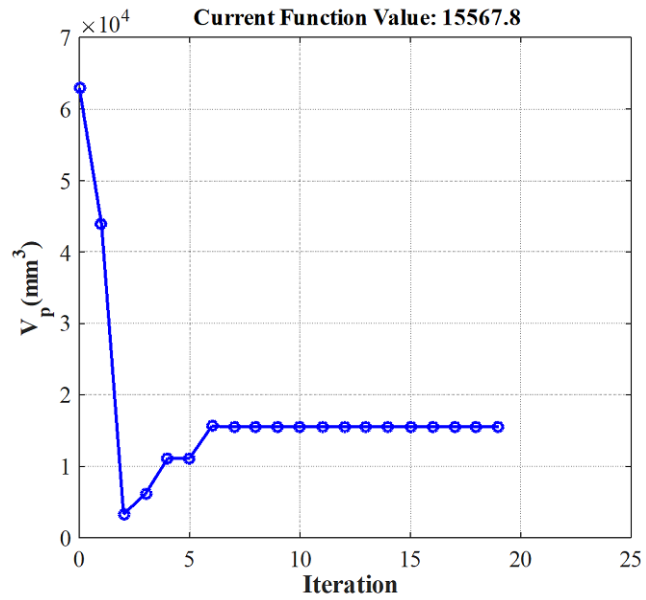
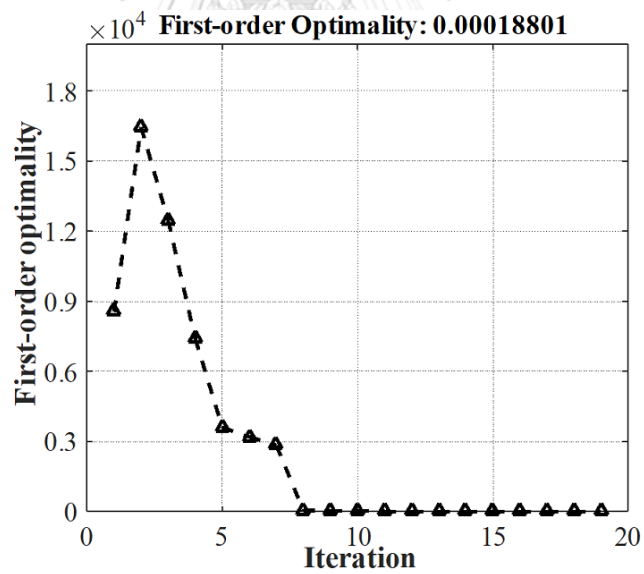


(a) V_p versus GA generation, 1st GA analysis



(b) V_p versus GA generation, 2nd GA analysis

Fig. 7.4. Evolution of patch volume in GA analyses for $2a = 0.3W_s$, $E_p = 460$ MPa, and $E_a = 2944$ MPa.

(a) V_p versus fmincon iteration

(b) First-order optimality evaluation

Fig. 7.5. Evolution of patch volume in fmincon analysis for $2a = 0.3W_s$, $E_p = 460$ MPa, and $E_a = 2944$ MPa

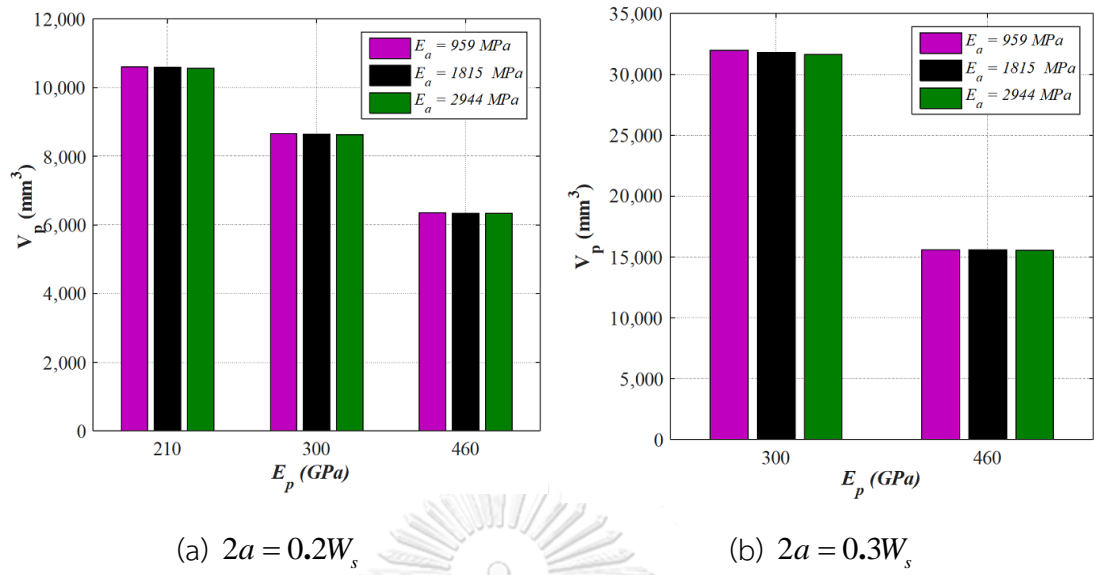


Fig. 7.6. Optimum patch volumes for different material combinations.

Table 7.1 Optimum FRP patch for different material combinations,
 $2a = 0.2W_s$.

Given parameters		Optimization solution								
		1 st GA analysis					2 nd GA analysis			
$2a / W_s$	E_p	E_a	W_p	L_p	t_p	V_p	W_p	L_p	t_p	V_p
	GPa	MPa	mm	mm	mm	mm ³	mm	mm	mm	mm ³
0.2	210	959	81.56	108.34	1.20	10615.5	79.7	110.94	1.20	10610.43
	210	1815	80.24	109.96	1.20	10590.27	80.56	109.54	1.20	10589.33
	210	2944	81.05	108.64	1.20	10566.49	79.97	109.52	1.21	10620.57
	300	959	72.37	99.72	1.20	8660.30	73.14	98.61	1.20	8654.73
	300	1815	72.26	99.61	1.20	8653.66	72.91	98.78	1.20	8642.77
	300	2944	73.57	97.63	1.20	8626.43	74.41	96.59	1.20	8627.13
	460	959	67.32	78.06	1.21	6372.46	65.97	79.94	1.21	6361.56
	460	1815	65.67	79.85	1.21	6361.47	65.94	80.22	1.20	6347.63
	460	2944	66.04	79.48	1.21	6346.47	65.61	78.41	1.24	6376.86

Table 7.1. Optimum FRP patch for different material combinations,
 $2a = 0.2W_s$ (cont.).

Given parameters		Optimization solution						
		Nonlinear programming						
$2a/W_s$	E_p	E_a	W_p	L_p	t_p	V_p	W_p/W_s	$L_p/2a$
	GPa	MPa	mm	mm	mm	mm ³		
	210	959	80.64	109.6	1.20	10606.66	0.90	6.09
	210	1815	80.58	109.51	1.20	10588.99	0.90	6.08
	210	2944	80.49	109.39	1.20	10565.18	0.89	6.08
0.2	300	959	73.64	97.93	1.20	8653.79	0.82	5.44
	300	1815	73.59	97.85	1.20	8640.96	0.82	5.44
	300	2944	73.53	97.73	1.20	8623.61	0.82	5.43
	460	959	66.28	79.90	1.20	6354.93	0.74	4.44
	460	1815	66.26	79.83	1.20	6347.28	0.74	4.44
	460	2944	66.23	79.73	1.20	6336.86	0.74	4.43

Table 7.2 Optimum FRP patch for different material combinations,

$$2a = 0.3W_s.$$

Given parameters		Optimization solution					Optimization solution				
		1 st GA analysis					2 nd GA analysis				
$2a / W_s$	E_p	E_a	W_p	L_p	t_p	V_p	W_p	L_p	t_p	V_p	
	GPa	MPa	mm	mm	mm	mm ³	mm	mm	mm	mm ³	
	210	959	n/a	n/a	n/a	n/a	n/a	n/a	n/a	n/a	
	210	1815	n/a	n/a	n/a	n/a	n/a	n/a	n/a	n/a	
	210	2944	n/a	n/a	n/a	n/a	n/a	n/a	n/a	n/a	
	300	959	90.00	183.14	1.98	32674.38	90.00	177.6	2.00	31965.31	
0.3	300	1815	90.00	176.76	2.00	31815.06	90.00	176.73	2.00	31810.88	
	300	2944	90.00	175.79	2.00	31633.78	90.00	175.64	2.00	31616.04	
	460	959	86.22	90.54	2.00	15612.72	86.02	90.76	2.00	15614.04	
	460	1815	86.38	90.27	2.00	15593.46	85.94	90.74	2.00	15596.06	
	460	2944	86.86	89.62	2.00	15567.89	85.37	91.23	2.00	15576.74	

n/a: not available

Table 7.2. Optimum FRP patch for different material combinations,
 $2a = 0.3W_s$ (cont.).

Given parameters		Optimization solution						
		Nonlinear programming						
$2a/W_s$	E_p	E_a	W_p	L_p	t_p	V_p	W_p/W_s	$L_p/2a$
	GPa	MPa	mm	mm	mm	mm ³		
	210	959	n/a	n/a	n/a	n/a	n/a	n/a
	210	1815	n/a	n/a	n/a	n/a	n/a	n/a
	210	2944	n/a	n/a	n/a	n/a	n/a	n/a
0.3	300	959	90.00	177.56	2.00	31960.67	1.00	6.58
	300	1815	90.00	176.73	2.00	31810.88	1.00	6.55
	300	2944	90.00	175.64	2.00	31616.02	1.00	6.51
	460	959	86.79	89.93	2.00	15611.09	0.96	3.33
	460	1815	86.76	89.87	2.00	15592.75	0.96	3.33
	460	2944	86.70	89.77	2.00	15567.78	0.96	3.32

n/a: not available

7.3. Assessment of composite patch and adhesive layer failures

To assess the possibility of FRP rupture and debonding failures, FE analyses on the optimum patch-repaired cracked plates in Tables 7.1 and 7.2 are conducted.

The rupture failure of FRP patch is assessed using the Tsai-Hill failure criterion [8], given as

$$T_s = \frac{\sigma_{11}^2}{S_{11}^2} - \frac{\sigma_{11}\sigma_{22}}{S_{11}^2} + \frac{\sigma_{22}^2}{S_{22}^2} + \frac{\sigma_{12}^2}{S_{12}^2} \geq 1 \quad (7.1)$$

where T_s = Tsai-Hill failure index; σ_{11} , σ_{22} , and σ_{12} = longitudinal, transverse, and shear stresses in the patch, respectively; S_{11} , S_{22} , and S_{12} = ultimate longitudinal, transverse, and shear stresses of patch material, respectively, taken from [89, 90]. The FRP rupture occurs if the condition in Eq. (7.1) is satisfied.

The debonding failure is assessed using some criteria described in [7]. Especially, the debonding occurs when at least one of the following condition is satisfied.

Failure in adhesive layer by the maximum shearing stress at the steel-adhesive interface where Tresca reaches a maximum, as shown in Fig. 7.7.

$$\text{Tresca} = \sigma_1 - \sigma_3 \quad (7.2)$$

$$T_{ay} = \frac{\text{Tresca}}{2p_{ay}} \geq 1 \quad (7.3)$$

Debonding occurs at the steel-adhesive interface by maximum normal stress

$$T_{as} = \frac{\sigma_{33}}{p_{as}} \geq 1 \quad (7.4)$$

Debonding occurs at the adhesive-patch interface by maximum normal stress

$$T_{ap} = \frac{\sigma_{33}}{p_{ap}} \geq 1 \quad (7.5)$$

where T_{ay} , T_{as} , T_{ap} = adhesive failure indexes; σ_1 , σ_3 = maximum and minimum principal stresses in the adhesive layer, respectively; σ_{33} = normal stress; p_{ay} , p_{as} ,

and p_{ap} = the shear strength of the adhesive material, peeling strengths of the adhesive-cracked structure interface, and peeling strengths adhesive-patch interface, respectively. Values of p_{ay} and p_a are taken from [91]. Assuming $p_{as} = p_{ap}$, $T_{as} > T_{ap}$ because the maximum normal stresses at steel-adhesive interface obtained from FE analyses are larger than ones at the adhesive-patch interface.

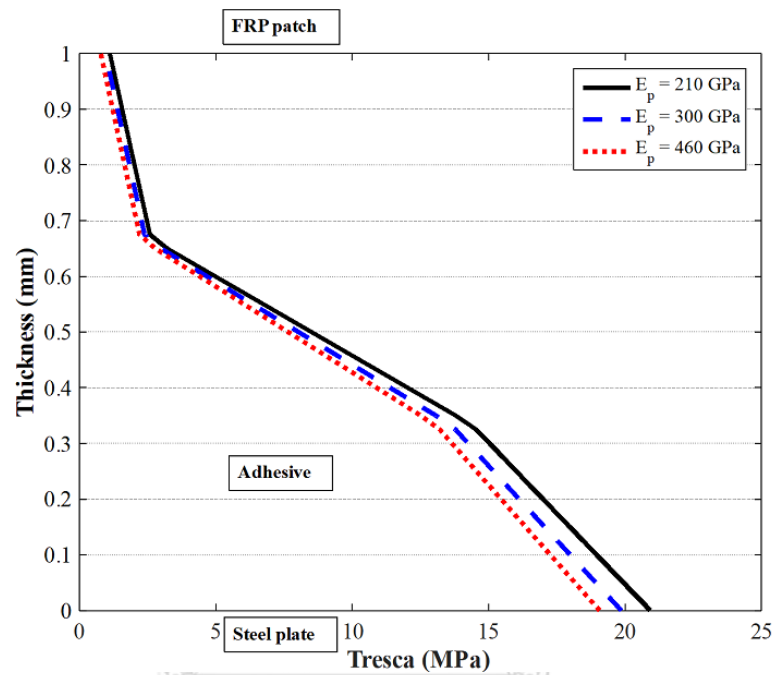


Fig. 7.7. Distribution of Tresca along adhesive thickness

$$(2a = 0.2W_s, E_a = 2944 \text{ MPa}).$$

In Table 7.3, all failure indexes T_s , T_{ay} , and T_{as} are less than one which indicates that FRP rupture and debonding failures are not possible for the optimum patch solution given in Tables 7.1 and 7.2. T_s values are quite low. Meanwhile, the maximum Tresca values in adhesive layer, detailed in Eq. (7.2), are pronounced, especially when high modulus adhesive is used, $T_s = 0.58$ for $2a = 0.2W_s$ and 0.64 for $2a = 0.3W_s$. If loading magnitude increases, failure in adhesive layer can occur as T_s increases. A function F_3 related to the debonding phenomenon can be added to the right-hand side of Eq. (5.3) in future works.

SIF value for the repaired plate when optimum patch design is used for the repair is numerically computed using ABAQUS and compared with the result obtained

from closed-form SIF solution as well as the fatigue threshold SIF range, as shown in Table 7.3. In some cases, SIFs from FE results violate the constraint in Eq. (6.4) with the maximum constraint violation is 4%.

Figs. 7.8 and 7.9 demonstrate the effects of elastic modulus of patch on the longitudinal stress in FRP patch and on Tresca in the adhesive layer, respectively. Figs. 7.10 and 7.11 show the effects of elastic modulus of adhesive material on Tresca and interfacial stresses in the adhesive layer at the two different crack lengths. Generally, a higher patch modulus causes more load transmitted from the structure to the patch [Fig. 7.8] but does not significantly influence the maximum Tresca in adhesive layer [Fig. 7.9]. A higher adhesive modulus causes an increase in maximum Tresca, shear stress, and normal stress in adhesive layer [Figs. 7.10 and 7.11]. In summary, the use of a high modulus patch and low modulus adhesive is recommended in this example.

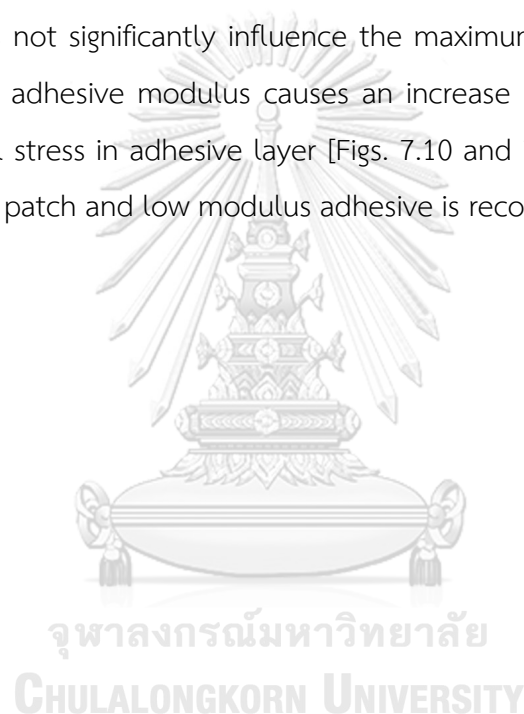


Table 7.3 Failure indexes for optimum patch design solutions

$2a/W_s$	E_p	E_a	SIF-Eq. (5.3)	SIF- FE	T_s	T_{ay}	T_{as}
	GPa	MPa	MPa.mm ^{1/2}	MPa.mm ^{1/2}	Eq. (7.1)	Eq. (7.3)	Eqs. (7.4)
0.2	210	959	209.00	214.40	0.002	0.2164	0.0741
	210	1815	209.00	208.30	0.002	0.3826	0.1329
	210	2944	209.00	199.50	0.001	0.5814	0.2191
	300	959	209.00	212.30	0.002	0.2133	0.0724
	300	1815	209.00	201.00	0.002	0.3690	0.1271
	300	2944	208.92	190.60	0.002	0.5519	0.2063
	460	959	209.00	213.20	0.002	0.2162	0.0726
	460	1815	209.00	198.50	0.003	0.3642	0.1239
	460	2944	209.00	190.20	0.003	0.5298	0.2067
	0.3	210	959	n/a	n/a	n/a	n/a
210		1815	n/a	n/a	n/a	n/a	n/a
210		2944	n/a	n/a	n/a	n/a	n/a
300		959	209.00	211.20	0.002	0.2593	0.0728
300		1815	209.00	198.80	0.002	0.4348	0.1237
300		2944	209.00	197.60	0.001	0.6368	0.1974
460		959	209.00	217.50	0.002	0.3001	0.0829
460		1815	208.99	206.60	0.002	0.4703	0.1315
460		2944	209.00	195.80	0.003	0.6432	0.1960

n/a = not available

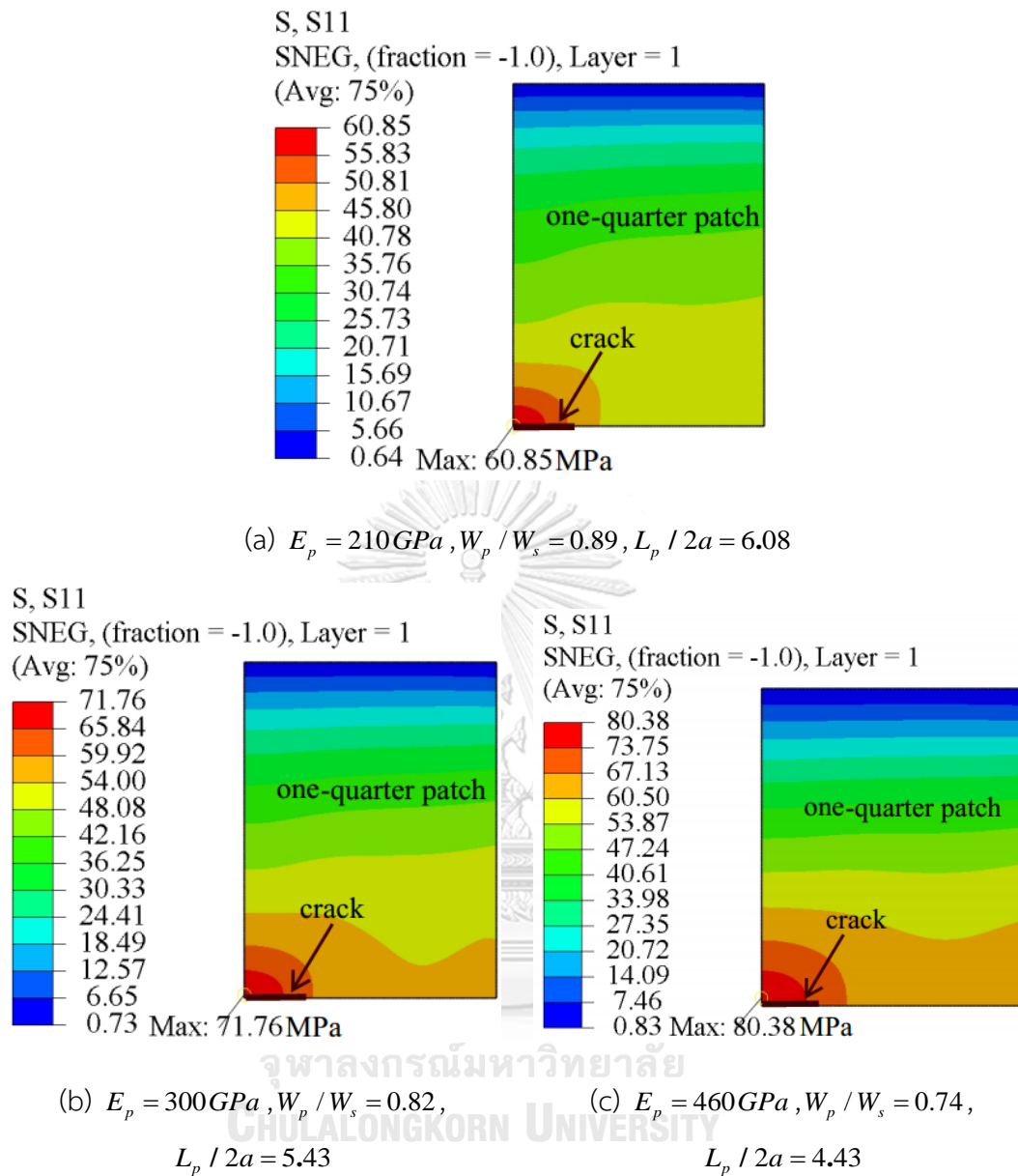
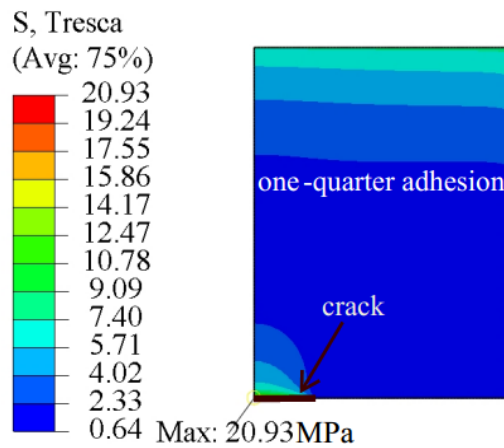
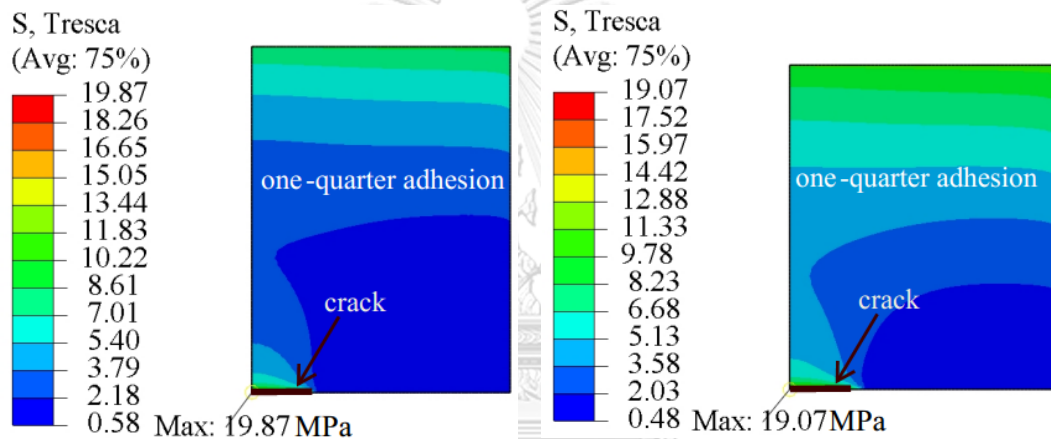


Fig. 7.8. Effect of patch modulus on longitudinal stress in FRP patch
($2a = 0.2W_s$, $E_a = 2944\text{MPa}$).



(a) $E_p = 210\text{GPa}$, $W_p / W_s = 0.89$, $L_p / 2a = 6.08$



(b) $E_p = 300\text{GPa}$, $W_p / W_s = 0.82$,

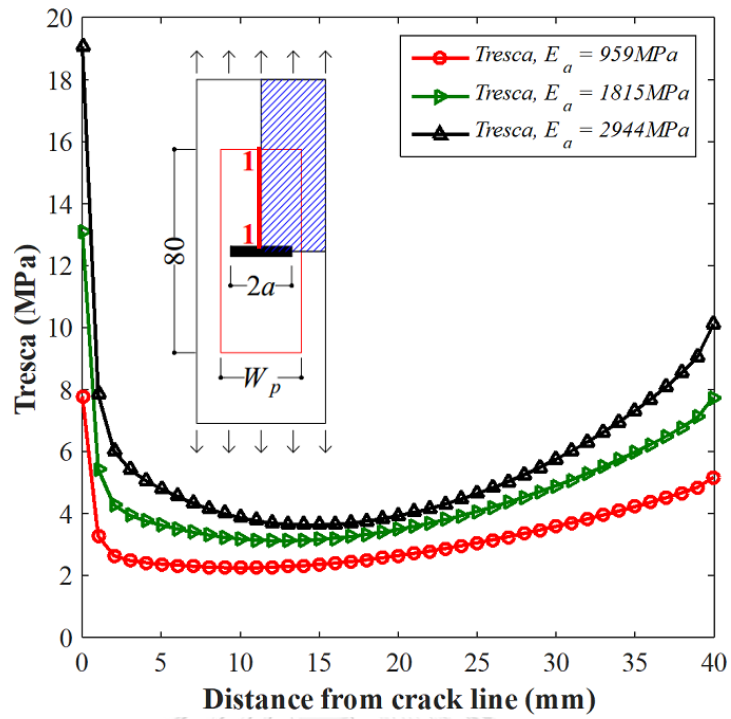
(c) $E_p = 460\text{GPa}$, $W_p / W_s = 0.74$,

$$L_p / 2a = 5.43$$

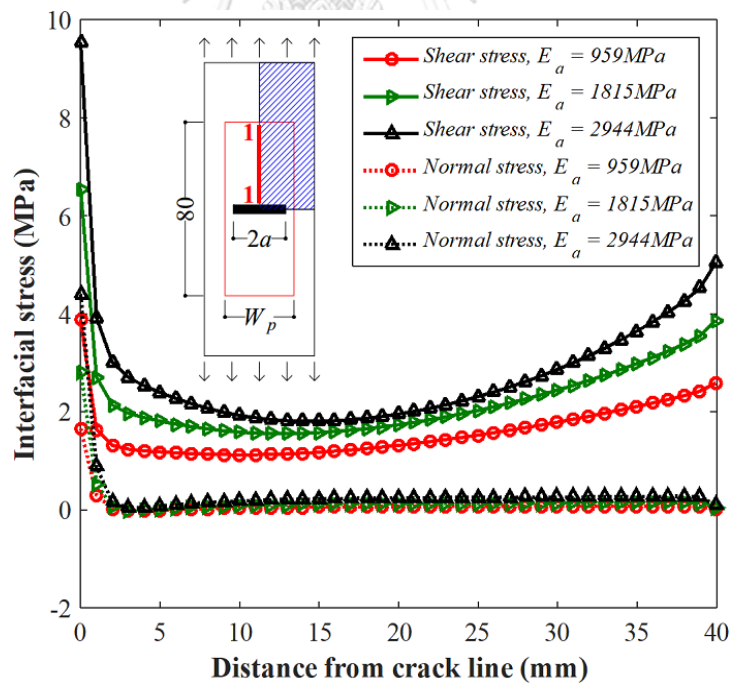
$$L_p / 2a = 4.43$$

Fig. 7.9. Effect of patch modulus on Tresca in adhesive layer

$$(2a = 0.2W_s, E_a = 2944 \text{ MPa}).$$



(a) Tresca along 1-1



(b) Interfacial stresses along 1-1

Fig. 7.10. Effect of adhesive modulus on Tresca and interfacial stresses in adhesive layer ($2a = 0.2W_s$, $E_p = 460 \text{ GPa}$).

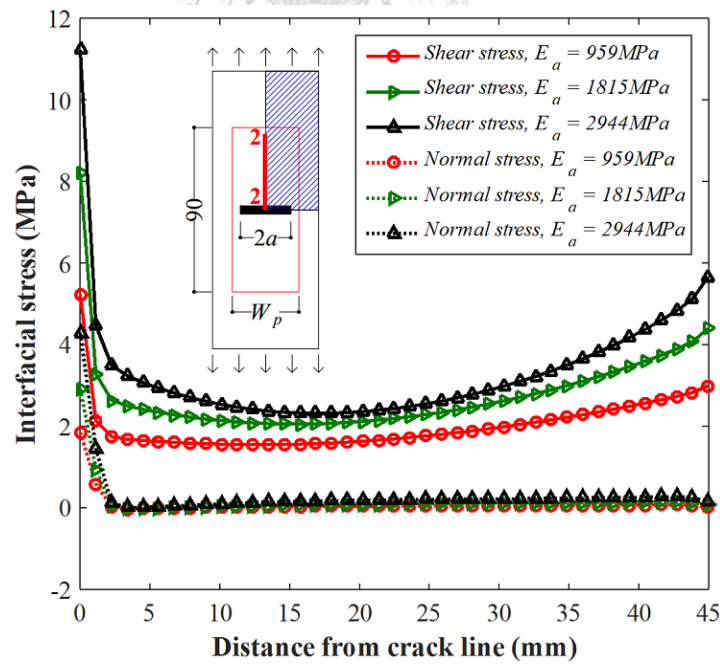
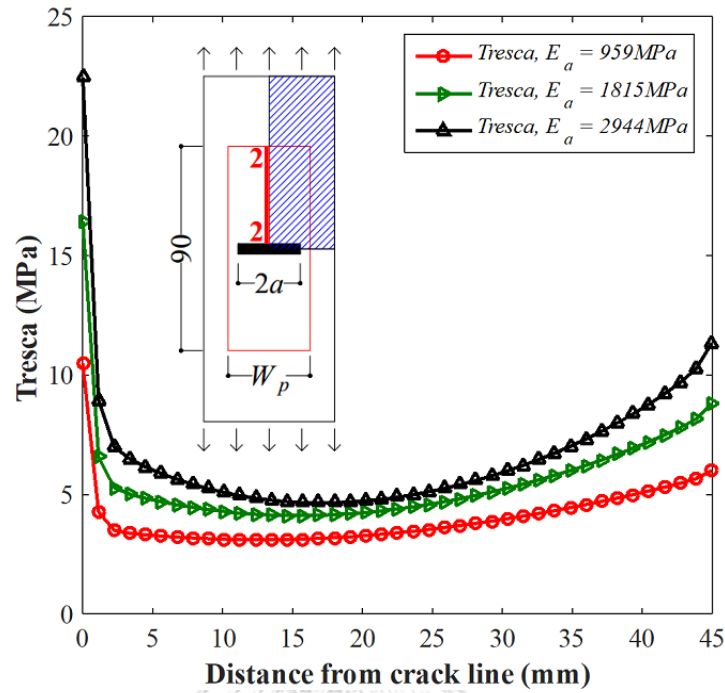


Fig. 7.11. Effect of adhesive modulus on Tresca and interfacial stresses in adhesive layer ($2a = 0.3W_s$, $E_p = 460$ GPa).

CHAPTER 8

CONCLUSIONS

8.1. Conclusions

This research introduces the numerical process that combines the finite element method, the genetic programming, and two optimization solvers for the design optimization of adhesive-bonded FRP patches used to repair cracked structures. An example design of double-sided FRP patches for repairing center-cracked steel plates subjected to tension fatigue loadings is used to illustrate the design process. The optimization problem has formulated and analyzed in the context of volume minimization of the FRP patch. The main conclusions are as follows:

1. FE model using continuum shell elements stacked through FRP patch thickness and tie constraints to represent the geometric compatibility conditions along steel-adhesive and adhesive-patch interfaces can characterize SIF of FRP-patched steel plates.
2. A symbolic regression via GP provides a nonlinear mathematical function of sufficient accuracy to predict a sensitive physical quantity, i.e., SIF, for patch-repaired cracked plates. This technique can be applied to other problems to provide an approximate model of a structural behavior in terms of design parameters. However, to obtain an effective prediction, the sufficiency property of the function and terminal sets of GP [72, 73] requires an engineer to have basic knowledge of the problem being treated.
3. Closed-form empirical solution for calculation of SIF of center-cracked steel plates repaired with two-sided adhesive-bonded FRP patches with sufficient accuracy are proposed for practicing engineers. The proposed solutions will help visualize the effects of design parameters on SIF which facilitates the repair design.
4. GA provides the near-optimal solutions for an inequality constrained optimization problem faster than nonlinear programming in this study.

5. For center-cracked steel plates under tension, the optimum patch design is significantly influenced by patch modulus. A significant reduction of patch volume can be achieved using high modulus FRP patches. Meanwhile, the effect of adhesive modulus is not pronounced. In the view of debonding failure, the maximum Tresca, and interfacial stresses significantly increase when adhesive modulus increases. As both stresses are relatively insensitive to patch modulus, the use of a high modulus patch and low modulus adhesive is recommended for fatigue crack repairs. For large cracks, the use of thick and high elastic modulus patch is the most effective

8.2. Recommendations for future works

Investigated ranges of the design parameters should be extended. The present research can be extended by investigating various crack types, structures, patch shapes, and loading conditions.

The debonding phenomenon should be considered by using coupled cohesive zone model, described in [92], to be assigned to the steel plate-adhesive and adhesive-patch interfaces where the phenomenon is prone to occur. SIF solution in Eq. (5.3) will be included the debonding by adding a new function F_3 into the right-hand side.

The genetic algorithm can be embedded in FE code to direct the FRP patch from a random initial configuration to an optimum one.

REFERENCES

- [1] US Department of Transportation (USDOT), Highway bridges for all states, 2016. <https://www.fhwa.dot.gov/bridge/nbi/ascii2016.cfm>. (Accessed 10 July 2017).
- [2] J. Bien, L. Elfgrén, J. Olofsson, Sustainable Bridges: Assessment for Future Traffic Demands and Longer Lives, Dolnoslaskie Wydawnictwo Edukacyjne 2007.
- [3] B. Kuehn, M. Lukić, A. Nussbaumer, H.-P. Guenther, R. Helmerich, S. Herion, M. Kolstein, S. Walbridge, B. Androic, O. Dijkstra, Assessment of existing steel structures: recommendations for estimation of remaining fatigue life, JRC Scientific and technical Report 43401 (2008).
- [4] J. Fisher, U. Yuceoglu, A survey of localized cracking in steel bridges, Interim Report, Dot-FH-111-9506, Federal Highway Administration (1981).
- [5] R.J. Dexter, J.M. Ocel, Manual for repair and retrofit of fatigue cracks in steel bridges. No. FHWA-IF-13-020, 2013.
- [6] S. Wilcox, Crack in PA & NJ Turnpike bridge forces immediate closure, 2017. <http://www.livetrucking.com/crack-in-pa-nj-turnpike-bridge-forces-immediate-closure/>. (Accessed July 7 2017).
- [7] P. Papanikos, K. Tserpes, G. Labeas, S. Pantelakis, Progressive damage modelling of bonded composite repairs, Theoretical and Applied Fracture Mechanics 43(2) (2005) 189-198.
- [8] G.H. Staab, 1 - Introduction to composite materials, Laminar Composites, Butterworth-Heinemann 2015, pp. 1-16.
- [9] D. Systèmes, ABAQUS-CAE User's Manual: Version 6.8. Pawtucket, Rhode Ireland: Hibbitt, Karlsson & Sorenson, Inc, 2008.
- [10] S. Wagner, G. Kronberger, A. Beham, M. Kommenda, A. Scheibenpflug, E. Pitzer, S. Vonolfen, M. Kofler, S. Winkler, V. Dorfer, M. Affenzeller, Architecture and design of the HeuristicLab optimization environment, in: R. Klempous, J. Nikodem, W. Jacak, Z.

Chaczko (Eds.), *Advanced Methods and Applications in Computational Intelligence*, Springer International Publishing, Heidelberg, 2014, pp. 197-261.

[11] A.M. Kumar, S. Hakeem, Optimum design of symmetric composite patch repair to centre cracked metallic sheet, *Composite Structures* 49(3) (2000) 285-292.

[12] H. Tada, P.C. Paris, G.R. Irwin, Two-dimensional stress solutions for various configurations with cracks, in: H. Tada, P.C. Paris, G.R. Irwin (Eds.), *The Stress Analysis of Cracks Handbook*, Third Edition, ASME, New York, NY, 2000.

[13] M.R. Ayatollahi, R. Hashemi, Computation of stress intensity factors (KI, KII) and T-stress for cracks reinforced by composite patching, *Composite Structures* 78(4) (2007) 602-609.

[14] J. Reddy, A generalization of two-dimensional theories of laminated composite plates, *International Journal for Numerical Methods in Biomedical Engineering* 3(3) (1987) 173-180.

[15] X.-L. Zhao, L. Zhang, State-of-the-art review on FRP strengthened steel structures, *Engineering Structures* 29(8) (2007) 1808-1823.

[16] A. Baker, Bonded composite repair of fatigue-cracked primary aircraft structure, *Composite Structures* 47(1-4) (1999) 431-443.

[17] The International Institute for FRP in Construction (IIFC), FRP-International-Vol-8-No-3-July-2011, 2011. <https://www.iifc.org/wp-content/uploads/2011/07/FRP-International-Vol-8-No-3-July-2011-website-version.pdf>. (Accessed July 11 2017).

[18] V.M. Karbhari, *Rehabilitation of metallic civil infrastructure using fiber reinforced polymer (FRP) composites: Types properties and testing methods*, Elsevier 2014.

[19] T.C. Miller, M.J. Chajes, D.R. Mertz, J.N. Hastings, Strengthening of a steel bridge girder using CFRP plates, *Journal of Bridge Engineering* 6(6) (2001) 514-522.

[20] A. Lenwari, T. Thepchatri, P. Albrecht, Flexural Response of Steel Beams Strengthened with Partial-Length CFRP Plates, *Journal of Composites for Construction* 9(4) (2005) 296-303.

- [21] A. Lenwari, T. Thepchatri, P. Albrecht, Debonding Strength of Steel Beams Strengthened with CFRP Plates, *Journal of Composites for Construction* 10(1) (2006) 69-78.
- [22] H. Sallam, S. Ahmad, A. Badawy, W. Mamdouh, Evaluation of steel I-beams strengthened by various plating methods, *Advances in Structural Engineering* 9(4) (2006) 535-544.
- [23] D. Schnerch, S. Rizkalla, Flexural Strengthening of Steel Bridges with High Modulus CFRP Strips, *Journal of Bridge Engineering* 13(2) (2008) 192-201.
- [24] J. Teng, T. Yu, D. Fernando, Strengthening of steel structures with fiber-reinforced polymer composites, *Journal of Constructional Steel Research* 78 (2012) 131-143.
- [25] L. Zhang, J. Teng, Elastic lateral buckling of I-section beams bonded with a thin plate, *The Third International Conference on Advanced Composites in Construction (ACIC 2007)*, University of Bath, UK, 2007, pp. 441-6.
- [26] M. Kabir, A. Seif, Lateral torsional buckling of steel i-beam retrofitted using FRP sheets: Analytical solution and optimization, *Advances in FRP Composites in Civil Engineering*, Springer2011, pp. 915-918.
- [27] X.-L. Zhao, *FRP-strengthened metallic structures*, CRC Press2013.
- [28] E. Ghafoori, M. Motavalli, Lateral-torsional buckling of steel I-beams retrofitted by bonded and un-bonded CFRP laminates with different pre-stress levels: experimental and numerical study, *Construction and Building Materials* 76 (2015) 194-206.
- [29] P. Colombi, A. Bassetti, A. Nussbaumer, Analysis of cracked steel members reinforced by pre-stress composite patch, *Fatigue & fracture of engineering materials & structures* 26(1) (2003) 59-66.
- [30] H. Liu, R. Al-Mahaidi, X.-L. Zhao, Experimental study of fatigue crack growth behaviour in adhesively reinforced steel structures, *Composite Structures* 90(1) (2009) 12-20.

- [31] B. Täljsten, C.S. Hansen, J.W. Schmidt, Strengthening of old metallic structures in fatigue with prestressed and non-prestressed CFRP laminates, *Construction and Building Materials* 23(4) (2009) 1665-1677.
- [32] H. Jiao, F. Mashiri, X.-L. Zhao, A comparative study on fatigue behaviour of steel beams retrofitted with welding, pultruded CFRP plates and wet layup CFRP sheets, *Thin-Walled Structures* 59 (2012) 144-152.
- [33] A. Belarbi, B. Acun, FRP systems in shear strengthening of reinforced concrete structures, *Procedia Engineering* 57 (2013) 2-8.
- [34] H.-T. Wang, G. Wu, J.-B. Jiang, Fatigue behavior of cracked steel plates strengthened with different CFRP systems and configurations, *Journal of Composites for Construction* 20(3) (2015) 04015078.
- [35] B. Zheng, M. Dawood, Fatigue strengthening of metallic structures with a thermally activated shape memory alloy fiber-reinforced polymer patch, *Journal of Composites for Construction* 21(4) (2016) 04016113.
- [36] Y.J. Kim, K.A. Harries, Fatigue behavior of damaged steel beams repaired with CFRP strips, *Engineering Structures* 33(5) (2011) 1491-1502.
- [37] P. Colombi, G. Fava, L. Sonzogni, Fatigue behavior of cracked steel beams reinforced by using CFRP materials, *Procedia Engineering* 74 (2014) 388-391.
- [38] P. Colombi, G. Fava, Experimental study on the fatigue behaviour of cracked steel beams repaired with CFRP plates, *Engineering Fracture Mechanics* 145 (2015) 128-142.
- [39] P. Colombi, G. Fava, Fatigue crack growth in steel beams strengthened by CFRP strips, *Theoretical and Applied Fracture Mechanics* 85 (2016) 173-182.
- [40] F. Erdogan, K. Arin, A sandwich plate with a part-through and a debonding crack, *Engineering Fracture Mechanics* 4(3) (1972) 449-458.
- [41] M. Ratwani, Analysis of cracked, adhesively bonded laminated structures, *AIAA journal* 17(9) (1979) 988-994.

- [42] L.R.F. Rose, An application of the inclusion analogy for bonded reinforcements, *International Journal of Solids and Structures* 17(8) (1981) 827-838.
- [43] L.R.F. Rose, A cracked plate repaired by bonded reinforcements, *International Journal of Fracture* 18(2) (1982) 135-144.
- [44] L.R.F. Rose, Theoretical analysis of crack patching, *Bonded Repair of Aircraft Structures*, Springer1988, pp. 77-106.
- [45] C.T. Sun, J. Klug, C. Arendt, Analysis of cracked aluminum plates repaired with bonded composite patches, *AIAA Journal* 34(2) (1996) 369-374.
- [46] S. Naboulsi, S. Mall, Modeling of a cracked metallic structure with bonded composite patch using the three layer technique, *Composite Structures* 35(3) (1996) 295-308.
- [47] C.C. Lam Angus, C.H. Yam Michael, J.J.R. Cheng, D. Kennedy Gaylene, Study of stress intensity factor of a cracked steel plate with a single-side CFRP composite patching, *Journal of Composites for Construction* 14(6) (2010) 791-803.
- [48] L. Gu, A.R.M. Kasavajhala, S. Zhao, Finite element analysis of cracks in aging aircraft structures with bonded composite-patch repairs, *Composites Part B: Engineering* 42(3) (2011) 505-510.
- [49] H.-T. Wang, G. Wu, Z.-S. Wu, Effect of FRP Configurations on the Fatigue Repair Effectiveness of Cracked Steel Plates, *Journal of Composites for Construction* 18(1) (2013) 04013023.
- [50] A. Baker, Crack patching: Experimental studies, practical applications, *Bonded Repair of Aircraft Structures*, Springer1988, pp. 107-173.
- [51] R. Mahajan, K. Ravi-Chandar, Experimental determination of stress-intensity factors using caustics and photoelasticity, *Experimental mechanics* 29(1) (1989) 6-11.
- [52] C. Taudou, K. Ravi-Chandar, Experimental determination of the dynamic stress-intensity factor using caustics and photoelasticity, *Experimental mechanics* 32(3) (1992) 203-210.

- [53] R. Marloff, M. Leven, T. Ringler, R. Johnson, Photoelastic determination of stress-intensity factors, *Experimental Mechanics* 11(12) (1971) 529-539.
- [54] D.G. Smith, C. Smith, Photoelastic determination of mixed mode stress intensity Factors, *Engineering Fracture Mechanics* 4(2) (1972) 357-366.
- [55] F. Diaz, E. Patterson, R. Tomlinson, J. Yates, Measuring stress intensity factors during fatigue crack growth using thermoelasticity, *Fatigue & Fracture of Engineering Materials & Structures* 27(7) (2004) 571-583.
- [56] Y. Fujimoto, E. Shintaku, G. Pirker, G. Liu, Piezoelectric sensor for stress intensity factor measurement of two dimensional cracks, *Engineering Fracture Mechanics* 70(9) (2003) 1203-1218.
- [57] Z. Marioli-Riga, D. Xenos, C. Vrettos, A standard analysis methodology for the stress analysis of repaired aircraft structures with the method of composite patch repair, *Applied Composite Materials* 11(4) (2004) 191-203.
- [58] C.N. Duong, C.H. Wang, *Composite repair: Theory and design*, Elsevier 2010.
- [59] R. Brighenti, Patch repair design optimisation for fracture and fatigue improvements of cracked plates, *International Journal of Solids and Structures* 44(3) (2007) 1115-1131.
- [60] A.A. Yala, A. Megueni, Optimisation of composite patches repairs with the design of experiments method, *Materials & Design* 30(1) (2009) 200-205.
- [61] M. Ramji, R. Srilakshmi, M. Bhanu Prakash, Towards optimization of patch shape on the performance of bonded composite repair using FEM, *Composites Part B: Engineering* 45(1) (2013) 710-720.
- [62] H. Errouane, Z. Sereir, A. Chateauneuf, Numerical model for optimal design of composite patch repair of cracked aluminum plates under tension, *International Journal of Adhesion and Adhesives* 49 (2014) 64-72.
- [63] A. Rasane, P. Kumar, M. Khond, Optimizing the size of a cfrp patch to repair a crack in a thin sheet, *The Journal of Adhesion* 93(13) (2017) 1064-1080.

- [64] A. Griffith, The Phenomena of Rupture and Flow in Solids, Philosophical transactions of the royal society of london. Series A, containing papers of a mathematical or physical character 221 (1921) 163-198.
- [65] G.R. Irwin, Analysis of stresses and strains near the end of a crack traversing a plate, Journal of Applied Mechanics (1957).
- [66] C.F. Shih, R.J. Asaro, Elastic-plastic analysis of cracks on bimaterial interfaces: Part I-small scale yielding, Journal of Applied Mechanics 55(2) (1988) 299-316.
- [67] B.D. M., S.L. A., The elastic energy of a straight dislocation in an infinite anisotropic elastic medium, Physica Status Solidi (b) 48(1) (1971) 419-428.
- [68] D. Systèmes, Abaqus theory manual, Dessault Systèmes, Providence, RI, 2007.
- [69] J.H. Holland, Adaptation in Natural and Artificial Systems. An Introductory Analysis with Application to Biology, Control, and Artificial Intelligence, Ann Arbor, MI: University of Michigan Press (1975).
- [70] D.E. Goldberg, Genetic Algorithms in Search, Optimization, and Machine Learning, Addison-Wesley Professional 1989.
- [71] M. Mitchell, An Introduction to Genetic Algorithms, Third Printing ed., MIT press 1998.
- [72] J.R. Koza, Genetic Programming: on the Programming of Computers by Means of Natural Selection, MIT press 1992.
- [73] S. Sette, L. Boullart, Genetic programming: principles and applications, Engineering Applications of Artificial Intelligence 14(6) (2001) 727-736.
- [74] J. Lee Rodgers, W.A. Nicewander, Thirteen ways to look at the correlation coefficient, The American Statistician 42(1) (1988) 59-66.
- [75] B. Do, A. Lenwari, Empirical Stress Intensity Factor Equations for Cracked Steel Plates Repaired with Double-Sided FRP Patches, IOP Conference Series: Materials Science and Engineering 371(1) (2018) 012056.

- [76] T. MathWorks, Global Optimization Toolbox User's Guide (r2018a), 2018. http://www.mathworks.com/help/pdf_doc/gads/gads_tb.pdf. (Accessed March 10 2018).
- [77] S.S. Rao, S.S. Rao, Engineering Optimization: Theory and Practice, 4th ed., John Wiley & Sons 2009.
- [78] H. Parisch, A continuum-based shell theory for non-linear applications, International Journal for Numerical Methods in Engineering 38(11) (1995) 1855-1883.
- [79] A. Hmidan, Y.J. Kim, S. Yazdani, Stress intensity factors for cracked steel girders strengthened with CFRP sheets, Journal of Composites for Construction 19(5) (2014) 04014085.
- [80] L. Pook, Analysis and application of fatigue crack growth data, Journal of Strain Analysis 10(4) (1975) 242-250.
- [81] Sika, Sika® CarboDur® Plates. Pultruded carbon fiber plates for structural strengthening, 2009. <https://irn.sika.com/dms/getdocument.get/2d1f35bc-066e-35ff-b45a-e8fc8099b43b/Carbodur.pdf>. (Accessed October 12 2017).
- [82] C. Wu, X. Zhao, W.H. Duan, R. Al-Mahaidi, Bond characteristics between ultra high modulus CFRP laminates and steel, Thin-Walled Structures 51 (2012) 147-157.
- [83] C.M. Bishop, Neural Networks for Pattern Recognition, Oxford university press, USA 2005.
- [84] T.L. Anderson, Fracture mechanics: fundamentals and applications, CRC press 2017.
- [85] S.K. Maiti, Fracture Mechanics, Cambridge University Press 2015.
- [86] Z. Yun, L.P. Ye, X.Z. Lu, Q.R. Yue, Finite Element Analysis for the Fatigue Behavior of Steel Plates Strengthened with CFRP Plates, Key Engineering Materials 324-325 (2006) 359-362.
- [87] Z. Yun, L.P. Ye, X.Z. Lu, Experimental study on fatigue behavior of tensile steel plates strengthened with CFRP plates, Proceeding Third International Conference on FRP Composites in Civil Engineering (CICE 2006), Miami, Florida, USA, 2006, pp. 733-736.

[88] S.T. Rolfe, J.M. Barsom, Fracture and fatigue control in structures: applications of fracture mechanics, ASTM International 1977.

[89] Performance Composites Ltd., Mechanical properties of carbon fibre composite materials, fibre / epoxy resin (120°C cure), 2009. http://www.performance-composites.com/carbonfibre/mechanicalproperties_2.asp. (Accessed March 30 2018).

[90] N.J. Aljabar, X.L. Zhao, R. Al-Mahaidi, E. Ghafoori, M. Motavalli, Y.C. Koay, Fatigue tests on UHM-CFRP strengthened steel plates with central inclined cracks under different damage levels, Composite Structures 160 (2017) 995-1006.

[91] J. Deng, J. Li, Y. Wang, W. Xie, Numerical study on notched steel beams strengthened by CFRP plates, Construction and Building Materials 163 (2018) 622-633.

[92] J.G. Teng, D. Fernando, T. Yu, Finite element modelling of debonding failures in steel beams flexurally strengthened with CFRP laminates, Engineering Structures 86 (2015) 213-224.



APPENDIX A

THREE-DIMENSIONAL FINITE ELEMENT MODELING

The following are the main code of ABAQUS input file to compute SIF for a 3D model of a center-cracked steel plate repaired with double-sided FRP patch under tension. Related figures that represent the results in a graphical user interface of each step are also given.

Step 1: Start the program

*Heading

** Job name: Job-OP1 Model name: Model-1

** Generated by: Abaqus/CAE

*Preprint, echo=NO, model=NO, history=NO, contact=NO

Step 2: Create four parts of the FE model

** PARTS

Two adhesive parts

*Part, name="Adhesive 1"

*End Part

*Part, name="Adhesive 2"

*End Part

Two FRP patch parts

*Part, name="CFRP 1"

*End Part

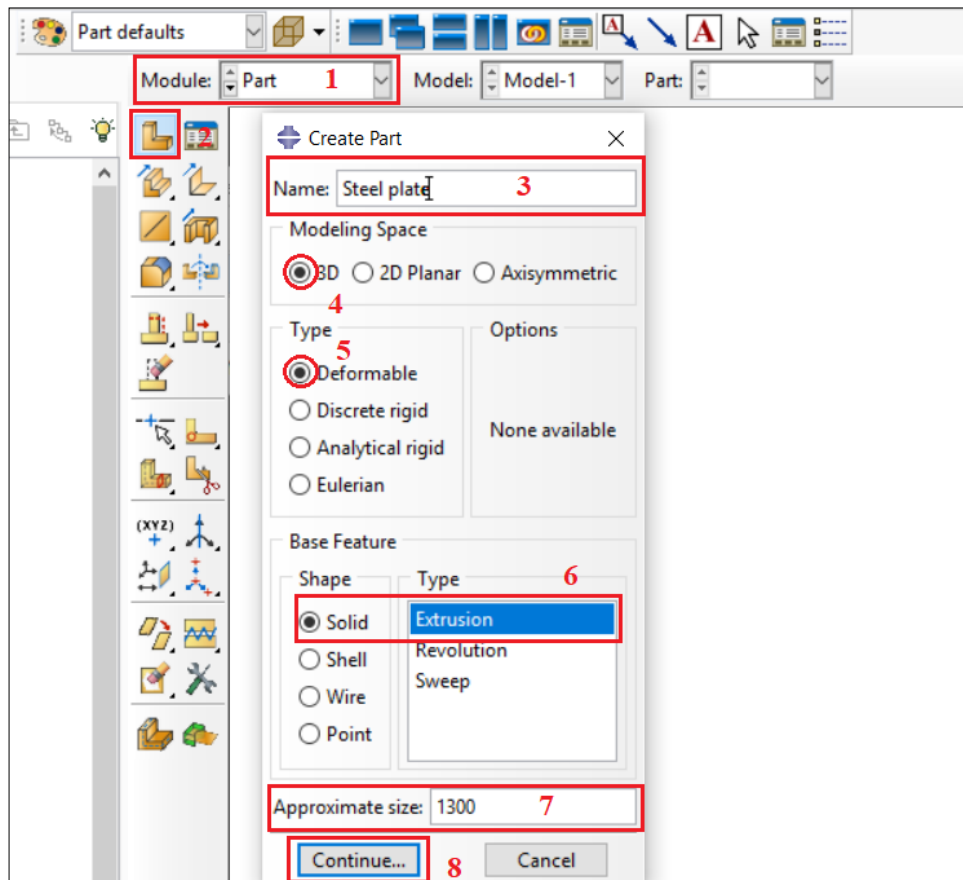
*Part, name="CFRP 2"

*End Part

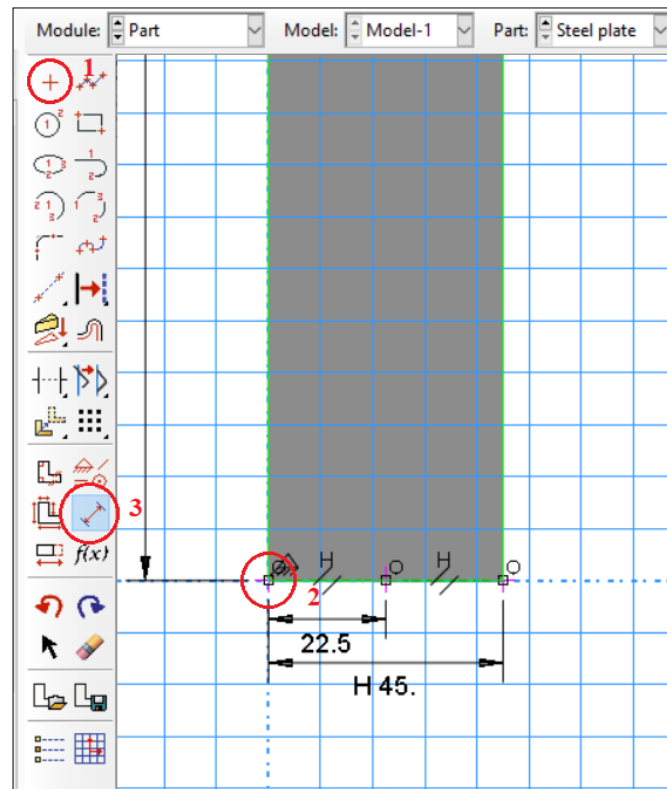
Steel plate part

*Part, name="Steel plate"

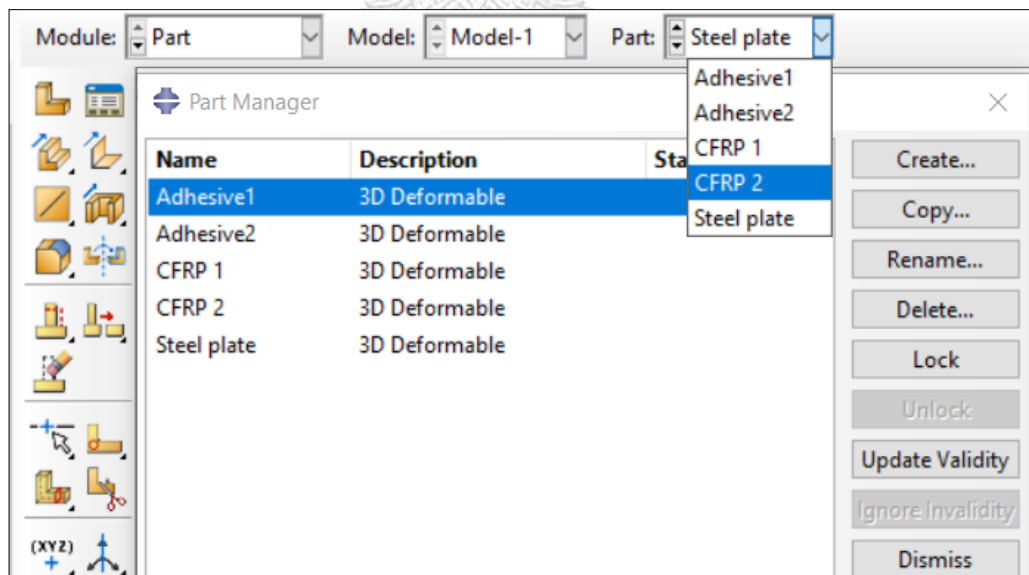
*End Part



(a) Create part dialogue



(b) Sketching geometry of the steel plate



(c) Five parts for the FE models created

Fig. A.1. Creating parts for FE model.

Step 3: Assembling created parts

** ASSEMBLY

*Assembly, name=Assembly

*Instance, name="Steel plate-1", part="Steel plate"

*Node

Node number, x, y, z

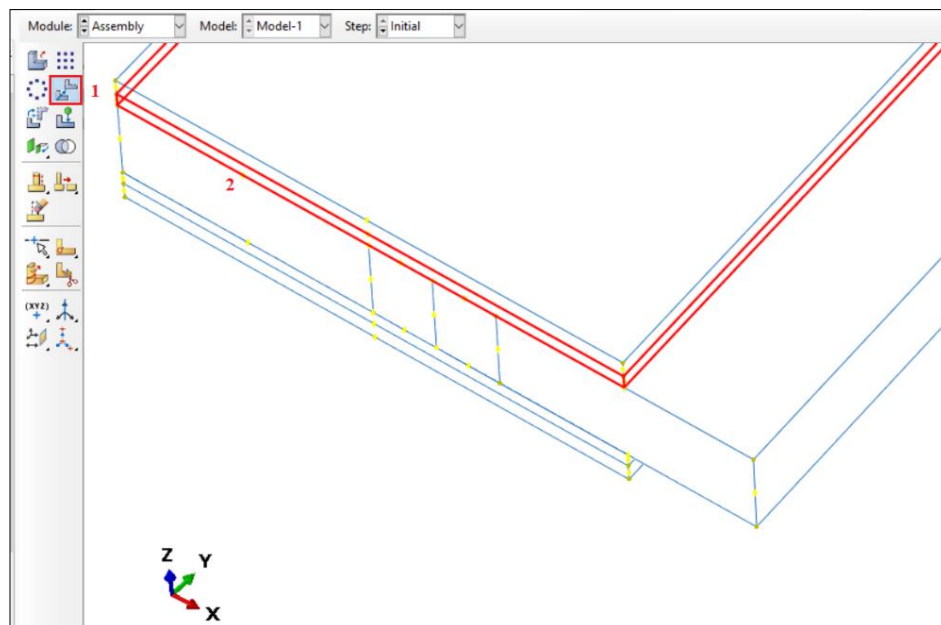


Fig. A.2. Assemblage of five parts of FE model.

*Element, type=C3D20

Element number, node 1, node 2, node 3, ..., node 20

*Nset, nset=Set-3, generate

1, 73302, 1

*Elset, elset=Set-3, generate

1, 59185, 1

** Section: Section-Steel

*Solid Section, elset=Set-3, material=Steel

,

*End Instance

*Instance, name=Adhesive 1-1, part="Adhesive 1"

0., 5., 10.

*Node

Node number, x, y, z

*Element, type=C3D20

Element number, node 1, node 2, node 3, ..., node 20

*Nset, nset=Set-2, generate

1, 18204, 1

*Elset, elset=Set-2, generate

1, 13200, 1

** Section: Adhesive

*Solid Section, elset=Set-2, material="Adhesive"

,

*End Instance

*Instance, name=Adhesive 2-1, part="Adhesive 2"

0., 5., -1

*Node

Node number, x, y, z

*Element, type=C3D20

Element number, node 1, node 2, node 3, ..., node 20

*Nset, nset=Set-3, generate

1, 12432, 1

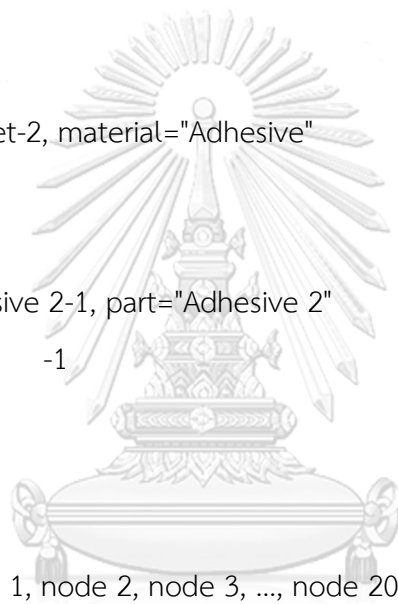
*Elset, elset=Set-3, generate

1, 8910, 1

** Section: Adhesive

*Solid Section, elset=Set-3, material="Adhesive"

,



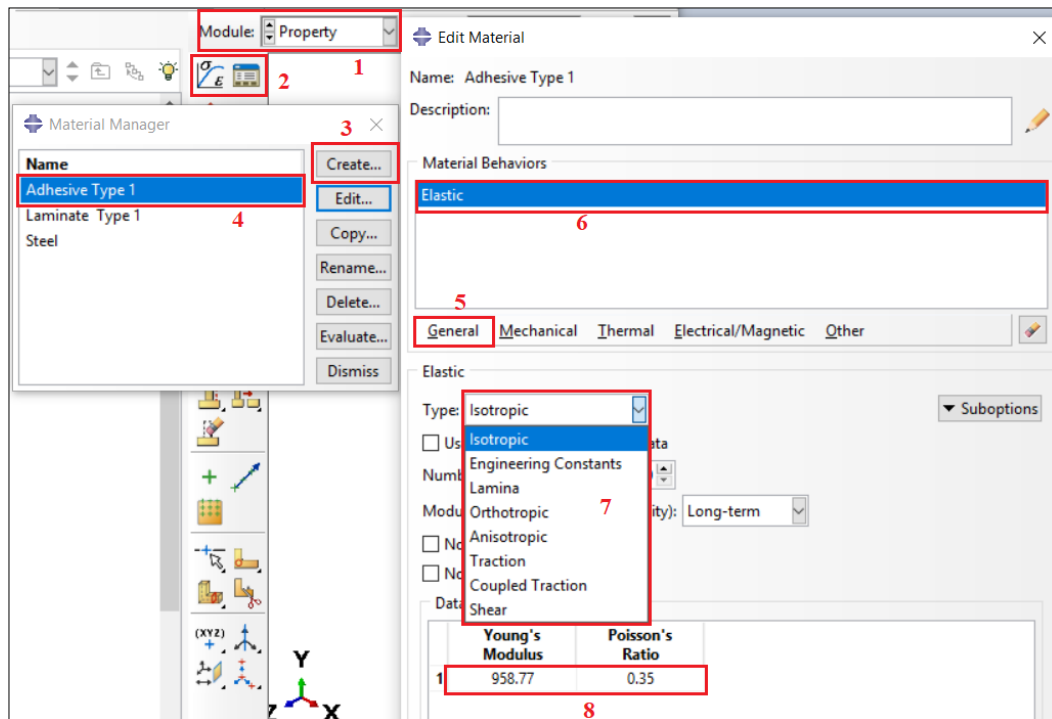


Fig. A.3. Creating steel and adhesive sections.

*End Instance

*Instance, name="CFRP 1-1", part="CFRP 1"

-12., -2.5, 11.

*Node

Node number, x, y, z

*Element, type=SC8R

Element number, node 1, node 2, node 3, ..., node 8

** Region: (CompositeLayup-1-1: Generated from Layup)

*Elset, elset=CompositeLayup-1-1, generate

1, 13200, 1

** Section: CompositeLayup-1

*Shell Section, elset=CompositeLayup-1, composite, stack direction=3,
layup=CompositeLayup-1

0.1, 3, "Laminate", 90., Ply-1

0.1, 3, "Laminate", 90., Ply-2

0.1, 3, "Laminate", 90., Ply-3

0.1, 3, "Laminate", 90., Ply-4
 0.1, 3, "Laminate", 90., Ply-5
 0.1, 3, "Laminate", 90., Ply-6
 0.1, 3, "Laminate", 90., Ply-7
 0.1, 3, "Laminate", 90., Ply-8
 0.1, 3, "Laminate", 90., Ply-9
 0.1, 3, "Laminate", 90., Ply-10
 0.1, 3, "Laminate", 90., Ply-11
 0.1, 3, "Laminate", 90., Ply-12

*End Instance

*Instance, name="CFRP 2-1", part="CFRP 2"

-12., 22.5, -2.2

*Node

Node number, x, y, z

*Element, type=SC8R

Element number, node 1, node 2, node 3, ..., node 8

** Region: (CompositeLayup-1: Generated From Layup)

*Elset, elset=CompositeLayup-1, generate

1, 13200, 1

** Section: CompositeLayup-1

*Shell Section, elset=CompositeLayup-1, composite, stack direction=3,

layup=CompositeLayup-1

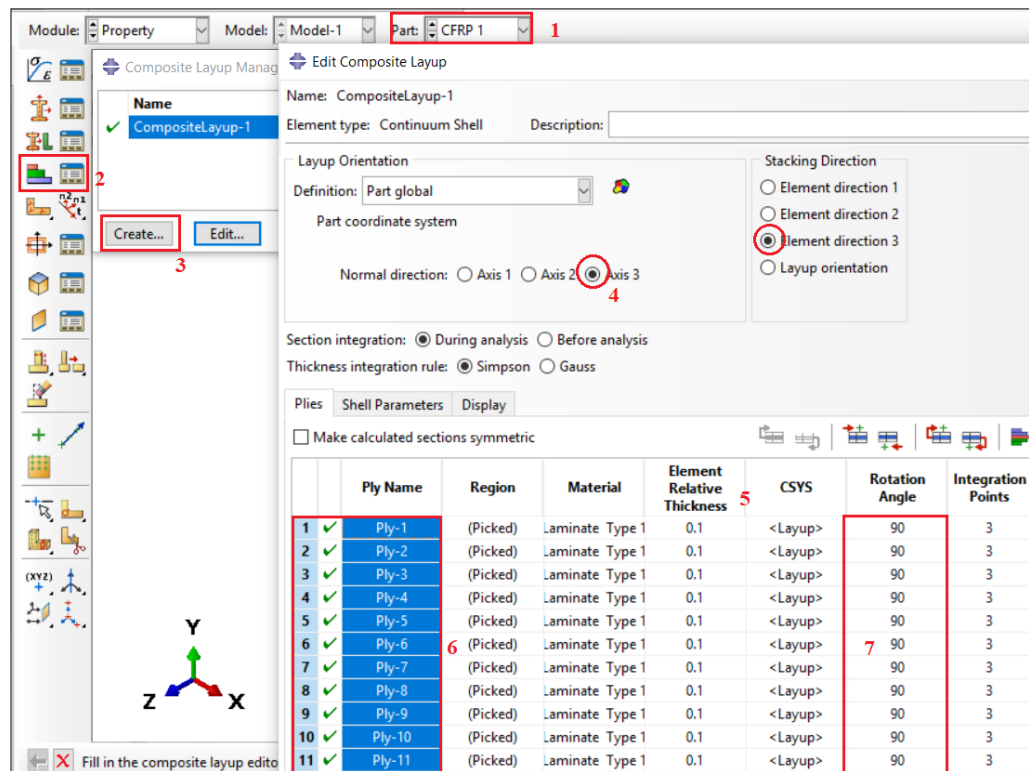
0.1, 3, "Laminate ", 90., Ply-1
 0.1, 3, "Laminate", 90., Ply-2
 0.1, 3, "Laminate", 90., Ply-3
 0.1, 3, "Laminate", 90., Ply-4
 0.1, 3, "Laminate", 90., Ply-5
 0.1, 3, "Laminate", 90., Ply-6
 0.1, 3, "Laminate", 90., Ply-7
 0.1, 3, "Laminate", 90., Ply-8
 0.1, 3, "Laminate", 90., Ply-9

0.1, 3, "Laminate", 90., Ply-10

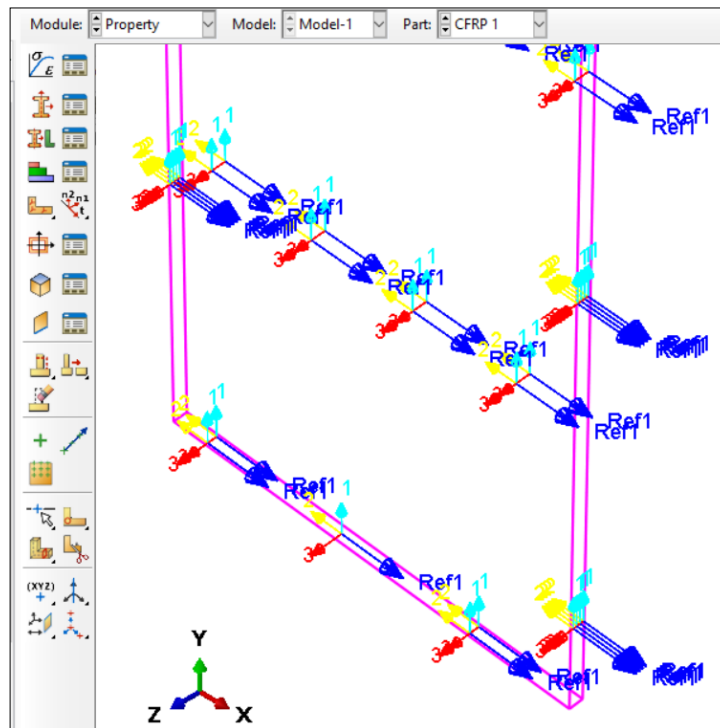
0.1, 3, "Laminate", 90., Ply-11

0.1, 3, "Laminate", 90., Ply-12

*End Instance



(a) Define the stacking direction and ply orientation for FRP patch



(b) Local coordinate of FRP path

Fig. A.4. Creating composite layup for FRP patch.

Step 4: Create sets of FE model

Example for Set-4

*Nset, nset=Set-4, instance="Steel plate-1"

node 1, node 2,....

*Nset, nset=Set-4, instance=Adhesive 1-1

node 1, node 2,....

*Nset, nset=Set-4, instance="CFRP 1-1", generate

node 1, node 2,....

*Nset, nset=Set-4, instance=Adhesive 2-1, generate

node 1, node 2,....

*Nset, nset=Set-4, instance="CFRP 2-1", generate

node 1, node 2,....

*Elset, elset=Set-4, instance="Steel plate-1"

element 1, element 2,....

*Elset, elset=Set-4, instance=Adhesive 1-1

element 1, element 2,....

*Elset, elset=Set-4, instance="CFRP 1-1", generate

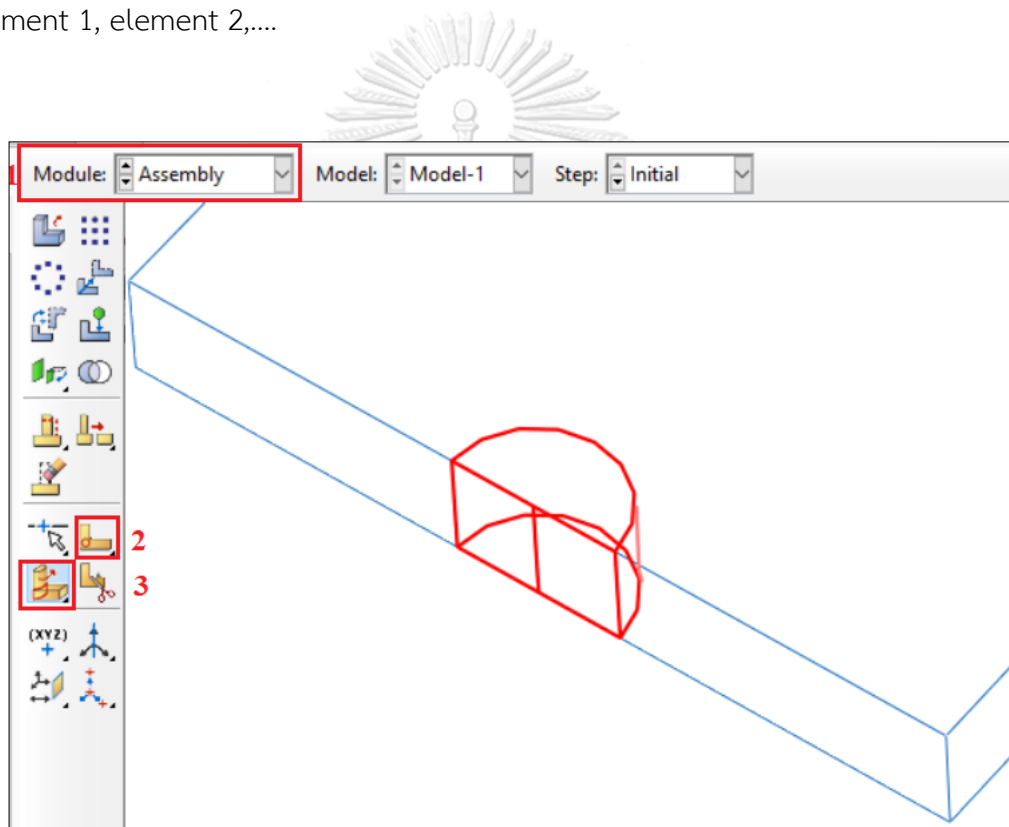
element 1, element 2,....

*Elset, elset=Set-4, instance=Adhesive 2-1, generate

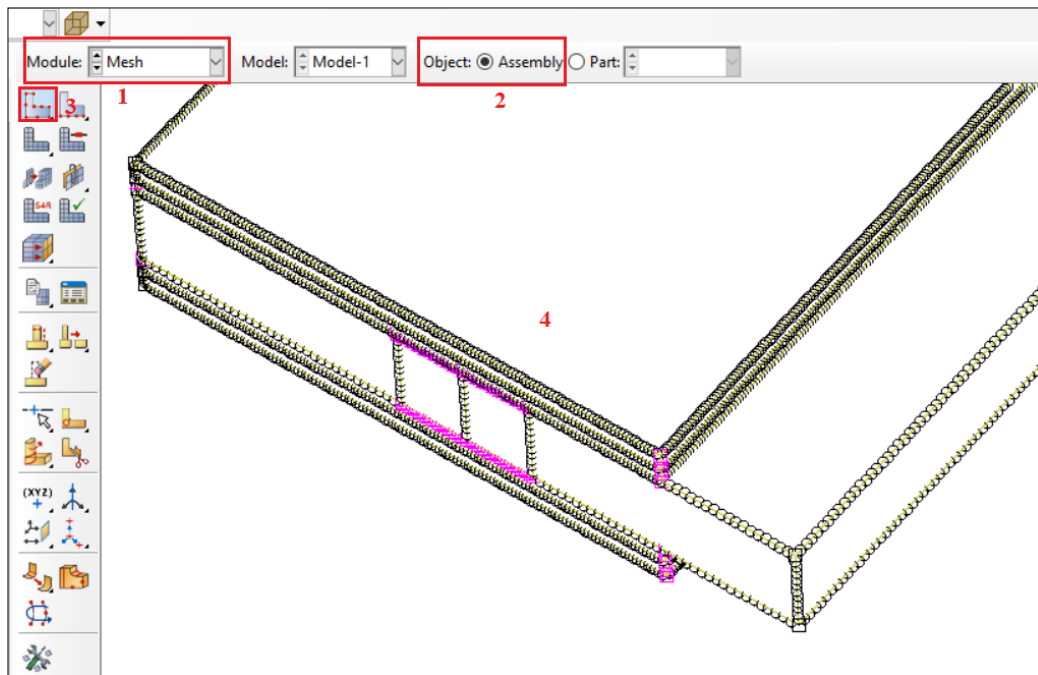
element 1, element 2,....

*Elset, elset=Set-4, instance="CFRP 2-1", generate

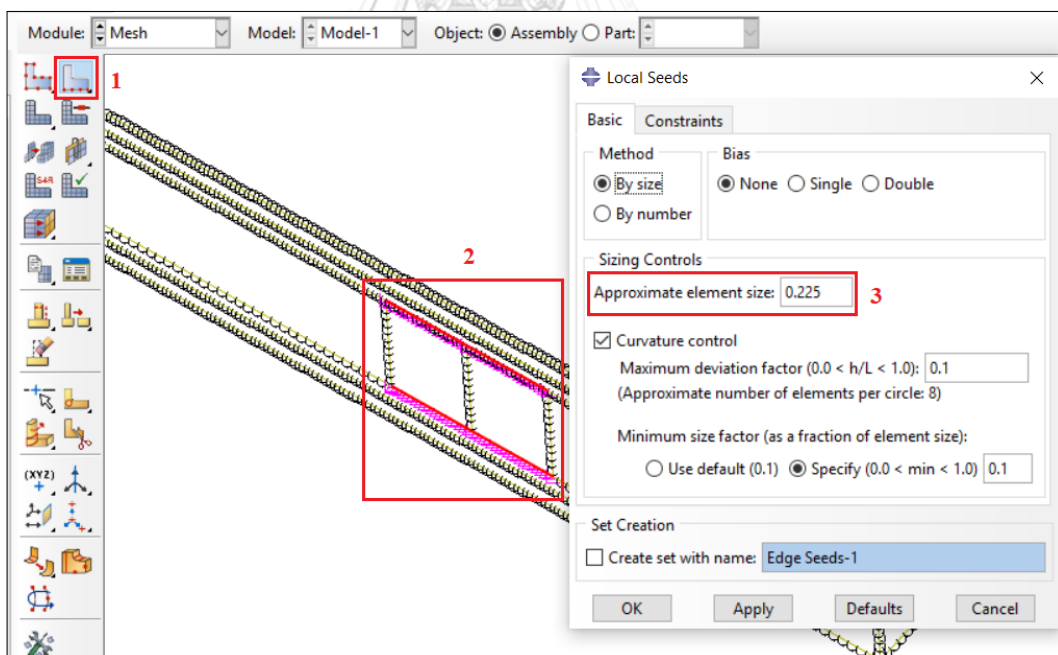
element 1, element 2,....



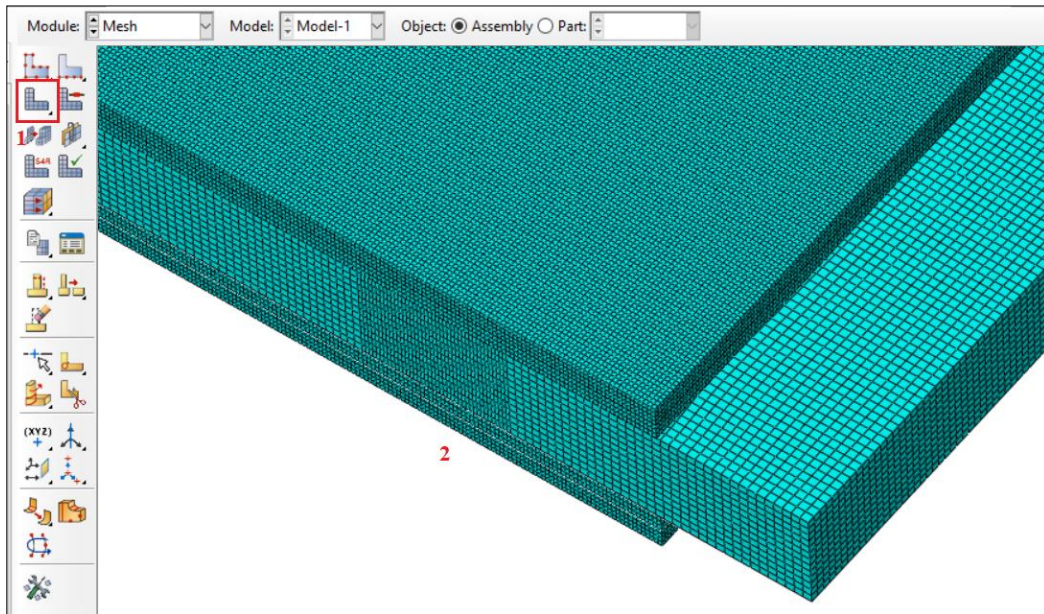
(a) Creating mesh instance for crack front region



(b) Define global mesh size for each part



(c) Define crack mesh size of front elements



(d) Meshed model of repaired plate

Fig. A.5. Meshing FE model.

Step 5: Define surfaces

Four adhesive surfaces: Surf-Adhesive1_1, Surf-Adhesive1_2, Surf-Adhesive2_1, and Surf-Adhesive2_2.

```
*Elset, elset=_Surf-Adhesive1_1_S1, internal, instance=Adhesive 1-1, generate
1, 4400, 1
```

```
*Surface, type=ELEMENT, name=Surf-Adhesive1_1
_Surf-Adhesive1_1_S1, S1
```

```
*Elset, elset=_Surf-Adhesive1_2_S2, internal, instance=Adhesive 1-1, generate
8801, 13200, 1
```

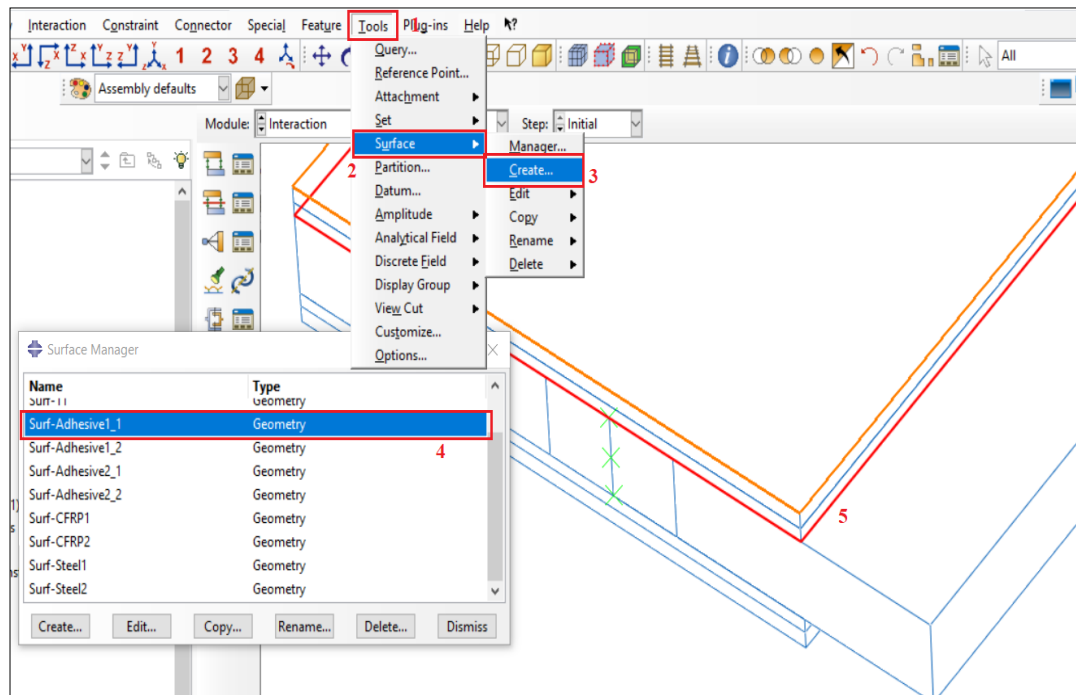


Fig. A.6. Defining surfaces for tie constraints.

*Surface, type=ELEMENT, name=Surf-Adhesive1_2
_Surf-Adhesive1_2_S2, S2

*Elset, elset=_Surf-Adhesive2_1_S2, internal, instance=Adhesive 2-1, generate
5941, 8910, 1

*Surface, type=ELEMENT, name=Surf-Adhesive2_1
_Surf-Adhesive2_1_S2, S2

*Elset, elset=_Surf-Adhesive2_2_S1, internal, instance=Adhesive 2-1, generate
1, 2970, 1

*Surface, type=ELEMENT, name=Surf-Adhesive2_2
_Surf-Adhesive2_2_S1, S1

Two patch surfaces: CFRP 1-1 and CFRP 2-1

*Elset, elset=_Surf-CFRP1_S1, internal, instance="CFRP 1-1", generate
1, 4400, 1

*Surface, type=ELEMENT, name=Surf-CFRP1
_Surf-CFRP1_S1, S1

```

*Elset, elset=_Surf-CFRP2_S2, internal, instance="CFRP 2-1", generate
8801, 13200, 1
*Surface, type=ELEMENT, name=Surf-CFRP2
_Surf-CFRP2_S2, S2
*Elset, elset=_Surf-Steel1_S6, internal, instance="Steel plate-1"
element 1, element 2,...
*Elset, elset=_Surf-Steel1_S4, internal, instance="Steel plate-1"
element 1, element 2,...
*Elset, elset=_Surf-Steel1_S2, internal, instance="Steel plate-1"
element 1, element 2,...
*Surface, type=ELEMENT, name=Surf-Steel1
_Surf-Steel1_S6, S6
_Surf-Steel1_S4, S4
_Surf-Steel1_S2, S2
*Elset, elset=_Surf-Steel2_S1, internal, instance="Steel plate-1"
element 1, element 2,...
*Elset, elset=_Surf-Steel2_S4, internal, instance="Steel plate-1"
element 1, element 2,...
*Elset, elset=_Surf-Steel2_S6, internal, instance="Steel plate-1"
element 1, element 2,...
*Surface, type=ELEMENT, name=Surf-Steel2
_Surf-Steel2_S1, S1
_Surf-Steel2_S4, S4
_Surf-Steel2_S6, S6

```

Step 6: Define tie constraints

```

** Constraint: Constraint-1
*Tie, name=Constraint-1, adjust=yes
Surf-Adhesive1_1, Surf-Steel1
** Constraint: Constraint-2

```

*Tie, name=Constraint-2, adjust=yes

Surf-Adhesive2_1, Surf-Steel2

** Constraint: Constraint-3

*Tie, name=Constraint-3, adjust=yes

Surf-CFRP1, Surf-Adhesive1_2

** Constraint: Constraint-4

*Tie, name=Constraint-4, adjust=yes

Surf-CFRP2, Surf-Adhesive2_2

*End Assembly

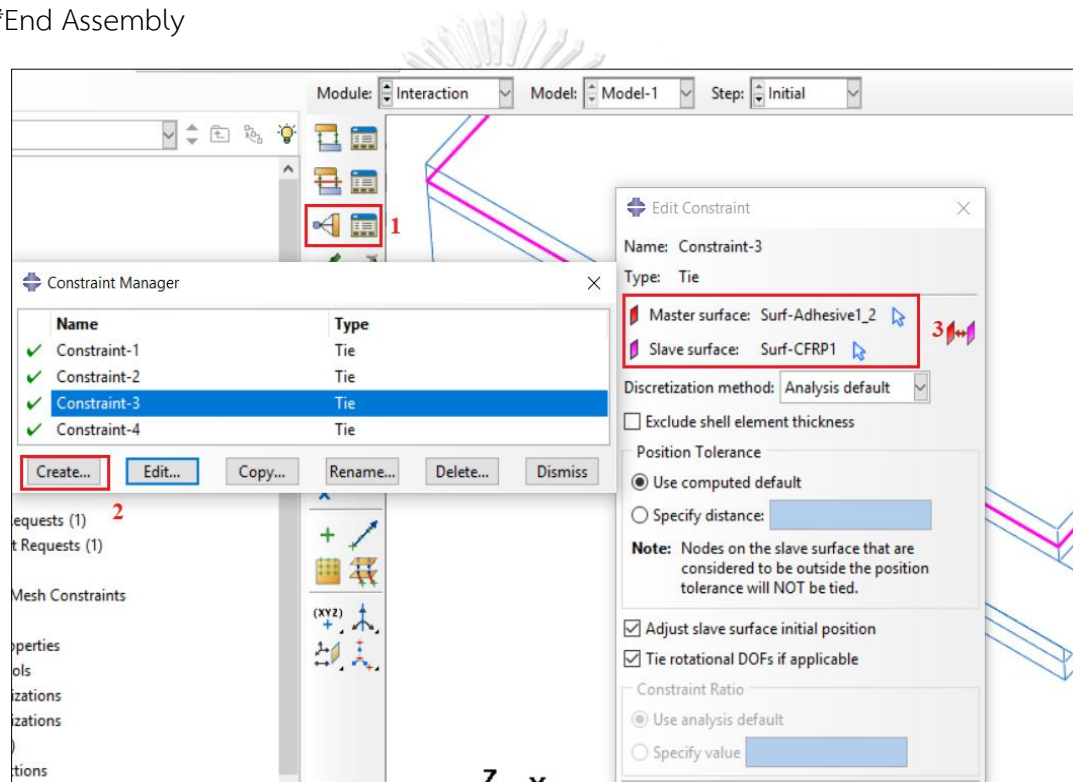


Fig. A.7. Creating four tie constraints.

Step 7: Material properties

** MATERIALS

*Material, name="Adhesive Type1"

*Elastic

958.77, 0.35

*Material, name="Laminate Type1"

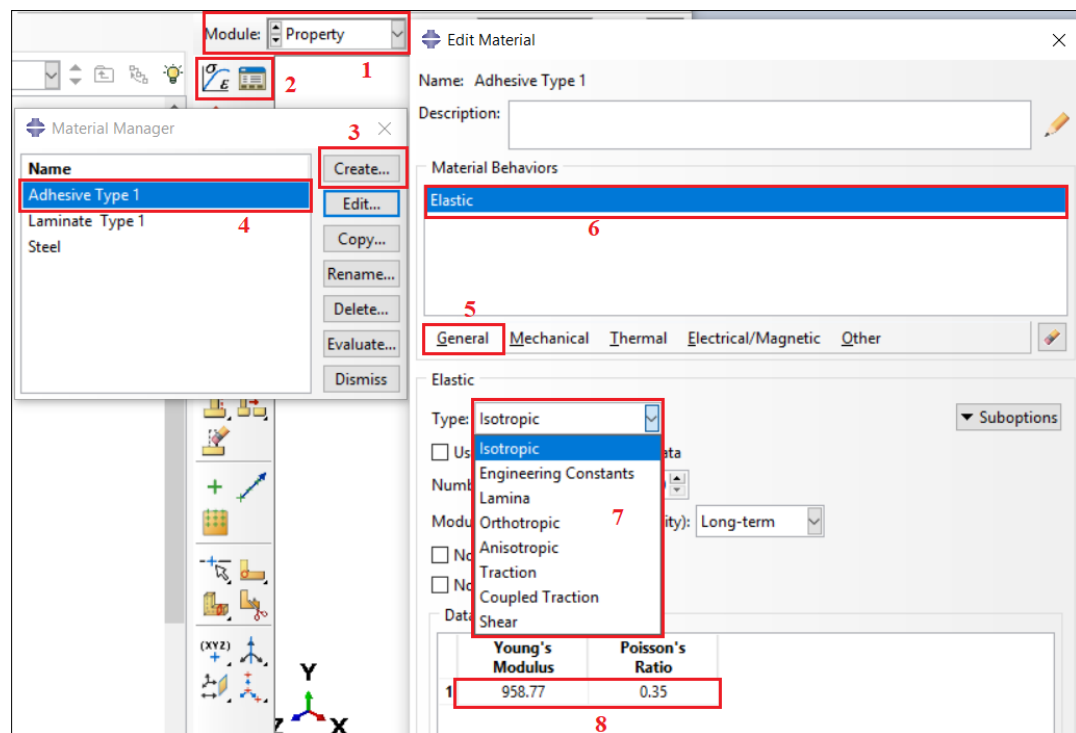
*Elastic, type=LAMINA

210000.,8000.,0.3,5000.,5000.,5000.

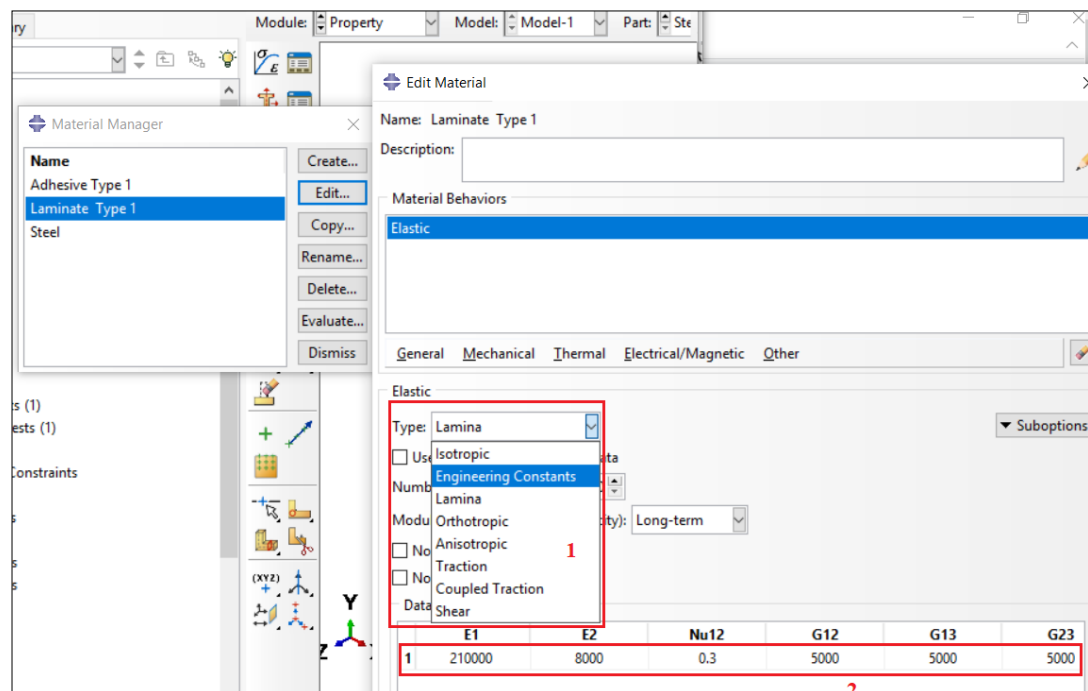
*Material, name=Steel

*Elastic

200000., 0.3



(a) Adhesive material properties



(b) FRP patch material properties

*Fig. A.8. Material properties.***Step 8: Boundary conditions**

** BOUNDARY CONDITIONS

** Name: BC-1 Type: Symmetry/Antisymmetry/Encastre

*Boundary

Set-4, XSYMM

** Name: BC-2 Type: Symmetry/Antisymmetry/Encastre

*Boundary

Set-5, YSYMM

** Name: BC-3 Type: Displacement/Rotation

*Boundary

Set-6, 3, 3

Set-6, 4, 4

Set-6, 5, 5

Set-6, 6, 6

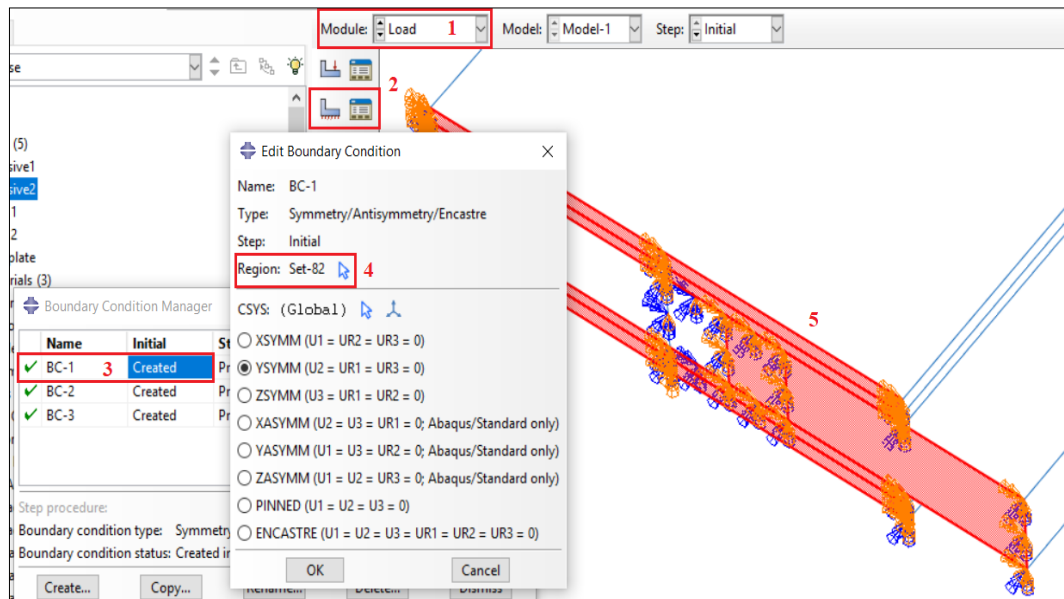


Fig. A.9. Assigning boundary conditions.

Step 9: Analysis step

** STEP: Step-1

*Step, name=Step-1, ngeom=NO

*Static

0.01, 1., 1e-06, 1.

Step 10: Assign loads

** LOADS

** Name: Load-1 Type: Pressure

*Dsload

Surf-11, P, -55.

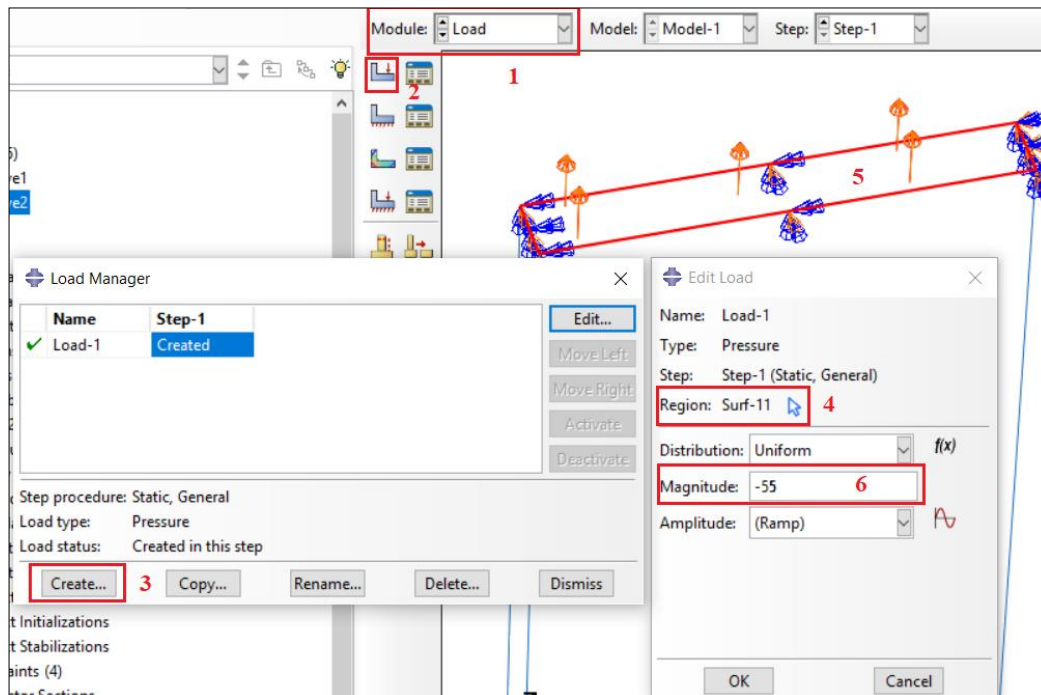


Fig. A.10. Creating tension load.

Step 11: Stress intensity factor extraction

** OUTPUT REQUESTS

*Restart, write, frequency=0

** FIELD OUTPUT: F-Output-1

*Output, field, variable=PRESELECT

*Output, history, frequency=0

** HISTORY OUTPUT: H-Output-1

*Contour Integral, crack name=H-Output-1_Crack-1, contours=5, crack tip nodes, type=K FACTORS, direction=MERR, symm

PickedSet219-1, _PickedSet220-1_, 1., 0., 0.

PickedSet219-2, _PickedSet220-2_, 1., 0., 0.

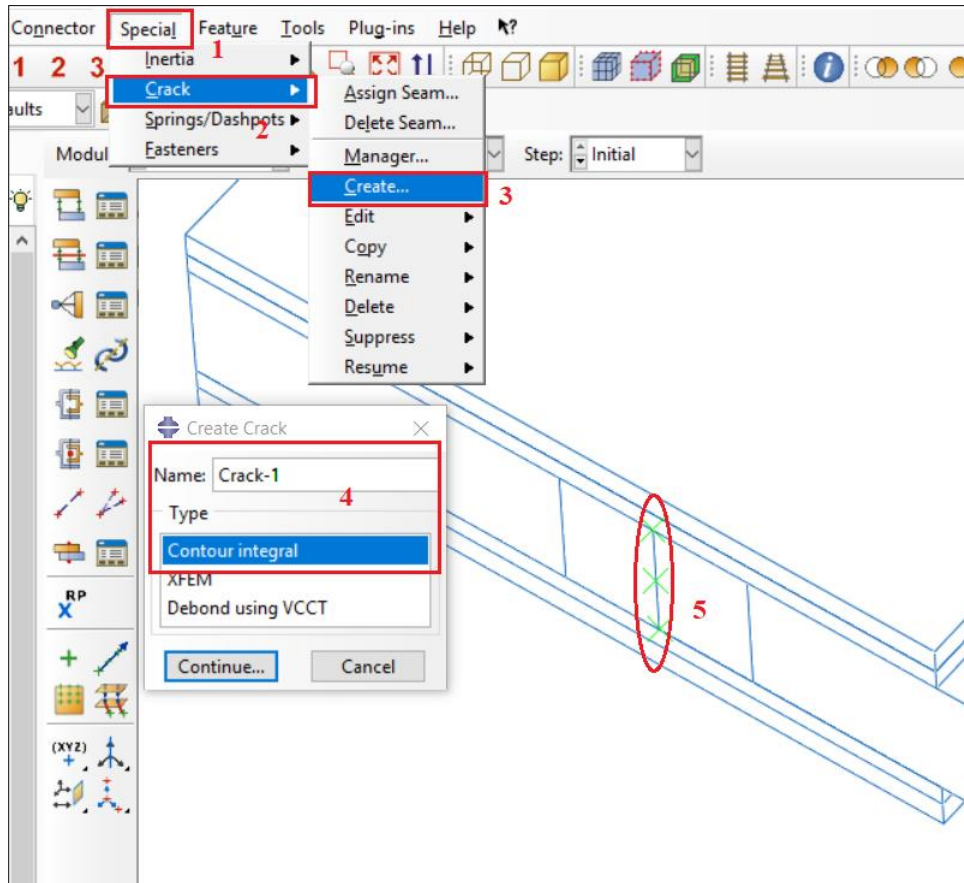
PickedSet219-3, _PickedSet220-3_, 1., 0., 0.

PickedSet219-4, _PickedSet220-4_, 1., 0., 0.

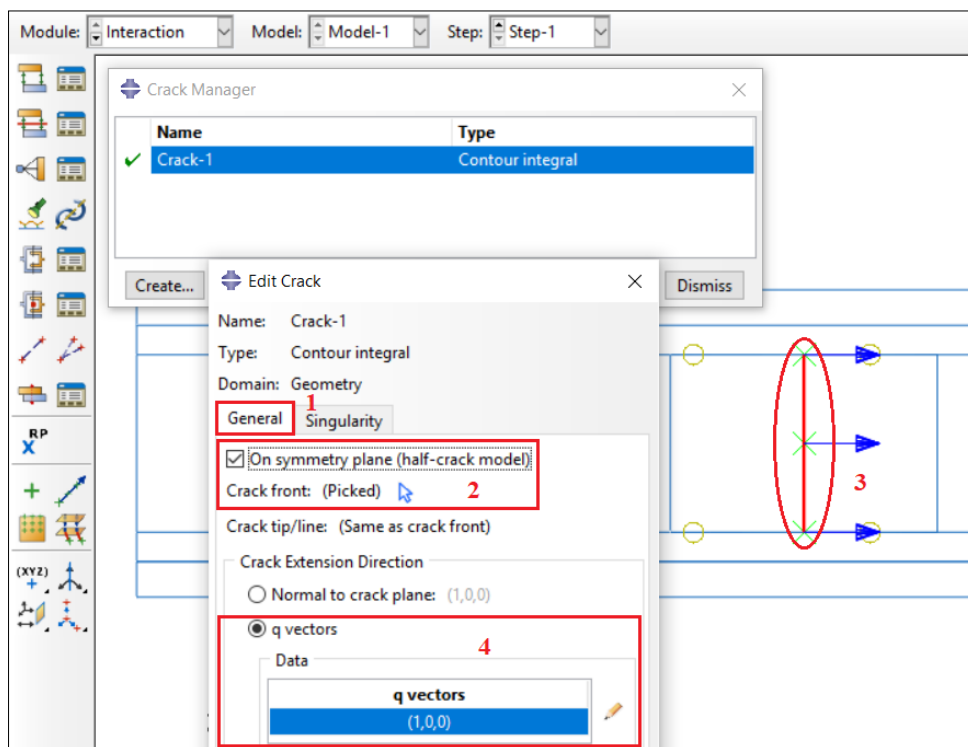
PickedSet219-5, _PickedSet220-5_, 1., 0., 0.

PickedSet219-6, _PickedSet220-6_, 1., 0., 0.

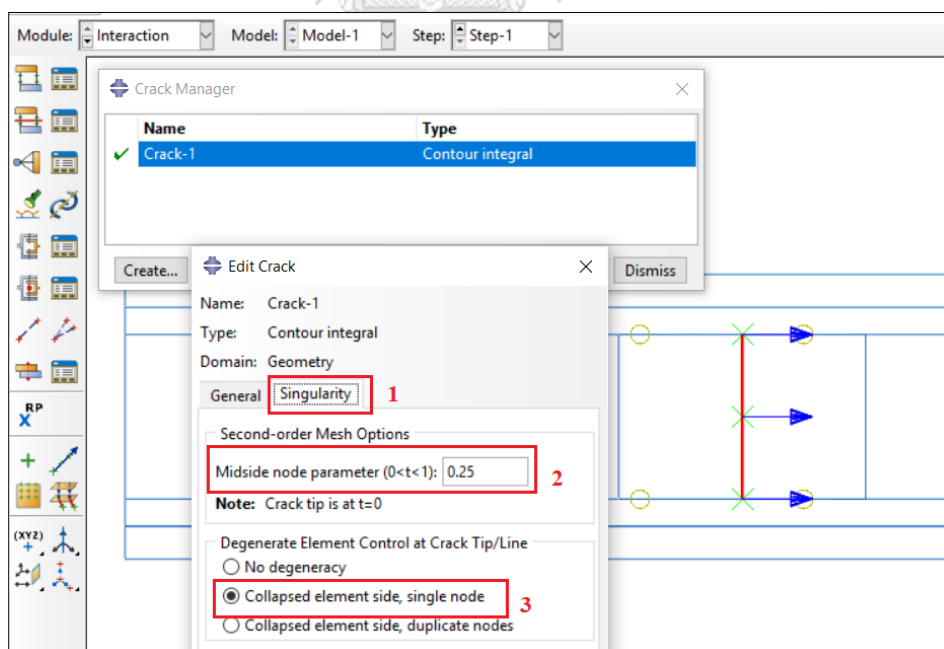
*End Step



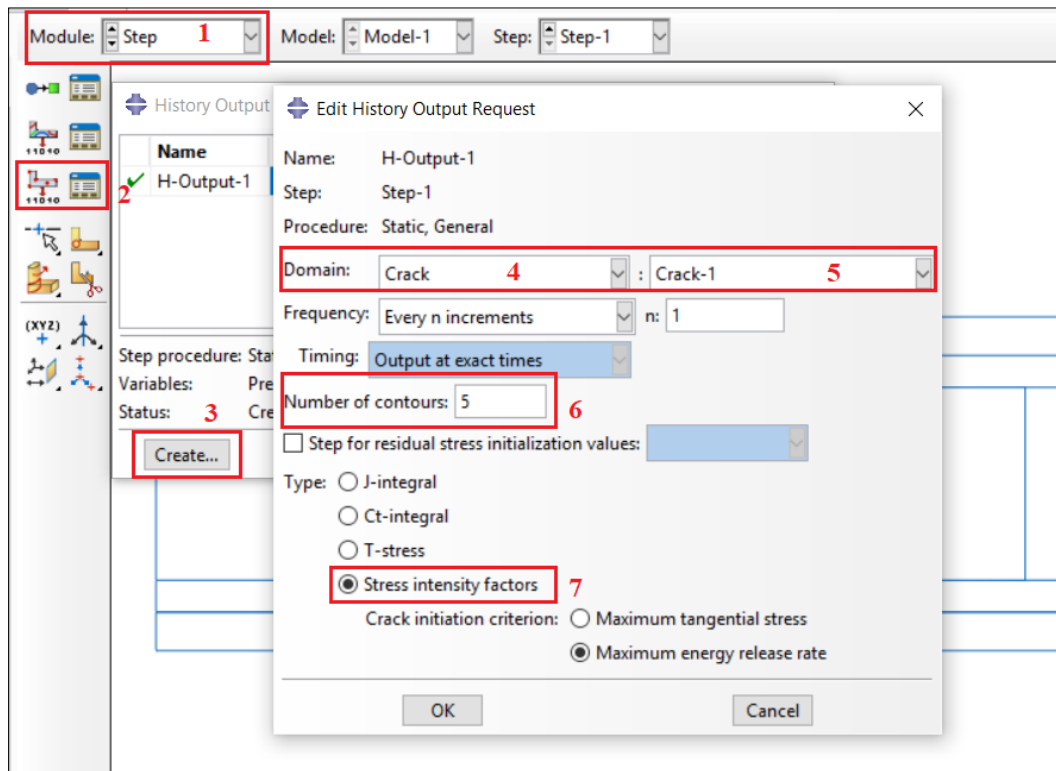
(a) Assign crack front



(b) Define crack extension direction (q vector)



(c) Assign collapsed element



(d) SIF output

Fig. A.11. Creating a crack and SIF output.

APPENDIX B

COMPARISON OF FINITE ELEMENT WITH PREVIOUS FE STUDY RESULTS

Tables B.1, B.2, and B.3 are comparisons between SIF values obtained from ABAQUS for both unrepaired and repaired cases (with a single-sided and a double-sided patch) and corresponding previous FE study results, respectively. Visualizations of the information in these tables correspond to Figs. 4.6, 4.7, and 4.8 in section 4.3.

Table B.1 Comparison of SIF from FE and handbook solutions [12] (unrepaired).

$2a/W_s$	Plate 1			Plate 2		
	SIF, FE MPa mm ^{1/2}	SIF, [12] MPa mm ^{1/2}	Diff. %	SIF, FE MPa mm ^{1/2}	SIF, [12] MPa mm ^{1/2}	Diff. %
0.1	570.13	567.36	0.49	800.77	802.36	0.20
0.2	823.54	817.13	0.78	1156.67	1155.60	0.09
0.3	1033.67	1033.06	0.06	1463.67	1460.97	0.18
0.4	1250.67	1250.99	0.03	1765.33	1769.16	0.22
0.5	1493.33	1495.99	0.18	2110.63	2115.65	0.24
0.6	1795.33	1799.73	0.24	2538.67	2545.20	0.26
0.7	2212.00	2219.39	0.33	3128.00	3138.69	0.34
0.8	2880.00	2894.24	0.49	4072.67	4093.08	0.50
0.9	4345.87	4359.64	0.32	6111.44	6165.47	0.88

Table B.2 Comparison of SIF from FE and solutions [13] (one-sided patch).

$2a/W_s$	Boron/epoxy				Graphite/epoxy					
	SIF,	FE	SIF,	[13]	Diff.	SIF,	FE	SIF,	[13]	Diff.
	MPa m ^{1/2}		MPa m ^{1/2}		%	MPa m ^{1/2}		MPa m ^{1/2}		%
0.1	12.45		12.50		0.40	12.01		12.25		1.99
0.2	15.64		16.13		3.04	16.98		17.25		1.57
0.3	17.98		18.25		1.47	19.06		19.50		2.32
0.4	19.56		20.00		2.18	21.12		21.25		0.64
0.5	21.86		21.50		1.67	22.94		23.25		1.35
0.6	24.51		24.00		2.13	24.97		24.75		0.87

Table B.3 Comparison of SIF from FE results and solutions [11] (two-sided patch).

Patch shape	Patch dimensions			SIF,	FE	SIF,	[11]	Diff.
	W_p	L_p	t_p	MPa m ^{1/2}		MPa m ^{1/2}		%
	(mm)	(mm)	(mm)					
Rectangular	72	24	2.25	5.33		5.33		0.14
	72	36	2.25	4.05		3.95		2.53
	72	48	2.25	3.77		3.65		3.16
	48	48	2.25	4.38		4.35		0.64
	72	48	2.25	3.77		3.65		3.16
	96	48	2.25	3.53		3.40		3.86
Square	60	60	2.25	4.08		4.03		1.22
	72	72	2.25	3.95		3.91		1.06
	84	84	2.25	3.85		3.78		2.11
	72	72	1.50	5.26		5.30		0.80
	84	84	1.50	5.16		5.13		0.60
	96	96	1.50	5.06		4.98		1.62

APPENDIX C

VERIFICATION OF CLOSED-FORM SIF SOLUTION

The following four tables are comparisons between proposed SIF solutions and FE results for four verification cases in Table 5.6. Visualizations of the information in these tables correspond to Figs. 5.4a), b), c), and d) in section 5.4.

Table C.1 Comparison of the proposed F_2 solution and ABAQUS for case 1.

$2a/W_s$	F_2 , plate 3			F_2 , plate 4		
	Eq. (5.5)	FE	error (%)	Eq. (5.5)	FE	error (%)
0.1	0.718	0.718	0.04	0.715	0.713	0.34
0.2	0.658	0.680	3.32	0.655	0.659	0.66
0.3	0.599	0.575	4.12	0.596	0.598	0.35
0.4	0.541	0.532	1.61	0.538	0.541	0.65
0.5	0.483	0.462	4.57	0.480	0.486	1.37
0.6	0.425	0.425	0.04	0.422	0.432	2.19
0.7	0.368	0.383	3.81	0.365	0.383	4.57
0.8	0.311	0.331	6.05	0.308	0.318	3.28
0.9	0.254	0.264	3.53	0.251	0.267	5.99

Table C.2 Comparison of the proposed F_2 solution and ABAQUS for case 2.

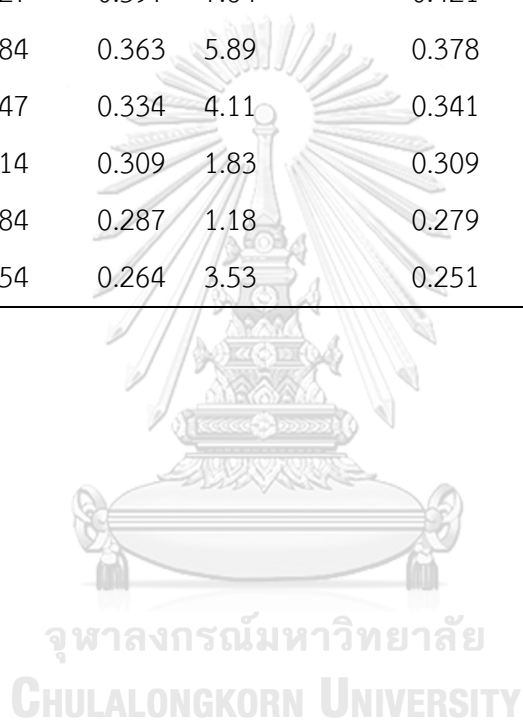
$L_p / 2a$	F_2 , plate 3			F_2 , plate 4		
	Eq. (5.5)	FE	error (%)	Eq. (5.5)	FE	error (%)
1	0.630	0.657	4.16	0.614	0.569	8.01
4	0.489	0.519	5.84	0.473	0.486	2.66
7	0.483	0.506	4.52	0.467	0.483	3.19
10	0.483	0.506	4.55	0.467	0.483	3.25
13	0.483	0.506	4.55	0.467	0.483	3.25
16	0.483	0.506	4.55	0.467	0.483	3.25

Table C.3 Comparison of the proposed F_2 solution and ABAQUS for case 3.

W_p / W_s	F_2 , plate 3			F_2 , plate 4		
	$2a = 0.5W_s$			$2a = 0.5W_s$		
	Eq. (5.5)	FE	error (%)	Eq. (5.5)	FE	error (%)
0.2	0.754	0.732	3.03	0.756	0.762	0.78
0.3	0.693	0.667	3.92	0.691	0.685	0.96
0.4	0.643	0.621	3.66	0.639	0.621	2.96
0.5	0.603	0.590	2.22	0.598	0.574	4.14
0.6	0.571	0.571	0.04	0.565	0.549	2.97
0.7	0.544	0.556	2.12	0.538	0.530	1.66
0.8	0.521	0.542	3.86	0.516	0.513	0.56
0.9	0.501	0.529	5.32	0.497	0.499	0.37
1.0	0.483	0.517	6.63	0.480	0.486	1.37

Table C.4 Comparison of the proposed F_2 solution and ABAQUS for case 4.

W_p/W_s	F_2 , plate 3			F_2 , plate 4		
	$2a = 0.9W_s$			$2a = 0.9W_s$		
	Eq. (5.5)	FE	error (%)	Eq. (5.5)	FE	error (%)
0.2	0.621	0.645	3.64	0.622	0.648	3.97
0.3	0.543	0.510	6.63	0.540	0.503	7.44
0.4	0.479	0.437	9.60	0.474	0.438	8.28
0.5	0.427	0.397	7.64	0.421	0.378	11.46
0.6	0.384	0.363	5.89	0.378	0.341	10.68
0.7	0.347	0.334	4.11	0.341	0.303	12.56
0.8	0.314	0.309	1.83	0.309	0.297	4.18
0.9	0.284	0.287	1.18	0.279	0.273	2.26
1.0	0.254	0.264	3.53	0.251	0.267	5.99




APPENDIX D

SYMBOLIC REGRESSION VIA GENETIC PROGRAMMING IN HEURISTICLAB

Step 1: Data preparation

The input for GP analyses in this study is a database containing five columns, as shown in Fig. D.1. $x_1 - x_4$ are variables given in Eq. (5.4) and y is the correction factor F_2 . A comma separated values text file (.csv) with Excel is used as the input file.



	A	B	C	D	E
1	x1	x2	x3	x4	y
2	0.5	0.6	1	0.4216	0.72171
3	0.1	0.6	1	1.53636	0.98415
4	0.5	1	10	1.53493	0.28053
5	0.9	1	10	1.53493	0.12864
6	0.1	1	1	0.42302	0.97663
7	0.1	1	5	0.4216	0.88577
8	0.5	0.2	16	1.53636	0.93695
9	0.5	0.2	5	1.53493	0.94831
10	0.5	0.6	5	1.53824	0.30991

Fig. D.1. Database for GP analyses.

CHULALONGKORN UNIVERSITY

Step 2: Start HeuristicLab > Select Genetic Programming Symbolic Regression.

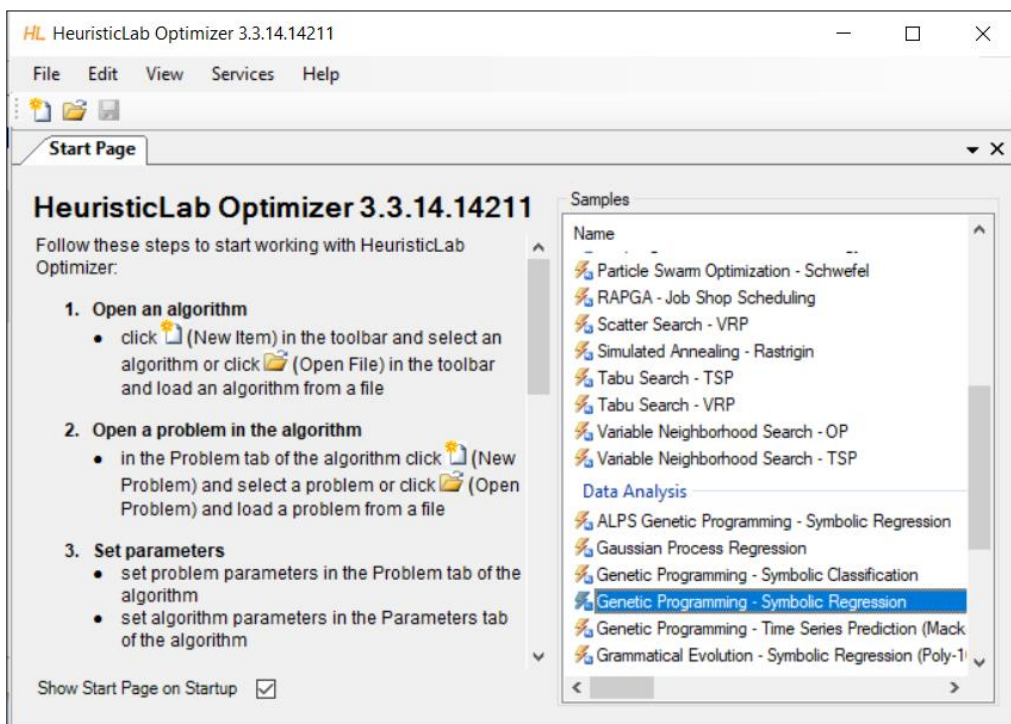


Fig. D.2. Starting HeuristicLab.

Step 3: Load the database > Shuffle the data > Define the target variable, as shown in Fig. D.2.

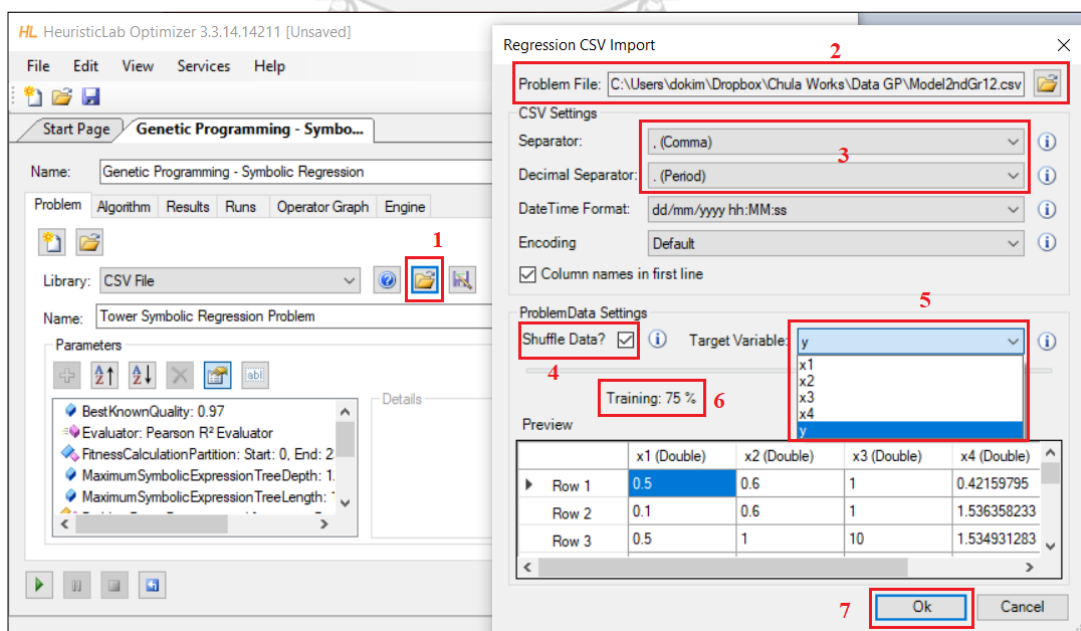


Fig. D.3. Import the database and define the target variable in HeuristicLab.

Step 4: Define the maximum numbers of tree depth (10) and tree length (30), as mentioned in Table 5.2 > Define the function and terminal sets for the GP analysis, detailed in Figs. D.3 and D.4.

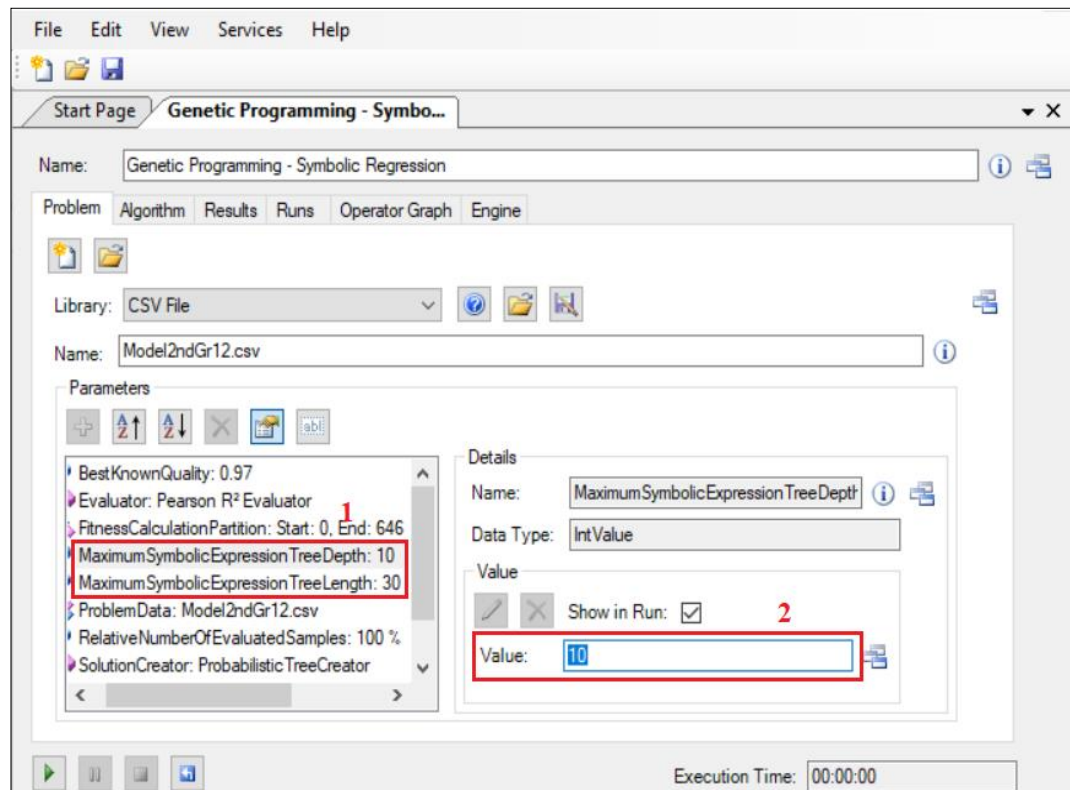


Fig. D.4. Define the maximum numbers of tree depth and tree length.

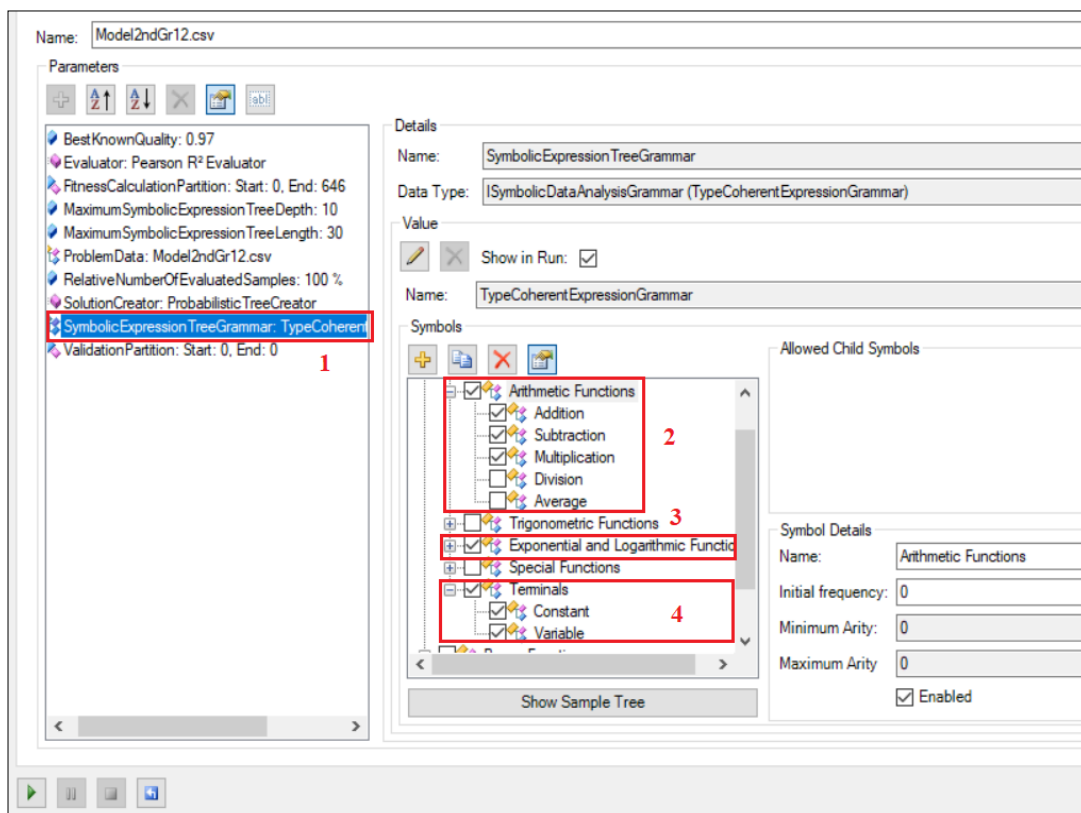


Fig. D.5. Definite function and terminal sets for GP.

Step 5: Define some control parameters for GP algorithm such as a number of the elites, mutation probability, GP population size, maximum number of GP generations, and run the program, detailed in Fig. D.5.

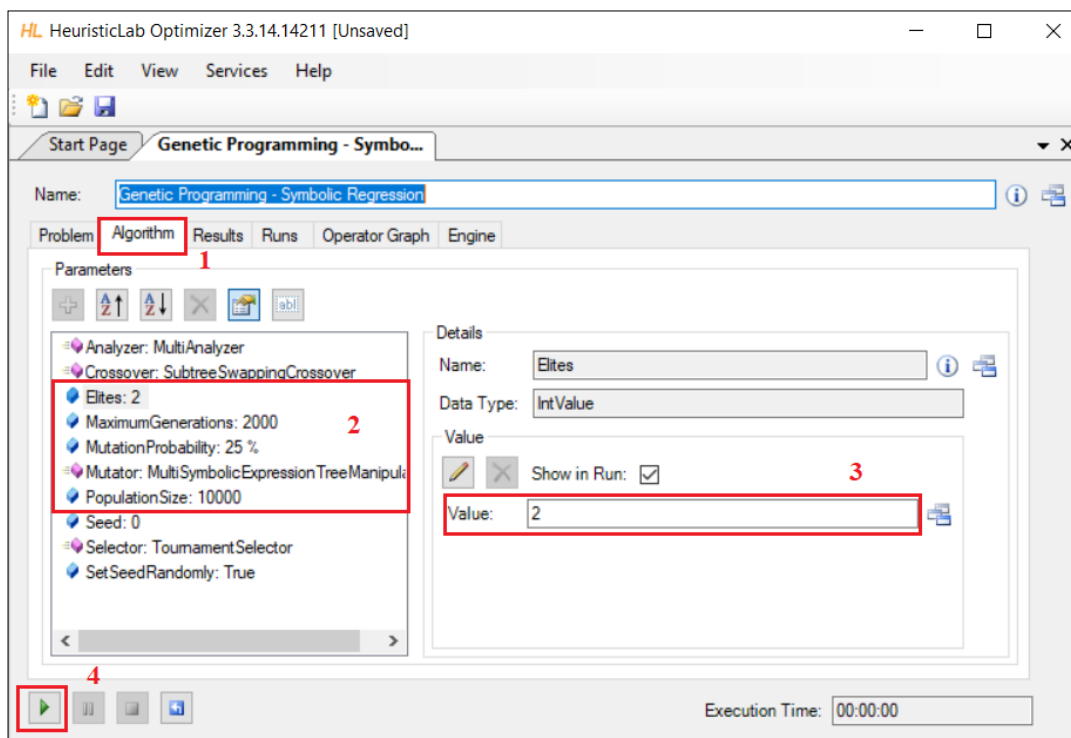


Fig. D.6. Define some control parameters for GP algorithm.

APPENDIX E

OPTIMIZATION SOLVERS IN MATLAB

E.1. Genetic algorithm

In this study, the “options”, mentioned in section 3.6, for GA is described as the following MATLAB commands.

```

%% Start with the default options
options = gaoptimset;

%% creates a structure called options that contains the parameters
%% for the genetic algorithm and sets parameters to [], indicating
%% default values will be used

%% Modify options setting
options = gaoptimset(options, 'PopulationSize', PopulationSize_Data);
options = gaoptimset(options, 'EliteCount', EliteCount_Data);
options = gaoptimset(options, 'Generations', Generations_Data);
options = gaoptimset(options, 'TolFun', TolFun_Data);
options = gaoptimset(options, 'TolCon', TolCon_Data);
options = ...
gaoptimset(options, 'InitialPopulation', InitialPopulation_Data);
options = gaoptimset(options, 'SelectionFcn', @selectionroulette);

%% including the population size (PopulationSize), number of elite
%% strings (EliteCount), maximum number of generations (Generations),
%% function and constraint tolerances (TolFun and TolCon), vector
%% specifying the range of the individuals in the initial population
%% (InitialPopulation), and selection function (@selectionroulette).

%% Plot option
options = gaoptimset(options, 'PlotFcns', {@gaplotbestf});

%% GA command
[x, fval] = ...
ga(@VolumeFun, nvars, [], [], [], [], lb, ub, @NonlconstraintFun, [], options);

%% x           : solution vector
%% fval        : objective function value at the solution
%% @VolumeFun  : objective function (patch volume function)
%% nvars       : number of design parameters
%% lb          : lower bound vector of design parameters
%% ub          : upper bound vector of design parameters
%% @NonlconstraintFun : nonlinear constraint function (SIF)

```

E.2. Nonlinear programming

The “options” in section 3.6 for nonlinear programming is described as the following MATLAB commands.

```

%% Start with the default options, detailed in reference [76]
options = optimoptions('fmincon');

%% Modify options setting
options = optimoptions(options, 'Display', 'iter');
options = optimoptions(options, 'TolFun', TolFun_Data);
options = optimoptions(options, 'TolX', TolX_Data);
options = optimoptions(options, 'PlotFcns', {@optimplotfval ...
@optimplotfirstorderopt });
options = optimoptions(options, 'MaxProjCGIter', MaxProjCGIter_Data);
options = optimoptions(options, 'TolCon', TolCon_Data);
options = optimoptions(options, 'TolProjCG', TolProjCG_Data);
options = optimoptions(options, 'TolProjCGAbs', TolProjCGAbs_Data);

%% 'Display','iter': displays output at each iteration, and gives the
%% default exit message
%% TolFun, TolX, and TolCon: function, variable, and constraint
%% tolerances
%% 'PlotFcns',{@optimplotfval @optimplotfirstorderopt}: plot the
%% function value and maximum constraint violation
%% TolProjCG: a stopping criterion for projected conjugate gradient
%% algorithm
%% TolProjCGAbs: a stopping criterion for projected conjugate
%% gradient algorithm

%% nonlinear programming command
[x,fval] = ...
fmincon(@VolumeFun,x0,[],[],[],[],lb,ub,@NonlconstraintFun,options);

%% x           : solution vector
%% fval        : objective function value at the solution
%% @VolumeFun  : objective function (patch volume function)
%% x0         : initial point to start the algorithm
%% lb         : lower bound vector of design parameters
%% ub         : upper bound vector of design parameters
%% @NonlconstraintFun : nonlinear constraint function (SIF)

```

E.3. A comparison between GA and nonlinear programming solutions

A comparison between the optimum solutions of Rastrigin's function obtained from GA and nonlinear programming is presented. Rastrigin's function has many local minima and a global minimum at (0,0) [76], as follow:

$$Ras(x_1, x_2) = 20 + x_1^2 + x_2^2 - 10(\cos 2\pi x_1 + \cos 2\pi x_2) \quad (E.1)$$

The following are MATLAB commands and solutions for both GA and nonlinear programming solvers. Note that these solvers start at (20,30), which is quite far from the global minimum (0,0).

GA commands:

```
>> rf2 = @(x)rastriginsfcn(x/10); % objective function
>> x0 = [20,30]; % start point away from the minimum
>> initpop = 10*randn(20,2) + repmat([10 30],20,1);
>> opts =gaoptimset('InitialPopulation',initpop);
>> [x,feval] = ga(rf2,2,[],[],[],[],[],[],[],[],opts);
```

GA solution:

```
x =
   -0.0173    0.0443
feval =
    0.0045
```

Nonlinear programming commands:

```
>> rf2 = @(x)rastriginsfcn(x/10); % objective function
>> x0 = [20,30]; % start point away from the minimum
>> [x,feval] = fmincon(rf2,x0)
```

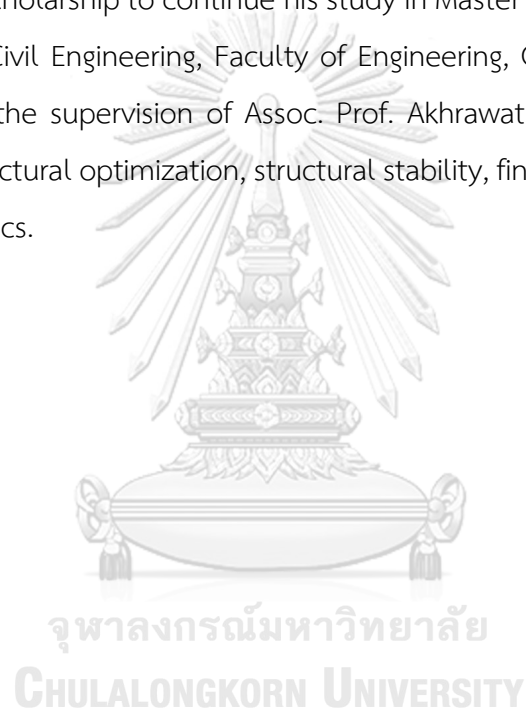
Nonlinear programming solution:

```
x =
   19.8991   29.8486
feval =
   12.9344
```

The above results show that GA works better than nonlinear programming for Rastrigin's function that has many local minima even the initial population (or starting point) of the algorithm is far from the real solution.

VITA

Bach Kim Do was born on August 17, 1992, in Binh Dinh province, Viet Nam. Do received his bachelor of engineering in civil engineering from the Faculty of Civil Engineering, the Ho Chi Minh University of Technology in 2015. Following his graduation, he spent one and a half years working as a structural engineer at Samsung Electronics Ho Chi Minh City Complex. In August 2016, he got the AUN/SEED-Net scholarship to continue his study in Master of Civil Engineering at the Department of Civil Engineering, Faculty of Engineering, Chulalongkorn University, Thailand under the supervision of Assoc. Prof. Akhrawat Lenwari. He is currently interested in structural optimization, structural stability, finite element method, and fracture mechanics.





จุฬาลงกรณ์มหาวิทยาลัย
CHULALONGKORN UNIVERSITY